

PRODUCTION MODELING AND FORECASTING OF NATURAL GAS  
PRODUCTION FROM BARROW METHANE HYDRATE DEPOSITS

By

Bahram F. Novruzaliyev

RECOMMENDED:



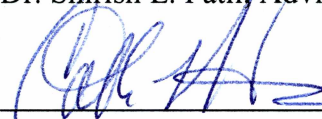
Dr. Santanu Khataniar



Dr. Abhijit Y. Dandekar

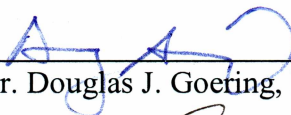


Dr. Shirish L. Patil, Advisory Committee Chair

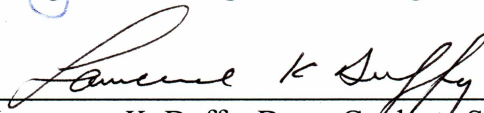


Dr. Catherine Hanks, Chair, Department of Petroleum Engineering

APPROVED:



Dr. Douglas J. Goering, Dean, College of Engineering and Mines



Dr. Lawrence K. Duffy, Dean, Graduate School

Dec 6, 2011

Date

PRODUCTION MODELING AND FORECASTING OF NATURAL GAS  
PRODUCTION FROM BARROW METHANE HYDRATE DEPOSITS

A

THESIS

Presented to the Faculty

of the University of Alaska Fairbanks

in Partial Fulfillment of the Requirements

for the Degree of

MASTER OF SCIENCE

By

Bahram F. Novruzaliyev, B.S.

Fairbanks, Alaska

December 2011

## ABSTRACT

In this work, state-of-the-art existing simulation models of East Barrow and Walakpa natural gas fields with associated gas hydrates were rebuilt, tuned with additional data (some of the data used were from the Mt. Elbert Well, which significantly improved earlier models), and updated in terms of production data and history matching. Fluid contacts, saturations and hydrate dissociation/formation reactions were initialized for both models, actual production was matched and planned wells were placed accordingly. For each model, a gas hydrate saturation sensitivity study was performed. Simulation models were run and production forecasts for Walakpa field were made. There is a clear picture of East Barrow field behavior, but the Walakpa model still involves significant approximations. Additional log data from new wells planned in the Walakpa field will reduce reservoir properties uncertainty and make the model a more realistic reservoir management tool.

A well choking study was performed on a hypothetical simplistic radial simulation grid with a vertical well. It was discovered that vertical gas wells drilled close to a hydrate zone tend to die due to hydrate blockage. Higher gas rates revealed improved production, but faster flow rate decline because of hydrate reformation. Horizontal wells could mitigate this problem due to their lower pressure drop per unit length of completed interval. They are also capable of higher production at lower drawdown. Since higher rate causes faster choking due to hydrate reformation, intermittent reduction of the flow rate is recommended for vertical wells in order to mitigate or at least delay the choking problem. Overall, both horizontal and vertical well designs are suitable for natural gas production from hydrate reservoirs.

## TABLE OF CONTENTS

	Page
SIGNATURE PAGE.....	i
TITLE PAGE.....	ii
ABSTRACT .....	iii
TABLE OF CONTENTS .....	iv
LIST OF FIGURES .....	vii
LIST OF TABLES.....	xi
LIST OF APPENDICES.....	xii
DISCLAIMER .....	xiii
ACKNOWLEDGMENTS .....	xiv
DEDICATION.....	xv
1. INTRODUCTION .....	1
1.1 Background .....	1
1.2 Objectives.....	2
1.3 Tasks Performed.....	3
2. LITERATURE REVIEW .....	4
2.1 Gas Hydrates .....	4
2.1.1 Structures.....	4
2.1.2 Occurrence and Stability Conditions.....	5
2.1.3 Natural Hydrate Morphology .....	7
2.2 Deposit Classes .....	8
2.3 Petrophysical Identification.....	9
2.4 Resource Estimation.....	10

	Page
3. METHODOLOGY .....	11
3.1 Barrow Gas Fields Reservoir Simulation.....	11
3.1.1 Background and Objectives.....	11
3.1.2 CMG-STARS Reservoir Simulator.....	11
3.1.2.1 Reservoir Grid .....	12
3.1.2.2 Reservoir Array Properties.....	12
3.1.2.3 Thermal Properties.....	12
3.1.2.4 Fluid/Component Properties.....	13
3.1.2.5 Wells and Production Constraints.....	14
3.1.2.6 Simulation Output Control.....	15
3.1.3 Model Revision .....	16
3.1.3.1 East Barrow Gas Field.....	16
3.1.3.2 Walakpa Gas Field.....	36
3.1.4 Sensitivity Study.....	45
3.1.5 Forecasting Study .....	46
3.2 Well Choking Study .....	47
3.2.1 Model Initialization .....	47
3.2.2 Study Procedures .....	50
4. RESULTS AND DISCUSSION.....	51
4.1 BGF Reservoir Simulation Study.....	51
4.1.1 Sensitivity Study.....	51
4.1.1.1 East Barrow Gas Field.....	51
4.1.1.2 Walakpa Gas Field.....	52

	Page
4.1.2 Reservoir Simulation Results .....	52
4.1.2.1 East Barrow Gas Field.....	52
4.1.2.2 Walakpa Gas Field.....	65
4.1.3 New Walakpa Wells .....	73
4.1.4 Forecasting Study .....	74
4.1.5 Horizontal Permeability .....	76
4.2 Well Choking Study .....	77
5. CONCLUSIONS AND RECOMMENDATIONS .....	85
5.1 Conclusions .....	85
5.1.1 BGF Reservoir Simulation .....	85
5.1.1.1 East Barrow Gas Field.....	85
5.1.1.2 Walakpa Gas Field.....	85
5.1.2 Well Choking Study .....	86
5.2 Recommendations .....	86
REFERENCES .....	88
APPENDICES .....	91

## LIST OF FIGURES

	Page
Figure 1.1: Barrow Gas Fields Location.....	1
Figure 1.2: Walakpa Sand Structural Map.....	2
Figure 2.1: Hydrate Stability Curve in Permafrost.....	6
Figure 3.1: Results Output Control Window .....	15
Figure 3.2: Reservoir Grid – 3D View.....	17
Figure 3.3: Reservoir Grid (K Layer 1) – IJ Plane View.....	17
Figure 3.4: Reservoir Grid (K Layer 13) – IJ Plane View .....	18
Figure 3.5: Reservoir Grid (K Layer 25) – IJ Plane View.....	18
Figure 3.6: Porosity Distribution – 3D View .....	19
Figure 3.7: Porosity – 5% (K Layer 16) – IJ Plane View .....	20
Figure 3.8: Permeability Distribution in I (North–South) Direction, md – 3D View.....	21
Figure 3.9: Permeability Distribution in J (East–West) Direction, md – 3D View .....	21
Figure 3.10: Permeability Distribution in K (Vertical) Direction, md – 3D View.....	22
Figure 3.11: Permeability of K Layer 16, md – IJ Plane View .....	22
Figure 3.12: Formula Editor – Temperature Distribution Initialization .....	23
Figure 3.13: Initial Temperature Distribution, °F – 3D View .....	24
Figure 3.14: Formula Editor – Gas Hydrate Distribution Initialization .....	26
Figure 3.15: Initial Gas Hydrate Saturation, lbmole/ft <sup>3</sup> – 3D View.....	26
Figure 3.16: Initial Gas Hydrate Saturation (K Layer 1), lbmole/ft <sup>3</sup> – IJ Plane View .....	27
Figure 3.17: Initial Gas Hydrate Saturation (K Layer 25), lbmole/ft <sup>3</sup> – IJ Plane View ...	27
Figure 3.18: Initial Hydrate–Gas Contact– IK Plane View .....	28
Figure 3.19: Formula Editor – Gas Saturation Initialization .....	29
Figure 3.20: Initial Gas Saturation – 3D View .....	30
Figure 3.21: Initial Gas Saturation (K Layer 1) – IJ Plane View .....	30
Figure 3.22: Initial Gas Saturation (K Layer 25) – IJ Plane View .....	31
Figure 3.23: Initial HGC and GWC – IK Plane View .....	31
Figure 3.24: Formula Editor – Water Saturation Initialization.....	33

	Page
Figure 3.25: Initial Water Saturation – 3D View.....	33
Figure 3.26: Initial Water Saturation (K Layer 1) – IJ Plane View .....	34
Figure 3.27: Initial Water Saturation (K Layer 25) – IJ Plane View .....	34
Figure 3.28: Initial HGC and GWC – IK Plane View .....	35
Figure 3.29: Walakpa Reservoir Grid – 3D View .....	36
Figure 3.30: Porosity Distribution – 3D View .....	37
Figure 3.31: Permeability Distribution, md – 3D View.....	38
Figure 3.32: Initial Reservoir Temperature Distribution, °F – 3D View .....	39
Figure 3.33: Initial Reservoir Pressure, psi – 3D View .....	40
Figure 3.34: Initial Gas Hydrate Saturation, lbmole/ft <sup>3</sup> – 3D View .....	41
Figure 3.35: Initial HGC – IK Plane View .....	42
Figure 3.36: Initial Gas Saturation – 3D View .....	43
Figure 3.37: Initial Water Saturation – 3D View.....	44
Figure 3.38: Well Locations – IJ Plane View .....	45
Figure 3.39: Simplistic Radial Grid – 3D View .....	48
Figure 3.40: Initial Temperature Distribution, °F – 3D View .....	49
Figure 3.41: Initial Gas Saturation – 3D View .....	50
Figure 4.1: East Barrow Cumulative Gas Production, ft <sup>3</sup> .....	53
Figure 4.2: Representative Grid Block Location .....	54
Figure 4.3: Gas Hydrate Saturation Profile at Grid Block 19,19,1.....	54
Figure 4.4: Gas Saturation Profile .....	55
Figure 4.5: Water Saturation Profile.....	56
Figure 4.6: Hydrate Saturation at Simulation End – 3D View .....	57
Figure 4.7: Hydrate Saturation at Simulation End (K Layer 19) – IJ Plane View .....	57
Figure 4.8: Gas Saturation at Simulation End – 3D View .....	58
Figure 4.9: Gas Saturation at Simulation End (K Layer 23) – IJ Plane View .....	59
Figure 4.10: Water Saturation at Simulation End – 3D View .....	59
Figure 4.11: Water Saturation at Simulation End (K Layer 23) – IJ Plane View.....	60



	Page
Figure 4.12: Temperature Distribution at Simulation End – 3D View .....	61
Figure 4.13: Pressure Distribution at Simulation End – 3D View .....	61
Figure 4.14: Initial HGC and GWC – IK Plane View .....	62
Figure 4.15: GWC at Simulation End– IK Plane View .....	62
Figure 4.16: Initial HGC – IK Plane View .....	63
Figure 4.17: HGC at Simulation End – IK Plane View .....	63
Figure 4.18: Initial HGC and GWC – IK Plane View .....	64
Figure 4.19: GWC at Simulation End – IK Plane View .....	64
Figure 4.20: Walakpa Cumulative Gas Production, ft <sup>3</sup> .....	65
Figure 4.21: Hydrate Saturation at Simulation End – 3D View .....	66
Figure 4.22: Hydrate Saturation at Simulation End (K Layer 7) – IJ Plane View .....	66
Figure 4.23: Water Saturation at Simulation End – 3D View .....	67
Figure 4.24: Water Saturation at Simulation End (K Layer 10) – IJ Plane View.....	68
Figure 4.25: Temperature Distribution at Simulation End – 3D View .....	68
Figure 4.26: Pressure Distribution at Simulation End – 3D View.....	69
Figure 4.27: Initial HGC and Gas Saturation – JK Plane View.....	70
Figure 4.28: Current HGC and Gas Saturation – JK Plane View .....	70
Figure 4.29: Initial HGC and Hydrate Saturation – JK Plane View.....	71
Figure 4.30: Current HGC and Hydrate Saturation – JK Plane View .....	71
Figure 4.31: Initial GWC and Water Saturation – JK Plane View .....	72
Figure 4.32: Current GWC and Water Saturation – JK Plane View .....	72
Figure 4.33: New Horizontal Wells in Walakpa Reservoir .....	73
Figure 4.34: First Case Cumulative Gas Production .....	74
Figure 4.35: Second Case Cumulative Gas Production .....	75
Figure 4.36: Dependence of Cumulative Production on $k_v/k_h$ .....	76
Figure 4.37: Production Profile for the First Case (10 Mscfd).....	77
Figure 4.38: Hydrate Saturation ( $S_h$ ) After 9.8 Years of Production at 10 Mscfd.....	78
Figure 4.39: Production Profile for the Second Case (30 Mscfd).....	79

	Page
Figure 4.40: Hydrate Saturation ( $S_h$ ) After 5.8 Years of Production at 30 Mscfd.....	80
Figure 4.41: Production Profile for the Third Case (100 Mscfd).....	81
Figure 4.42: Hydrate Saturation ( $S_h$ ) After 3.2 Years of Production at 100 Mscfd.....	81
Figure 4.43: Cumulative Production Comparison of All Three Cases.....	82
Figure 4.44: Representative Grid Block (10, 1, 7).....	83
Figure 4.45: Hydrate Equilibrium Curve.....	84
Figure A.1: Component Initialization.....	91
Figure A.2: Forward Reaction Initialization.....	92
Figure A.3: Backward Reaction Initialization.....	92
Figure B.1: Wellbore Diagram of EB #12.....	93
Figure B.2: Wellbore Diagram of EB #14.....	94
Figure B.3: Wellbore Diagram of EB #15.....	95
Figure B.4: Wellbore Diagram of EB #18.....	96
Figure B.5: Wellbore Diagram of EB #19.....	97
Figure B.6: Wellbore Diagram of EB #21.....	98
Figure C.1: Wellbore Diagram of WAL #2.....	99
Figure C.2: Wellbore Diagram of WAL #3.....	100
Figure C.3: Wellbore Diagram of WAL #4.....	101
Figure C.4: Wellbore Diagram of WAL #5.....	102
Figure C.5: Wellbore Diagram of WAL #6.....	103
Figure C.6: Wellbore Diagram of WAL #7.....	104
Figure C.7: Wellbore Diagram of WAL #8.....	105
Figure C.8: Wellbore Diagram of WAL #9.....	106
Figure C.9: Wellbore Diagram of WAL #10.....	107
Figure D.1: Wellbore Diagram of WAL #11.....	108
Figure D.2: Wellbore Diagram of WAL #12.....	109
Figure D.3: Wellbore Diagram of WAL #13.....	110
Figure D.4: Wellbore Diagram of WAL #14.....	111

## LIST OF TABLES

	Page
Table 3.1: Walakpa Horizontal Wells' Completion Lengths.....	45
Table 3.2: Forecasting Summary.....	47
Table 4.1: East Barrow field sensitivity study summary.....	51
Table 4.2: Walakpa field sensitivity study summary.....	52
Table 4.3: Summary of Production Simulation for Walakpa Field.....	75

## LIST OF APPENDICES

	Page
Appendix A.....	91
Appendix B.....	93
Appendix C.....	99
Appendix D.....	108

## **DISCLAIMER**

This thesis was prepared as an account of work sponsored by an agency of the United States Government. Neither the United States Government nor an agency thereof, nor any of their employees makes any warranty, expressed or implied, or assumes any legal liability or responsibility for the accuracy, completeness, or usefulness of any information, apparatus, product, or process disclosed, or represents that its use would not infringe privately owned rights. References herein to any specific commercial product, process, or service by trade name, trademark, manufacturer, or otherwise do not necessarily constitute or imply its endorsement, recommendation, or favoring by the United States Government or any agency thereof. The views and opinions of authors expressed herein do not necessarily state or reflect those of the United States Government or any agency thereof.

## ACKNOWLEDGMENTS

This is a great opportunity to express my sincere gratitude to my advisory committee: Dr. Shirish L. Patil, Dr. Abhijit Y. Dandekar, and Dr. Santanu Khataniar for vital comments and recommendations on this work. I owe my deepest appreciation to my academic advisor, Dr. Shirish L. Patil for his consistent encouragement, scientific guidance, truthful caring, and superior managerial skills.

I would like to thank Mrs. Melody Hughes, Petroleum Engineering department office manager for her everlasting helpfulness.

I convey my heartfelt gratitude to PRA (Petrotechnical Resources Alaska) for the research I was kindly entitled to carry out. I would like to personally thank Mr. Thomas Walsh for timely communication and technical guidance.

The funding for this work was provided by the U.S. Department of Energy (US DOE) (DE-FC26-06NT42962), through Petrotechnical Resources Alaska, Inc.

I am thankful to Computer Modelling Group (CMG) for the exceptional software, and for extended grid block license. Without those this research would be virtually impossible. Special thanks to CMG Customer Support Team.

I would also like to thank SPT Group for granting me the OLGA licensed software. Due to time limitations I was not able to use the software and include any results; however, I very much appreciate SPT Group for granting the license to University of Alaska Fairbanks.

Lastly, I would like to show my gratefulness to my loving family and friends who always supported me regardless the distance separating us.

## **DEDICATION**

This thesis is dedicated to my grandparents.

## 1. INTRODUCTION

### 1.1 Background

The city of Barrow, northernmost town of the United States of America, is located on the North Slope of Alaska, remote from most infrastructure. Constantly growing energy demand of the city and adjacent villages has been successfully met by the Barrow Gas Fields (BGF) for almost 30 years. The BGF consist of East Barrow (EB), South Barrow (SB), and Walakpa (WAL) fields, located to the south and southeast of Barrow (Figure 1.1). According to field report (Glenn and Allen, 1991) and simulation results, the BGF are capable of maintaining gas supply in the region for another 100 years.

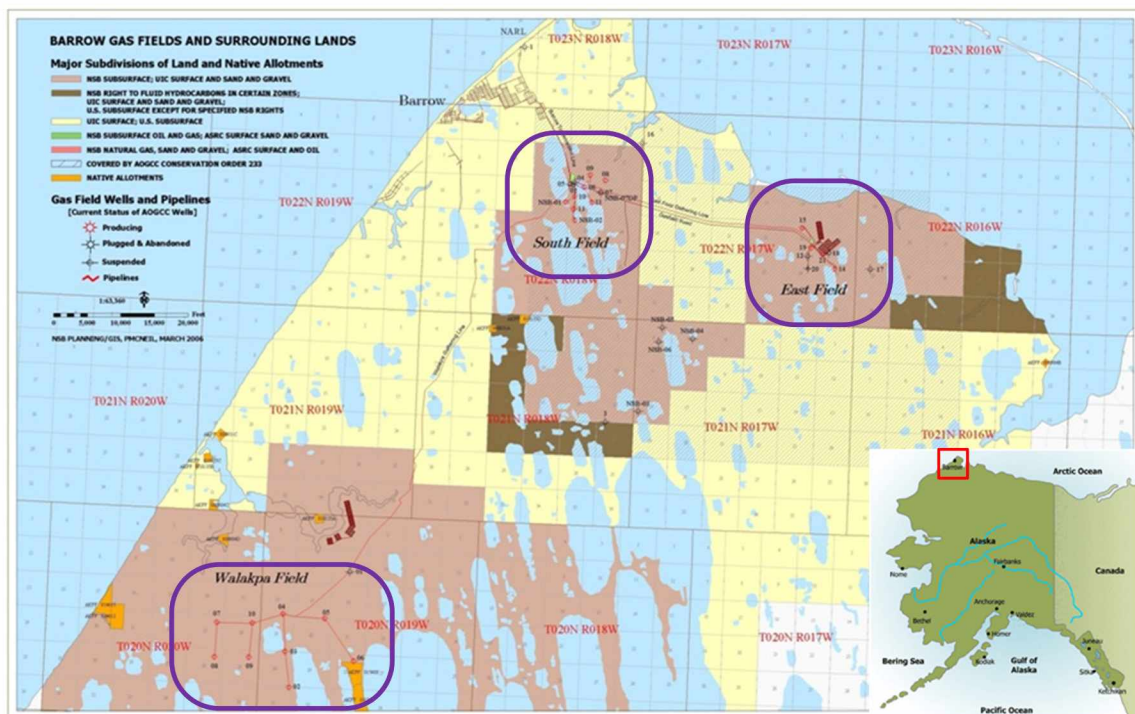


Figure 1.1: Barrow Gas Fields Location (Modified from NETL Website)

BGF pay-zone depth ranges between 1900 ft and 3100 ft (Glenn and Allen, 1991), hence they are quite shallow. The main productive formation is Walakpa sand (Glenn and Allen, 1991). A structural map of the formation is provided in Figure 1.2. Initial pressure



and temperature conditions in the updip portion of Walakpa sand were sufficient for gas hydrate formation (Glenn and Allen 1991). In the BGF, free gas is being produced; however, the upper portion of the fields lies within the gas hydrate stability region. It turns BGF into gas fields with gas hydrates associated on the top.

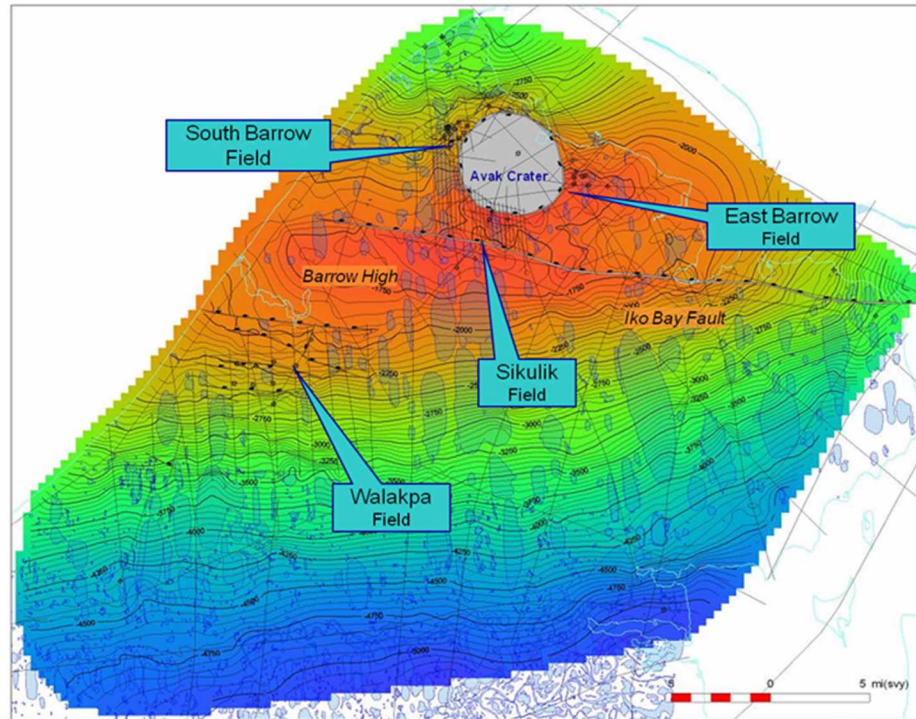


Figure 1.2: Walakpa Sand Structural Map (Modified from Petrotechnical Resources Alaska)

Previous studies reported possible gas recharge from dissociating gas hydrates in the gas hydrate zone (Stokes et al., 2005; Stokes and Walsh, 2007). Gas hydrate stability depth was estimated within the range of 2000–2550 ft (Singh, 2008; Glenn and Allen, 1991).

The BGF project is of extreme importance as it is one of the first studies on gas hydrate deposit exploitation in this region.

## 1.2 Objectives

This project was undertaken to evaluate potential of gas hydrates as an energy resource, simulate hydrate processes in the field, and get a better understanding of field

performance. The work was focused on building state of the art simulation models, simulation of hydrate-bearing reservoirs with maximum accuracy in the inputs, obtaining precise outputs, and their analysis.

### **1.3 Tasks Performed**

The tasks successfully completed in this study are summarized as follows:

- a. Existing BGF reservoir models were reviewed for initialization errors and fixed.
- b. Outdated property-distribution formulas were rewritten and assigned accordingly.
- c. The hydrate zone was initialized for the first time. This required input of chemical reactions, their equilibrium parameters, etc.
- d. A sensitivity study was performed in order to achieve adequate hydrate saturation values and dissociation rates. It also minimized the material balance error during simulation runs.
- e. Forecasting was completed for the Walakpa field for two scenarios. First scenario involved only existing Walakpa producers. The second one included four new planned horizontal wells.
- f. Well choking due to hydrate reformation in the near-wellbore zone was studied by simulation.

## 2. LITERATURE REVIEW

### 2.1 Gas Hydrates

Gas hydrates are solid chemical compounds resembling ice. They consist of gas molecules entrapped within the lattice structures of water molecules (Moridis et al., 2008). Such substances are called clathrates or cage compounds. In clathrates, host molecules form a crystalline cage-like lattice with voids occupied by guest molecules. In the case of gas hydrates, host molecules of water connect to each other by hydrogen bonds and trap guest molecules of gas (Klauda and Sandler, 2005). To form hydrates generally require low temperatures and high pressures (Makogon, 1966). Apparently, clathrates do not flow in porous media whereas some flow through them might be possible.

Theoretically, all gasses can form hydrates under certain conditions (Klauda and Sandler, 2005; Makogon, 1982). Exceptions are hydrogen, helium, and neon. They do not form hydrates (Makogon, 1982). In most cases natural gas hydrates are formed with methane gas; followed by ethane, propane, CO<sub>2</sub>, and butane (Makogon, 1982). Structure and stability properties of the hydrates depend on the type of gas with which they are formed.

#### 2.1.1 Structures

There are 3 gas hydrate structures discovered so far: Structure I (sI), Structure II (sII), and Structure H (sH). Cubic structures I and II are the most common encountered in nature (Kvenvolden, 1993). Structure I hydrates consist of 46 water molecules with 8 cavities (Miller, 1961). These cavities have average diameters of about 4.3 Å (Miller, 1961). They can entrap only small guest molecules of a size ranging between 4.0 and 5.5 Å, most frequently methane and sometimes ethane (Miller, 1961). Also within the range to form Structure I hydrates are H<sub>2</sub>S and CO<sub>2</sub> molecule sizes, but their occurrence is rare. Since methane gas hydrates are the most abundant in nature, Structure I hydrates are found in vast amounts (Kvenvolden, 1993; Moridis et al., 2008).

Structure II hydrates are formed by 136 water molecules with 24 cavities (Miller, 1961). These include 16 small cavities that can hold a guest molecule of 5.0 Å or less and 8 large cavities that can have a guest of 6.7 Å or less (Miller, 1961). These larger cavities are capable of holding propane molecules, of about 6.3 Å in diameter (Collett and Ehlig-Economides, 1983), whereas smaller cavities can be occupied by methane molecules of a diameter equal to 4.4 Å.

Structure H hydrates have a hexagonal shape, and their discovery was relatively recent (Mehta and Sloan, 1999). In order to form, Structure H hydrates require light molecules such as methane, hydrogen sulfide, or nitrogen as well as heavier molecules such as isopentane, hexane, or methylcyclohexane (Mehta and Sloan, 1999; Schulz and Zabel, 2006). Therefore, Structure H hydrates can occur in the presence of oil or condensate and are most frequently observed in manifolds and pipelines where multiphase flow takes place. Structure H hydrates contain 34 water molecules and 6 cavities, five of which are small and can hold guests with diameters about 4.5-5.5 Å (Schulz and Zabel, 2006). The remaining cavity is exceptionally large and accepts heavy guest molecules of diameters up to 8-9 Å (Schulz and Zabel, 2006).

### **2.1.2 Occurrence and Stability Conditions**

Gas hydrates have been discovered and samples have been recovered from numerous sites in the world (Moridis et al., 2008). Apparently gas hydrates occur in two distinctive and quite dissimilar settings: hydrates associated with permafrost in polar regions and hydrate occurrences in deep water sediments. The latter were found all over the world on the beds of oceans, seas, and even deep lakes. These deposits contain enormous amounts of natural gas (Makogon et al., 2007). However, existing technologies have not yet been tested for commercial production of natural gas from marine hydrates and thus such operations are considered to be currently unfeasible (Moridis et al., 2008).

Of major interest are gas hydrate accumulations associated with permafrost. From development perspective they have numerous advantages over deep water hydrate deposits: onshore location, existence of impermeable caprock, shallow depth, and

frequent association with conventional gas fields are foremost among these advantages. In permafrost regions, natural gas in the subsurface can possibly occur partially or completely in the hydrate state (Makogon, 1966). A typical hydrate stability curve in a permafrost region is displayed in Figure 2.1.

Special pressure and temperature conditions are required for gas hydrates to stay in a stable state (Katz, 1971). These conditions depend on various rock and fluid parameters such as entrapped gas composition, hydrate saturation, formation water salinity, and formation mineralogy. However, even if certain stability conditions are maintained within a formation, hydrates do not necessarily exist in it (Makogon, 1966).

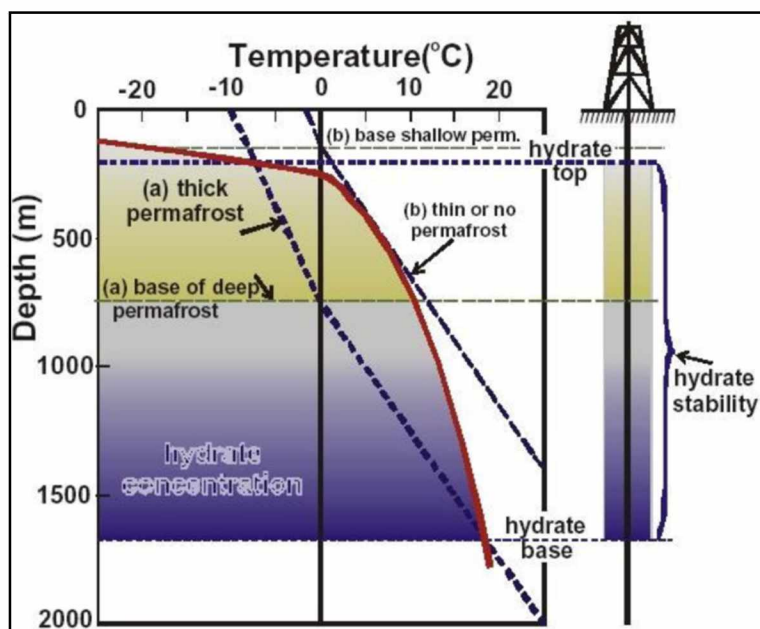


Figure 2.1: Hydrate Stability Curve in Permafrost (Geologic Survey of Canada, [www.nrcan.gc.ca](http://www.nrcan.gc.ca))

Gas hydrate stability properties highly depend on gas composition (Godbole et al., 1988). Godbole et al. (1988) conducted laboratory experiments to reveal that dependence. The estimation of hydrate stability parameters for methane-ethane mixtures was chosen as an objective for their study. They discovered that with increased ethane presence from 0 to 9.8 vol% in a methane-ethane mixture, stability pressure decreases and stability

temperature increases. Hence, within the experiment range, with increase of ethane fraction in methane, gas hydrates become more stable (Maekawa, 2001).

Increase in water salinity causes reduction of hydrate stability temperature at a rate of 5–7 deg. per 100,000 ppm (Katz, 1971). Overall, brine is more inert and less readily reacts with gas to form hydrates, therefore more energy is required to start the reaction. Nevertheless, hydrate layers can occur at considerably high temperatures. For this reason, in some cases hydrate layers can have significant thickness. Onshore hydrate stability zone thickness lies in a range between 700 and 1500m, whereas offshore it is expected to be only from 100 to 400m thick (Makogon,1982). Hydrate zone thickness is a considerable property directly affecting hydrate production project viability (Godbole et al., 1988). Hydrate formation is also possible at temperatures higher than the freezing point of water (Katz, 1971). This explains why gas hydrate layers can occur beneath the base of permafrost. Apparently, the base of permafrost has a temperature close to 0°C, the freezing point of water. In a case when they were formed before the freezing of soil, hydrates can even be located above the base of permafrost (Katz, 1971).

Synthetic gas hydrates have been obtained repeatedly in different laboratories (Jaiswal, 2004; Singh, 2008). Some experiments included hydrate formation in porous media. Hydrates have been formed experimentally in porous media long ago, and they were able to conduct fluids (Evernos et al., 1971). A number of experiments were conducted at the University of Alaska Fairbanks (UAF) in order to estimate gas hydrate relative permeability values (Jaiswal, 2004). Almost all of the experiments led to the conclusion that an increase in hydrate saturation leads to decrease in relative and effective permeability of the sample (Evernos et al., 1971; Jaiswal, 2004).

### **2.1.3 Natural Hydrate Morphology**

Gas hydrates can occur in the subsurface as disseminated inclusions, nodules, thin layers, or large bodies (Worthington, 2008). If gas hydrates are present in the form of disseminated inclusions, their volume is considered usually to be too small for economical gas production. In cases of large hydrate body occurrences with high hydrate

saturations, the formations are frequently hydrate-bonded rather than matrix-bonded (Stokes and Walsh, 2007). This means that the formation grains are cemented by hydrate and will disaggregate if the hydrates start to dissociate. This raises additional difficulties in production, such as risk of formation collapse possibly leading to overburden subsidence and wellbore stability issues (Stokes and Walsh, 2007).

## **2.2 Deposit Classes**

Since most of the deposits containing gas hydrates have certain common features, the following classification has been suggested (Moridis and Collett, 2004):

Class 1 hydrate deposits refer to gas hydrates associated with conventional gas reservoirs in which the gas-bearing formation is overlain by a gas hydrate layer. There is impermeable rock above the gas hydrate layer and below the productive formation. Natural gas can be supported by an aquifer. In Class 1 reservoirs, the gas hydrate-free gas contact (HGC) is the base of the hydrate stability region. This class of deposits is most common onshore associated with permafrost regions such as the North Slope of Alaska, northern Canada and the northern part of Siberia. Messoyakha and Barrow Gas Fields serve as possible examples of this class of deposits (Makogon, 1966; Stokes and Walsh, 2007). Methane hydrates in the Barrow Gas Fields are believed to contribute lots of methane gas to the total gas production (Stokes and Walsh, 2007).

Class 2 deposits are ones in which there is no free gas below the gas hydrate layer, but there is an aquifer below it. In deposits of this class, the hydrate layer and aquifer are isolated by impermeable rocks just as in Class 1 deposits; however gas hydrate-water contact is likely to be above the base of the hydrate stability region. This can be the case when all of the gas has been trapped in the hydrates.

Class 3 hydrate deposits are characterized by hydrate accumulation entirely bound by impermeable formations and a free fluid zone is absent. Since the formation of hydrates is usually accompanied by volume reduction, a reasonable conclusion can be made that in

the absence of water flux, gas hydrate formations might be at abnormally low pressure (Makogon, 1966).

Class 4 deposits refer to gas hydrate accumulations dispersed in the deep water on ocean, sea, and lake beds, not bound by any caprock from above. Due to their unique occurrence and technical recovery difficulties, these hydrate deposits are least regarded as a prospective energy resource (Moridis and Collett, 2004).

### **2.3 Petrophysical Identification**

Of key importance is to identify and locate hydrate bearing formations precisely. On the well-scale, the fastest way to do this is thorough utilization of LWD (Logging While Drilling) tools. Luckily gas hydrates have certain characteristic petrophysical properties that can be used to distinguish them in the subsurface section.

In most cases gas hydrates are identified by characteristic log response such as high electrical resistivity, high sonic velocity, and low density (Worthington, 2008). Mud gas logs are also recommended for hydrate identification (Worthington, 2008). Several authors have suggested utilization of sonic and neutron porosity logs to effectively distinguish hydrate-bearing formations (Collett and Ehlig-Economides, 1983; Godbole et al., 1988). However, a neutron porosity log by itself is unable to identify gas hydrates in permafrost regions (Worthington, 2008). The reason for that is the high porosity reading for both hydrates and ice layers. Hence, application of all aforementioned tools together will lead to the most precise hydrate identification.

Even though gas hydrates have specific log response, some difficulties may arise with the distinguishing of gas hydrates from ice (Worthington, 2008). Very thin gas hydrate layers are also often difficult to spot, even though modern logging tools have quite high resolution. However, production from such thin layers is highly unlikely due to low volumes, so they can be neglected in most cases.



## 2.4 Resource Estimation

Different estimations have been made on gas reserves trapped in the hydrate state, but even the most pessimistic forecasts indicate enormous volumes of gas. Onshore gas reserves trapped in hydrates alone were estimated at  $57 \cdot 10^{12} \text{ m}^3$  (2,013 TCF) (Makogon, 1982). Milkov (2004) estimated marine hydrate reserves of  $1\text{--}5 \cdot 10^{15} \text{ m}^3$  (35,315–176,573 TCF). Kluda and Sandler (2005) made a more optimistic estimate of hydrates trapped in ocean sediments at  $1.2 \cdot 10^{17} \text{ m}^3$  (4,237,760 TCF). One of the most recent estimates, however, suggests global resource of natural gas in hydrate state of  $1.5 \cdot 10^{16} \text{ m}^3$  (529,720 TCF), (Makogon et al., 2007).

## **3. METHODOLOGY**

### **3.1 Barrow Gas Fields Reservoir Simulation**

#### **3.1.1 Background and Objectives**

Reservoir models for Barrow Gas Fields were built in Roxar RMS commercial geomodelling software by Panda and Morahan (2008). Afterward, the models were imported into the STARS module of the CMG commercial reservoir simulation suite pack (Singh, 2008). So far, the Barrow Gas Fields simulation models have been adapted to simulate gas hydrates as heavy oil with such high viscosity as to be virtually immobile (Singh, 2008). This was done due to lack of a hydrate phase in the simulator database. As a result of such adaptation the simulator was able to simulate gas hydrate dissociation; however gas hydrate reservoir behavior was not perfectly represented. One reason for that was lack of backward reaction (gas hydrate formation). If the reaction were specified, it would allow the adapted models to produce oil. Moreover, the simulator was producing results for oil phase, which was impractical since no oil was produced. The latest versions of CMG STARS software are capable of detailed gas hydrate specification and simulation. Both Walakpa and East Barrow field models were updated accordingly. The following objectives were chosen:

- Update simulation models with actual production data.
- Incorporate gas hydrates into history matched simulation models.
- Perform sensitivity study of hydrate saturation.

#### **3.1.2 CMG-STARS Reservoir Simulator**

STARS stands for Steam, Thermal, and Advanced processes Reservoir Simulator and is a commercial product of Computer Modelling Group Ltd. Designed for advanced purposes, STARS is capable of both 2D and 3D reservoir simulation. It allows multi-phase multi-component fluid flow, accounts for heat losses, dynamic rock and fluid properties, and many other features. All inputs can be specified using the simulator's user-friendly interface, or they can be directly imported from existing files. STARS supports and

accepts all file formats considered standard in the energy industry. Most of figures in this thesis are standard CMG outputs, having title and units on the top and color bar on the right side.

### ***3.1.2.1 Reservoir Grid***

There are several ways to initialize the reservoir grid in STARS. One way is to construct a grid manually by specifying grid type, number of blocks and their dimensions. The grid can be either Cartesian or Radial. Another method is to build the grid by importing existing structural and isopach maps, well trajectories, and log data that brings STARS to the level of the geomodelling software. The simplest way, if the reservoir grid has already been built in some geomodelling software (such as GOCAD, RMS, Petrel, or another CMG dataset), is to directly import it into STARS.

Static reservoir models of Barrow Gas Fields were built based on well log data in ROXAR RMS commercial software (Panda and Morahan, 2008). The resulting reservoir grids were directly imported into STARS (Singh, 2008).

### ***3.1.2.2 Reservoir Array Properties***

In the STARS user interface, all of the reservoir properties can be specified in the Array Properties subdivision of the Reservoir section. Reservoir properties can be specified for the entire grid, for a single layer (in K direction), or for each grid block individually. Some reservoir properties such as porosity and permeability were imported with the static grid. Reservoir properties such as pressure, temperature, fluid contacts, and saturations were specified in STARS. To establish dependence between certain reservoir properties, formulas were created as part of this work using the CMG formula editor. These formulas were then specified as properties in the Array Properties subdivision of the Reservoir section.

### ***3.1.2.3 Thermal Properties***

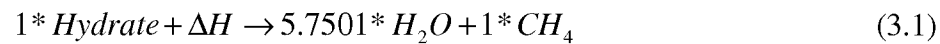
Thermal factor is critical for a simulation model with hydrates, since heat flux impacts hydrate stability as well as depressurization. Volumetric heat capacity and thermal

conductivities of rock and fluids were specified for both models. The “Keywords” in CMG for thermal conductivity phase mixing, specified as SIMPLE earlier, was changed to COMPLEX as part of this work, in order to better predict the thermal factor. Upon this change hydrate models account for very small porosity values (less than one percent).

#### ***3.1.2.4 Fluid/Component Properties***

Three fluid components were specified in the simulation models. Methane gas was specified as the gaseous phase and formation water as the water phase. Gas hydrate was initially specified as the oleic phase; however, within this study, hydrate was changed to solid phase. This was followed by several oil properties being deleted and specified for hydrate. Water and gas mole fractions were kept equal to 1 (no dissolved gas in water and no water vapor in gas). The oil mole fraction was deleted. Hydrate density and enthalpy were specified for solid phase, whereas viscosity data was deleted.

Gas hydrate dissociation is accompanied by methane and water release. One mole of hydrate releases one mole of gas and about 5.75 mole of water. This is an endothermic process described by forward chemical reaction (3.1).



where  $\Delta H$  – reaction enthalpy, BTU/lbmole. Enthalpy is negative for endothermic reactions. The STARS interface allows straightforward reaction specification with automatic mass balance calculation in order to reduce the error percentage. The reaction rate,  $k$ , is governed by Arrhenius equation (3.2).

$$k = Ae^{-E_a/RT} \quad (3.2)$$

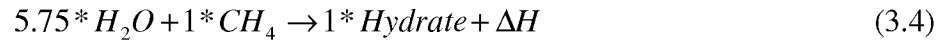
Where  $k$  – reaction rate constant, lbmole/lb-day;  $A$  – pre-exponential factor, or frequency factor (CMG keyword \*FREQFAC), dimensionless;  $E_a$  – activation energy (CMG keyword \*EACT), BTU/lbmole;  $R$  – universal gas constant, BTU/lbmole-°R; and  $T$  – reservoir temperature, °R.

Subsequently, reaction K values for vapor-liquid equilibrium were specified. In STARS, K value is represented by equation (3.3).

$$K(p, T) = \left( \frac{rxk1}{p} + rxk2 * p + rxk3 \right) * e^{\left( \frac{rxk4}{T - rxk5} \right)} \quad (3.3)$$

where  $p$  – pressure, psi;  $T$  – temperature, °K; and  $rxk1$ ,  $rxk2$ ,  $rxk3$ ,  $rxk4$ ,  $rxk5$  are reaction coefficients of which  $rxk1$  is in psi,  $rxk2$  is in 1/psi,  $rxk3$  is dimensionless,  $rxk4$  and  $rxk5$  are in °K.

Gas hydrate dissociation is a reversible process, hence hydrates can form again given favorable conditions and required components are present. In order to input this process, a backward reaction was specified as in equation (3.4)



Apparently, reaction (3.4) is a backward reaction of (3.1). Enthalpy  $\Delta H$  is positive in this case. Reaction frequency factor (\*FREQFAC), activation energy (\*EACT), and K value correlation coefficients were specified similarly to the forward reaction.

### **3.1.2.5 Wells and Production Constraints**

Wells can be effectively identified and located in the reservoir using the CMG interface, or they can be imported in cases of survey data availability. It is possible to define vertical, horizontal, and also multi-lateral wells. The user-friendly interface provides simple control of well events, allowing one to open or shut-in a well at certain date, to change the operational constraints, and to alter completion at any time during field life.

Operational constraints control the well production/injection. Among the constraints numerous options are available in CMG to be optimally selected for every specific case. Primary constraint value can be altered at any date (\*ALTER keyword). Primary constraint can also be substituted by another one (\*TARGET keyword) at any date during production, allowing for further manipulations with the new one. If a production/injection

data file is available, it can be imported directly into the model. This option was used for each of the wells in both models (Singh, 2008) and updated as part of this work.

### 3.1.2.6 Simulation Output Control

Each model requires different outputs depending on simulation purposes. Usually for a particular problem only a few variables are required. In order to save computational time, unnecessary simulation outputs can be deactivated using the simulator interface (Figure 3.1). In case where all the output variables are selected, simulation runs will be long. In STARS a limited number of variables are active by default. The ones required for this study had to be activated manually and some of the active variables had to be switched off.

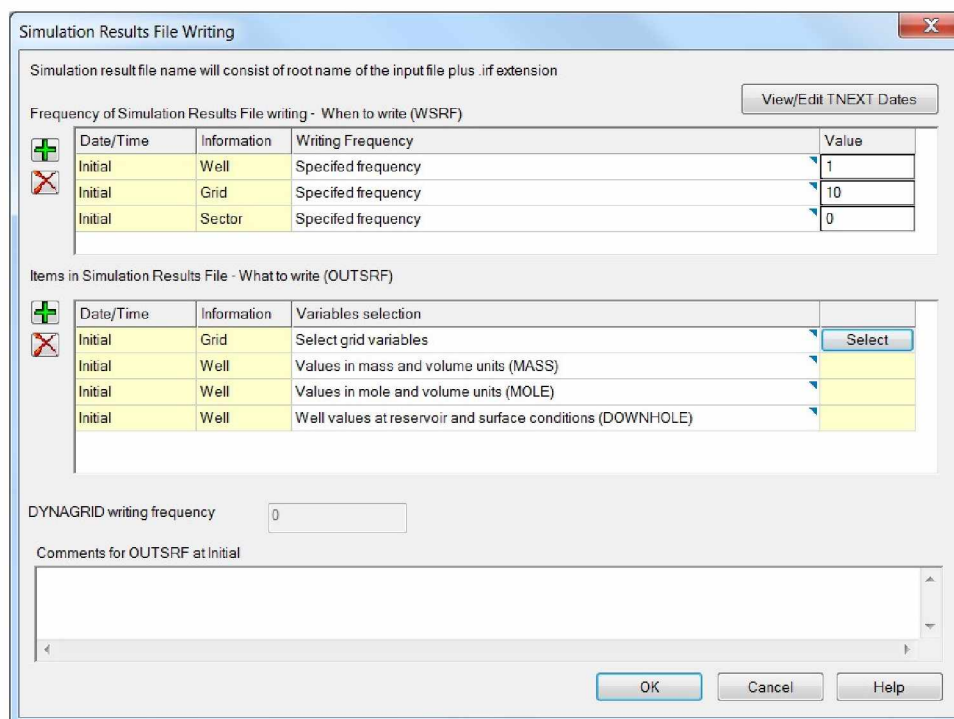


Figure 3.1: Results Output Control Window

Variables crucial for the current study are (respective keywords are provided in parentheses): gas saturation (SG), water saturation (SW), temperature (TEMP), pressure (PRES), water viscosity (VISW), gas viscosity (GASW), water relative permeability (KRW), gas relative permeability (KRG), I direction absolute permeability (PERMI), and

component solid concentration (SOLCONC). Volume units (VOL keyword) are recommended for the latter in order to see hydrate saturation as volume fraction.

### **3.1.3 Model Revision**

#### ***3.1.3.1 East Barrow Gas Field***

Within this study, the simulation model originally initialized and history matched by Singh (2008), was brought to the next level by numerous modifications and updated. The models were upgraded with gas hydrate initialization. A sensitivity study to analyze the dependence of hydrate saturation on solid concentration was performed. Based on the sensitivity study, a suitable best-case model with desired hydrate saturation was selected.

The best-case setting takes account of gas hydrate in place in such a way that simulation outputs demonstrate actual production and reasonable forecast, with material balance error reduced to a minimum. This section describes the reservoir properties attained for the best-case setting.

#### **a. Reservoir Grid**

The reservoir grid was built based on reservoir geology and well log data in ROXAR RMS (Panda and Morahan, 2008), and later imported directly into CMG (Singh, 2008).

Due to reservoir structure (i.e. high dipping angles of the formation), a corner point grid was used. The grid consisted of 54 blocks in I, 37 blocks in J, and 25 blocks in K directions respectively, rendering 49,950 grid blocks in total. Some grid blocks were specified inactive as they were not considered as part of the reservoir. Those grid blocks mostly represented Avak crater, which provides field closure at the west. A single grid block is 600 ft in both length and width (I and J directions), whereas thickness (K direction) varies between 1.09 ft and 3.22 ft. The top of the structure is located at 1900 ft TVD below sea level and the lowest portion of the reservoir is at a depth of 2330 ft TVD in the water leg. Figure 3.2 illustrates a 3D view of the reservoir grid. 2D views of the IJ plane for Layers 1 (K=1), 13 (K=13), and 25 (K=25) are shown in Figures 3.3, 3.4, and 3.5, respectively. Color denotes depth.

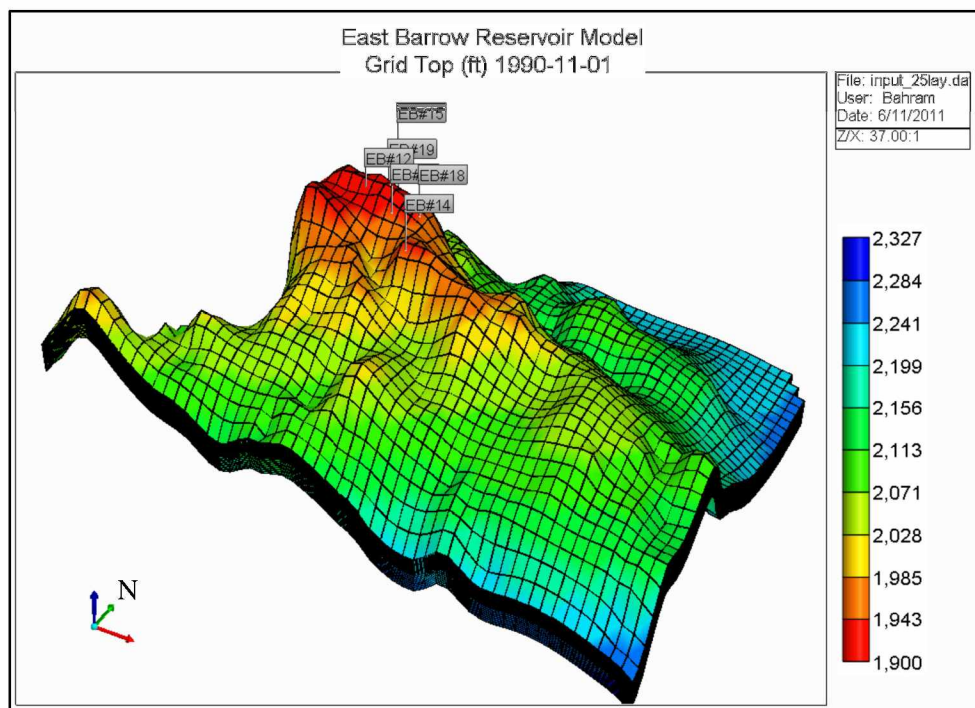


Figure 3.2: Reservoir Grid – 3D View

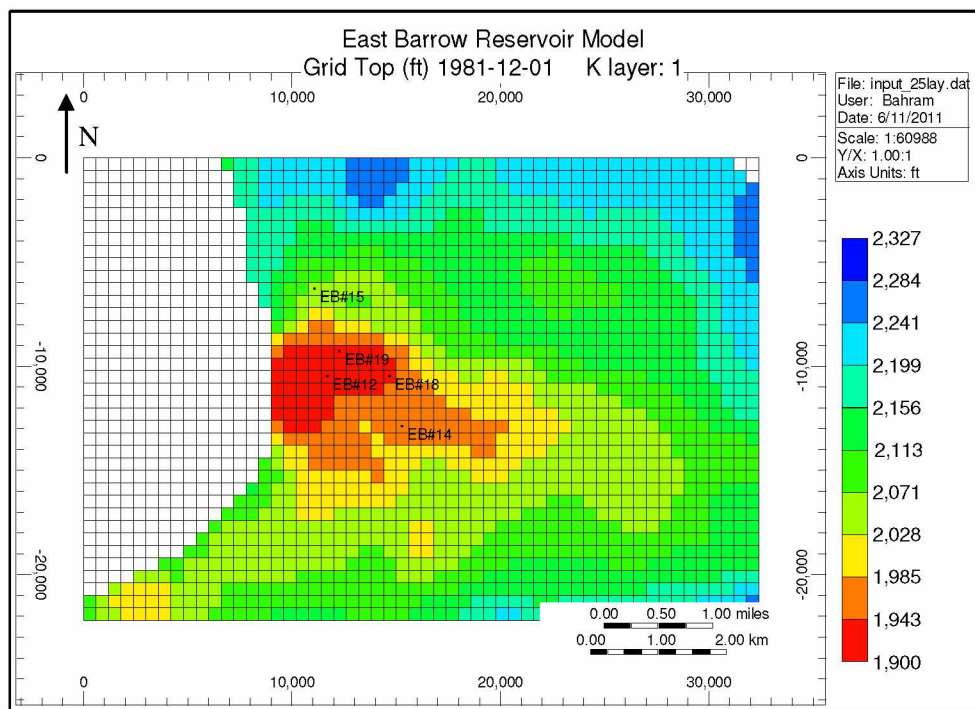


Figure 3.3: Reservoir Grid (K Layer 1) – IJ Plane View



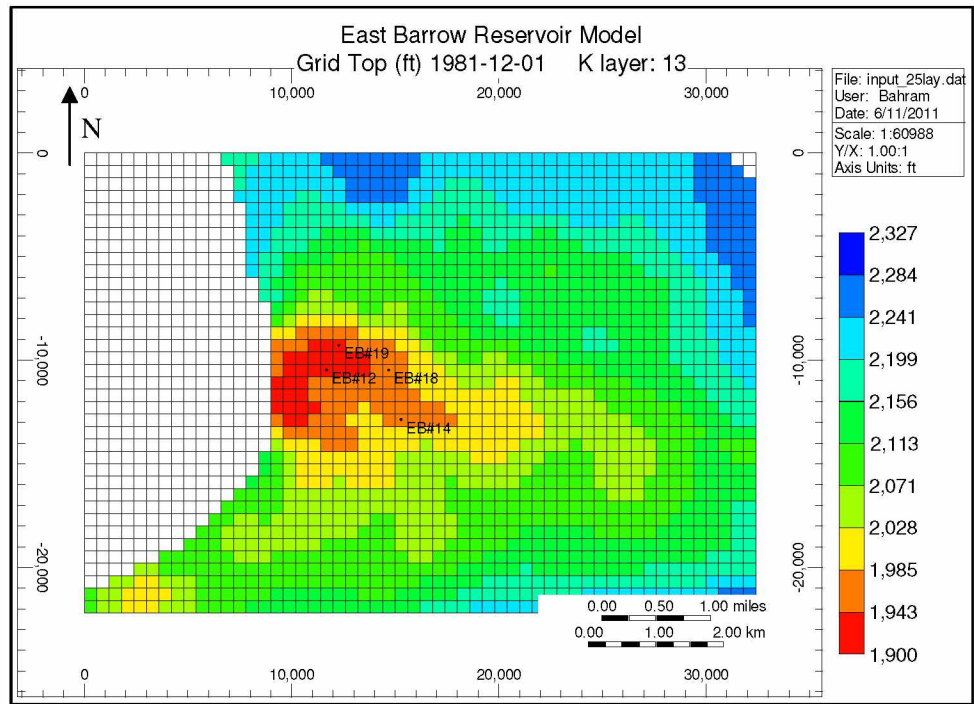


Figure 3.4: Reservoir Grid (K Layer 13) – IJ Plane View

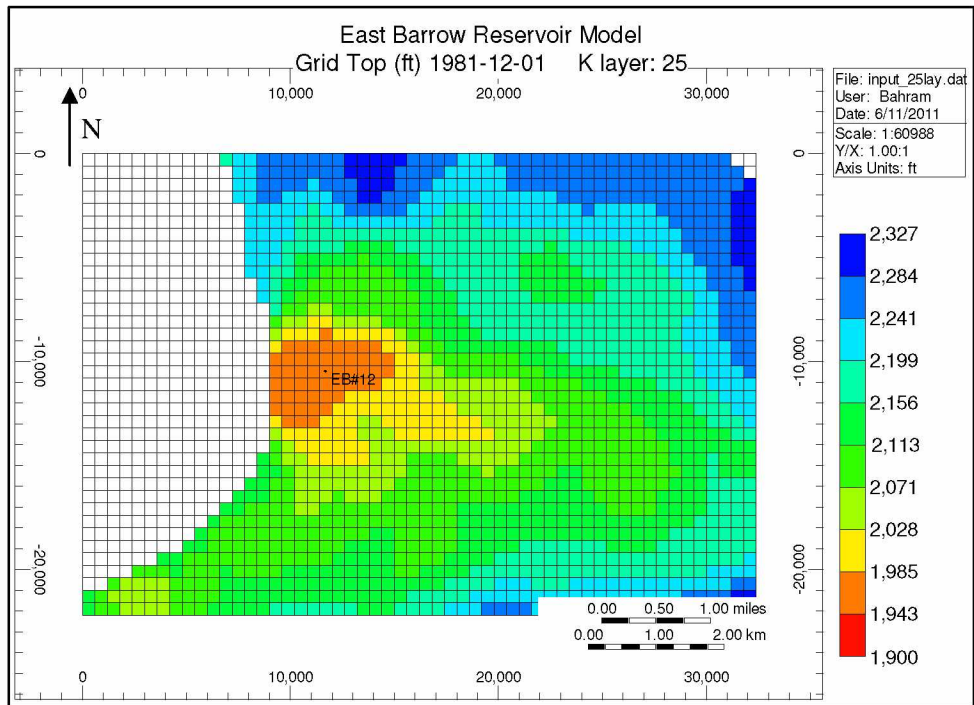


Figure 3.5: Reservoir Grid (K Layer 25) – IJ Plane View

## b. Reservoir Properties

### 1. Porosity

The geological model was populated with porosity values (Panda and Morahan, 2008), and then imported into CMG (Singh, 2008). Reservoir porosity ranged from 5% to 24%. A 3D view of porosity distribution is shown in Figure 3.6.

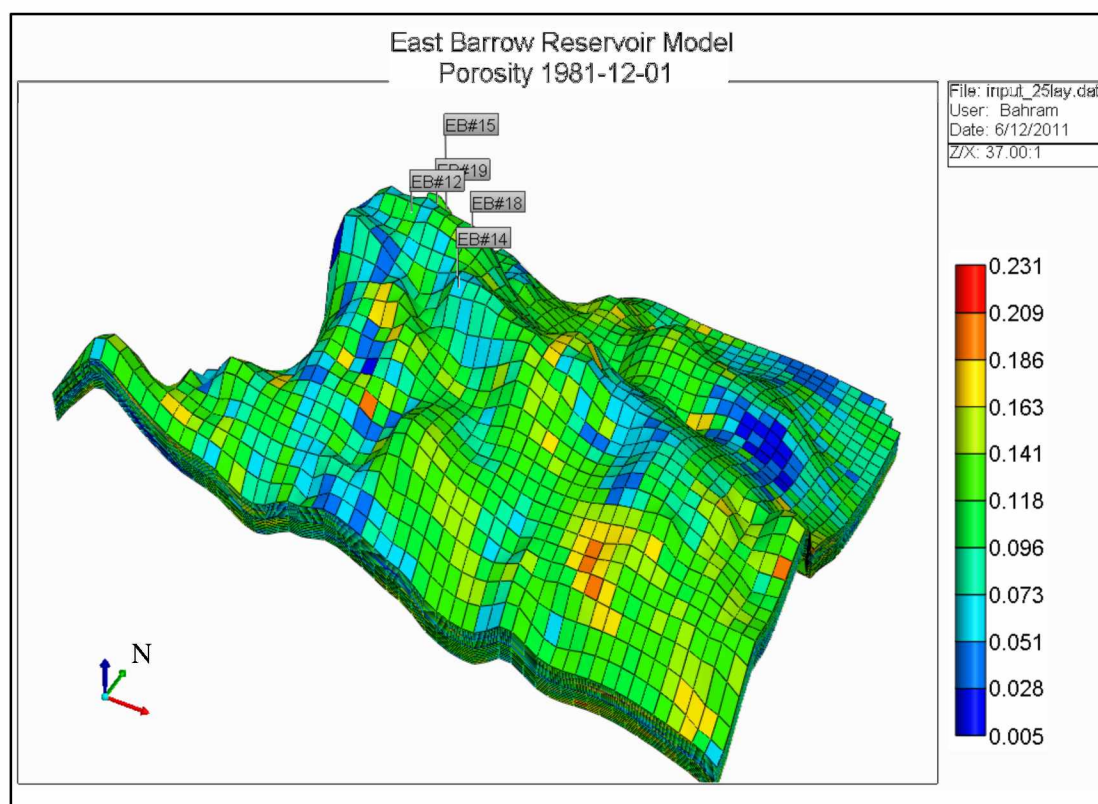


Figure 3.6: Porosity Distribution – 3D View

The productive formation is subdivided into the Upper and Lower Barrow sand (Panda and Morahan, 2008) which are separated by a semi-permeable shaly sand layer. That layer is represented by Layer 16 (K=16) of 5% porosity. The layer is permeable enough to maintain fluid flow. A 2D view of that layer in the IJ plane is presented in Figure 3.7. In all other layers porosity is varying similar to what is shown on 3D image, Figure 3.6.

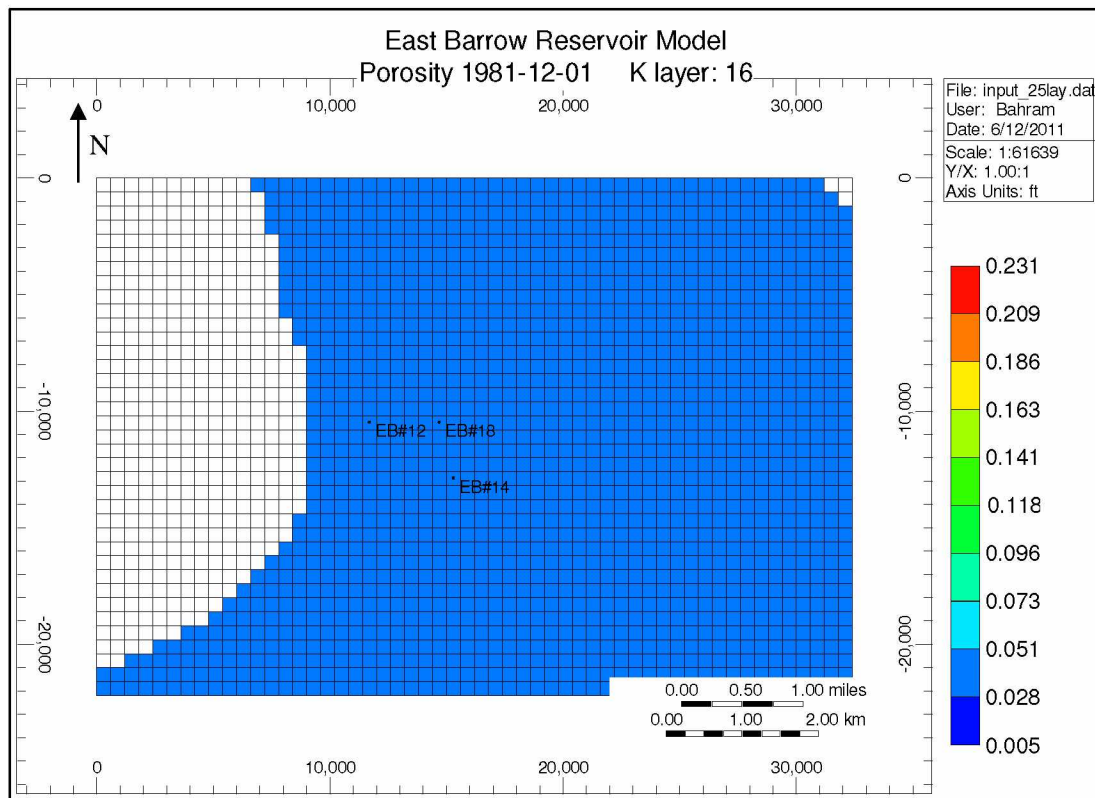


Figure 3.7: Porosity – 5% (K Layer 16) – IJ Plane View

## 2. Permeability

The reservoir was populated with permeability obtained from well logs (Panda and Morahan, 2008). Within the reservoir section of the formation, permeability varies between 1 and 50 md. The reservoir has a lower permeability layer represented by shaly stratum, assigned as Layer 16 (K=16). Permeability value assigned for the entire layer is 5md in all directions (I, J, K). 3D views of permeability distribution in I, J, and K directions are displayed in Figures 3.8, 3.9, and 3.10, respectively. Top 2D view of permeability for shaly Layer 16 is shown in Figure 3.11.

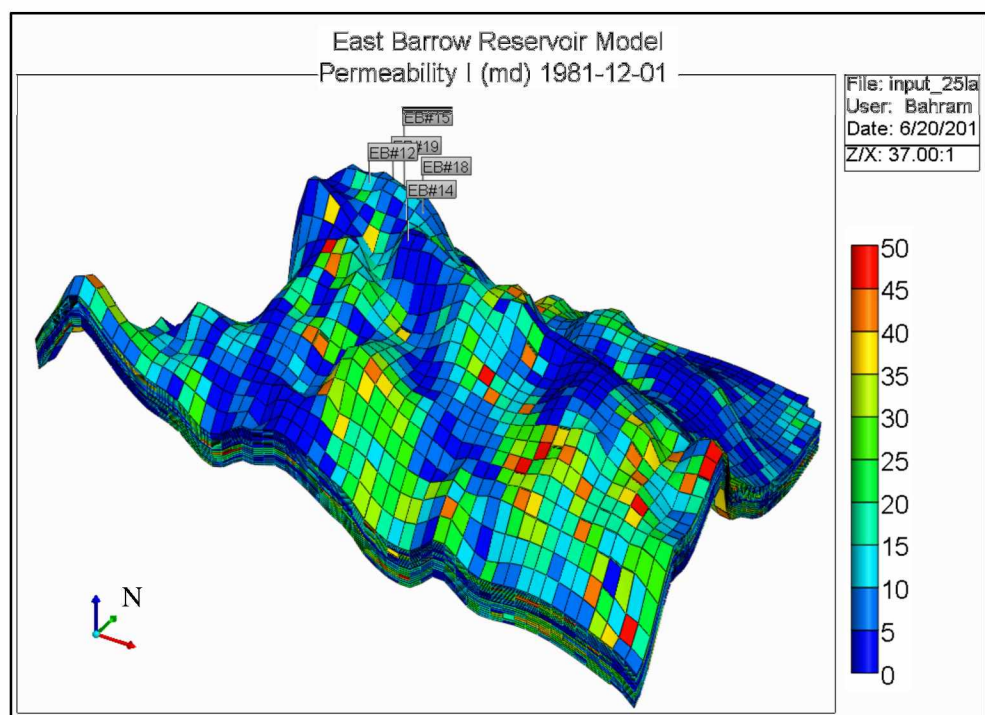


Figure 3.8: Permeability Distribution in I (North–South) Direction, md – 3D View

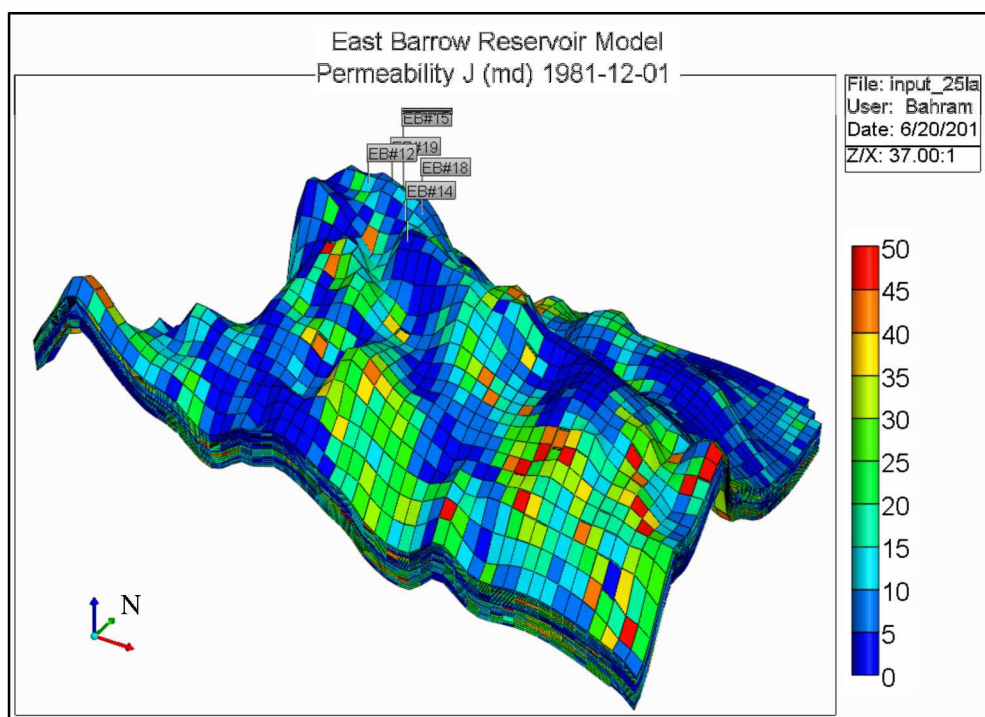


Figure 3.9: Permeability Distribution in J (East–West) Direction, md – 3D View

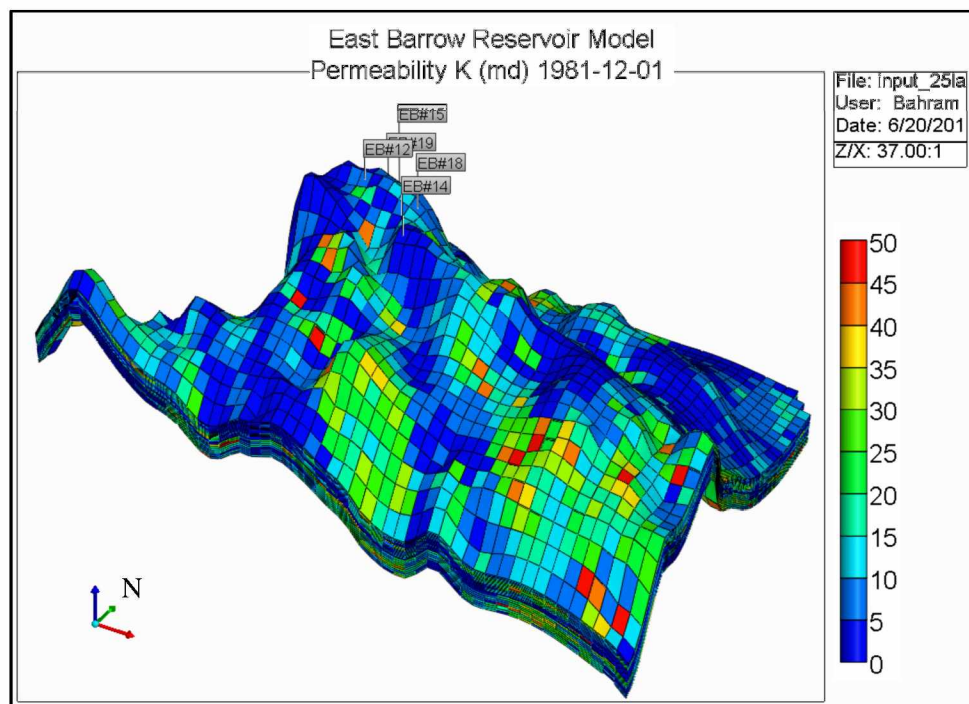


Figure 3.10: Permeability Distribution in K (Vertical) Direction, md – 3D View

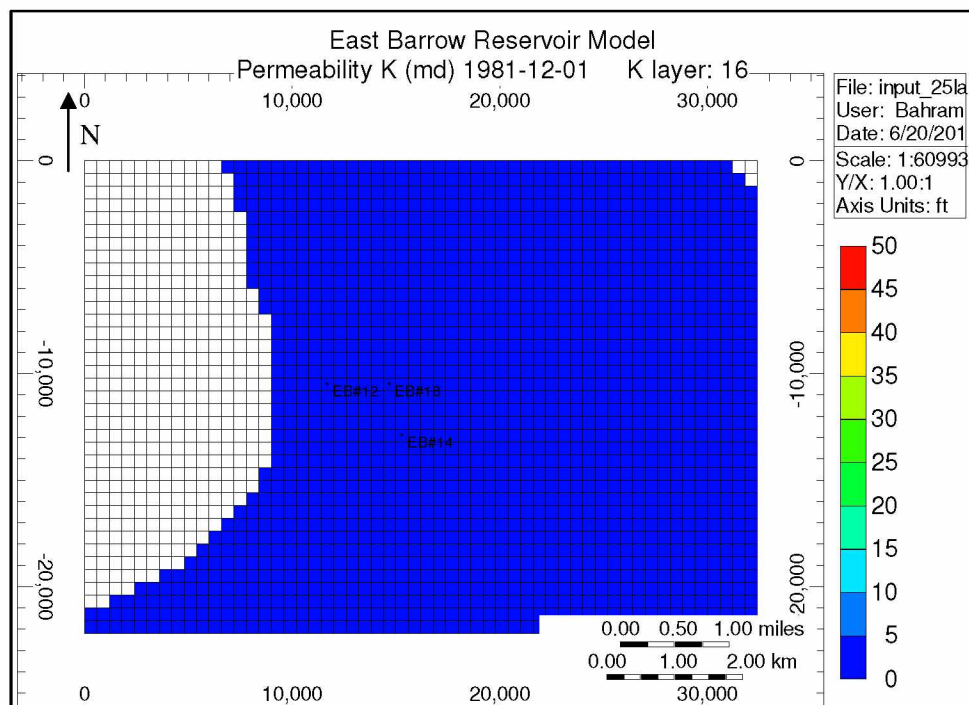


Figure 3.11: Permeability of K Layer 16, md – IJ Plane View

### 3. Temperature

Initial formation temperature at the top of the reservoir was equal to 41°F. The geothermal gradient was estimated at 1.6°F/100 ft (Panda and Morahan, 2008). Initially, a formula editor was used to write a formula for temperature distribution with respect to depth (Singh, 2008). According to formula specification rules in latest versions of CMG, the temperature distribution formula was rewritten (Figure 3.12). Afterwards, initial reservoir temperature was specified as formula dependent. The temperature distribution in the entire reservoir is illustrated in Figure 3.13.

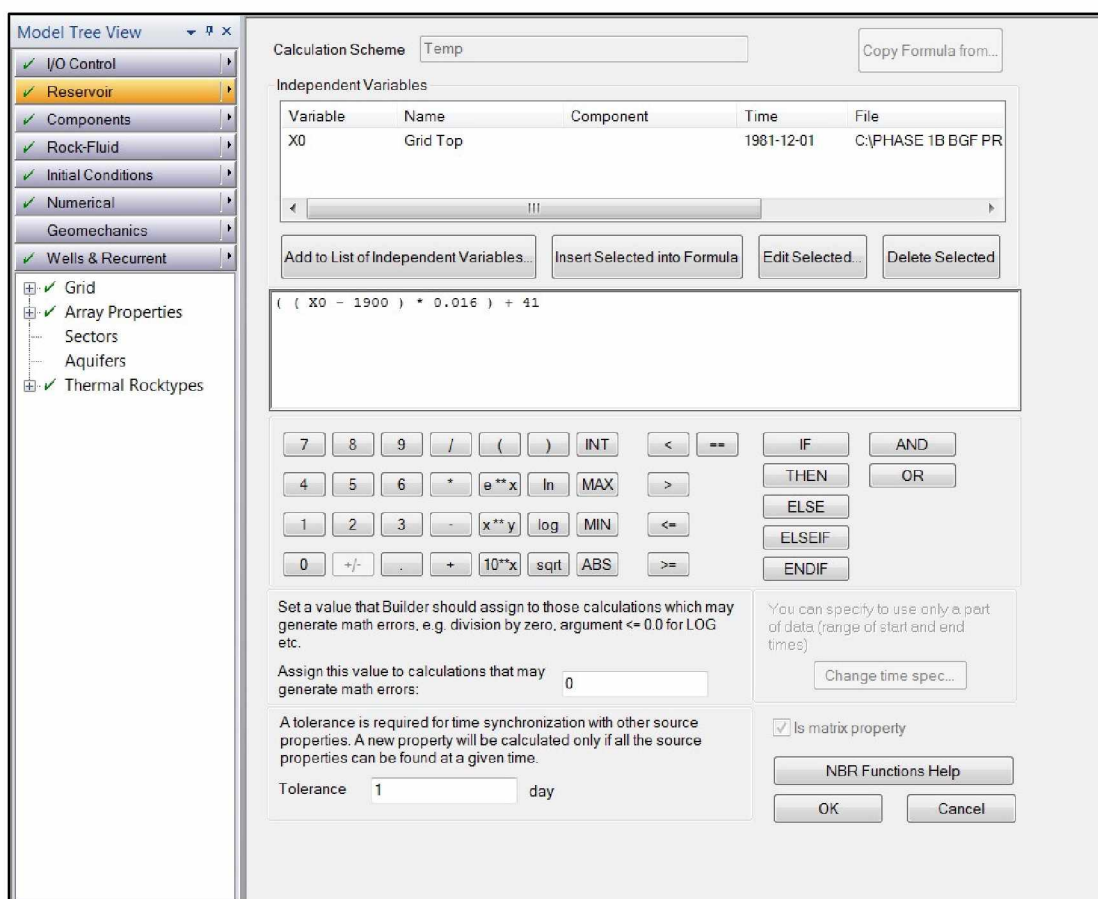


Figure 3.12: Formula Editor – Temperature Distribution Initialization

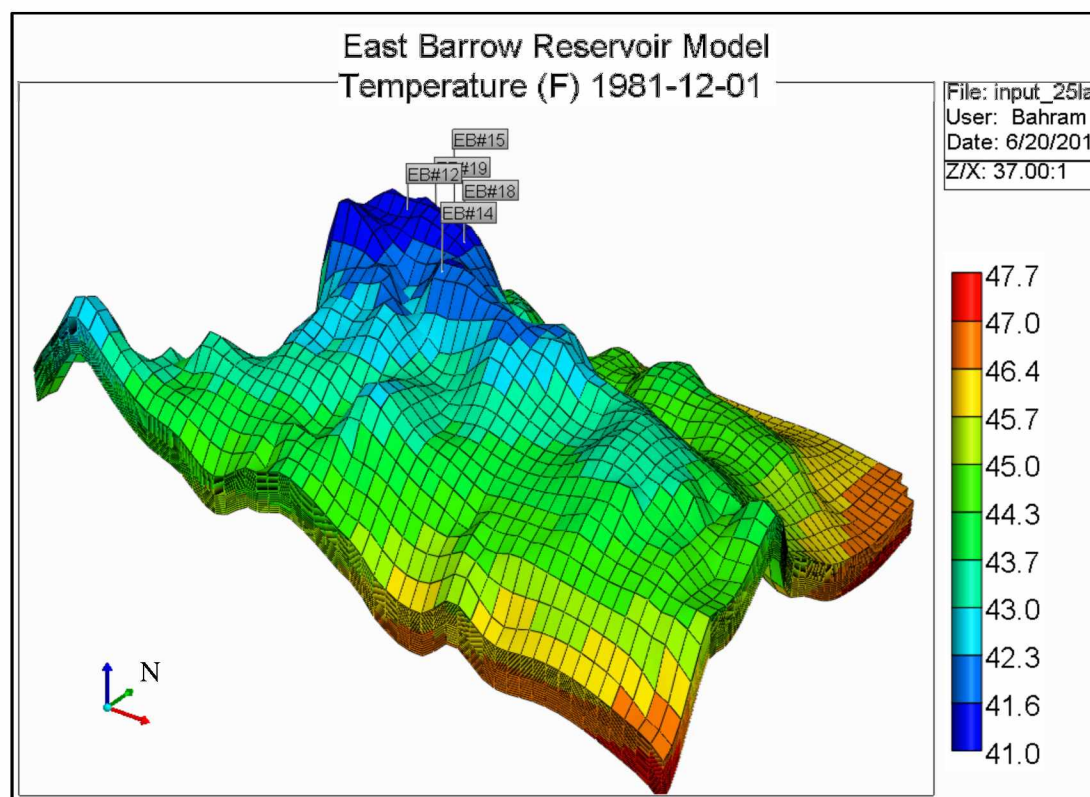


Figure 3.13: Initial Temperature Distribution, °F – 3D View

#### 4. Reservoir Pressure

Initial reservoir pressure was equal to 975 psi (Panda and Morahan, 2008; Singh, 2008). Pressure dependence on gravity was neglected due to hydrate zone underlain with free gas and weak aquifer (Singh, 2008). The entire model was assumed to be at initial pressure of 975 psi.

#### 5. Initial Hydrate Saturation

Since initial conditions in the hydrate layer of East Barrow gas field matched the three-phase pressure-temperature stability curve, all three phases were assumed to be present in the hydrate layer (Singh, 2008). Field zones shallower than 2050 ft were marked as hydrate-bearing (Panda and Morahan, 2008). Hence, 2050 ft was the initial HGC. The previous phase of research included a sensitivity study of reservoir to drive mechanisms

confirming 31% gas hydrate saturation in the hydrate layer (Singh, 2008). In that model, gas hydrates were specified as oil with high viscosity.

In the latest versions of CMG STARS, gas hydrates are specified as an Initial Solid Concentration reservoir property (SOLCONC keyword). Upon completion of the sensitivity study (discussed in a later section), it was concluded that a solid concentration of 0.1586 lbmole/ft<sup>3</sup> matches reservoir performance and represents 31% of hydrate saturation. A formula representing hydrate distribution was created in the CMG formula editor and was directly specified as a solid concentration property. Hydrate saturation was assigned for each grid block located deeper than 1900 ft but shallower than 2050 ft. The remaining grid blocks of the reservoir were assigned with hydrate saturation of 0%. The formula is given as

```
IF ((X0 > 1900) AND (X0 <= 2050)) THEN ((0.158591)) ELSE ((0))
```

where X0 is grid bottom depth, ft (Figure 3.14).

The 3D view of hydrate distribution within the reservoir is shown in Figure 3.15. Top (K=1) and bottom (K=25) layers' 2D hydrate distribution is presented in Figures 3.16 and 3.17, respectively. Figure 3.18 displays a magnified 2D view of HGC.



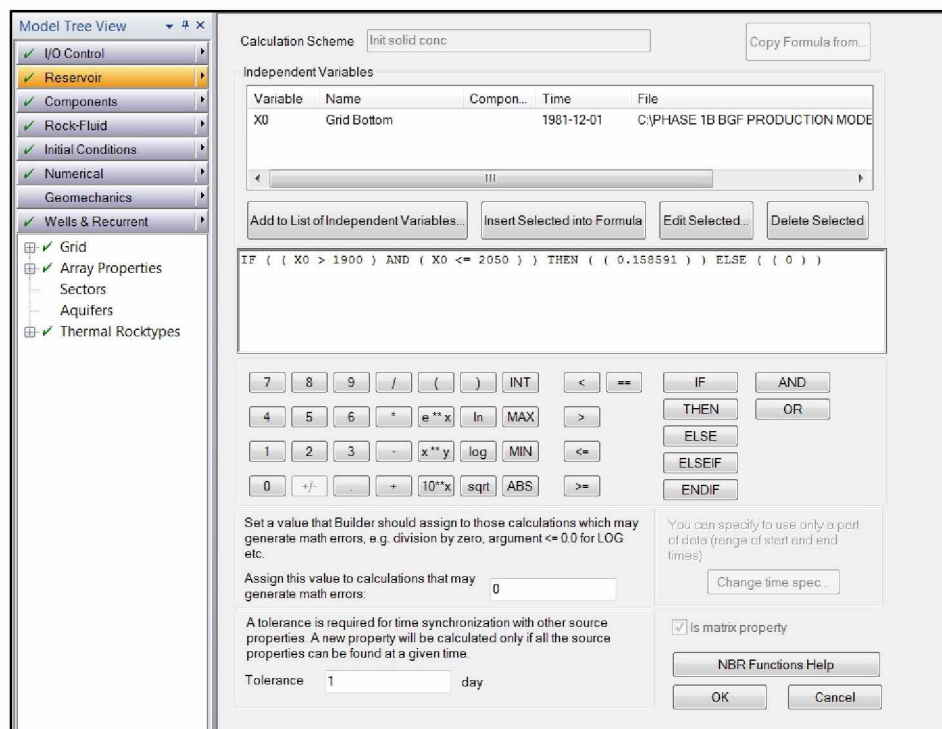


Figure 3.14: Formula Editor – Gas Hydrate Distribution Initialization

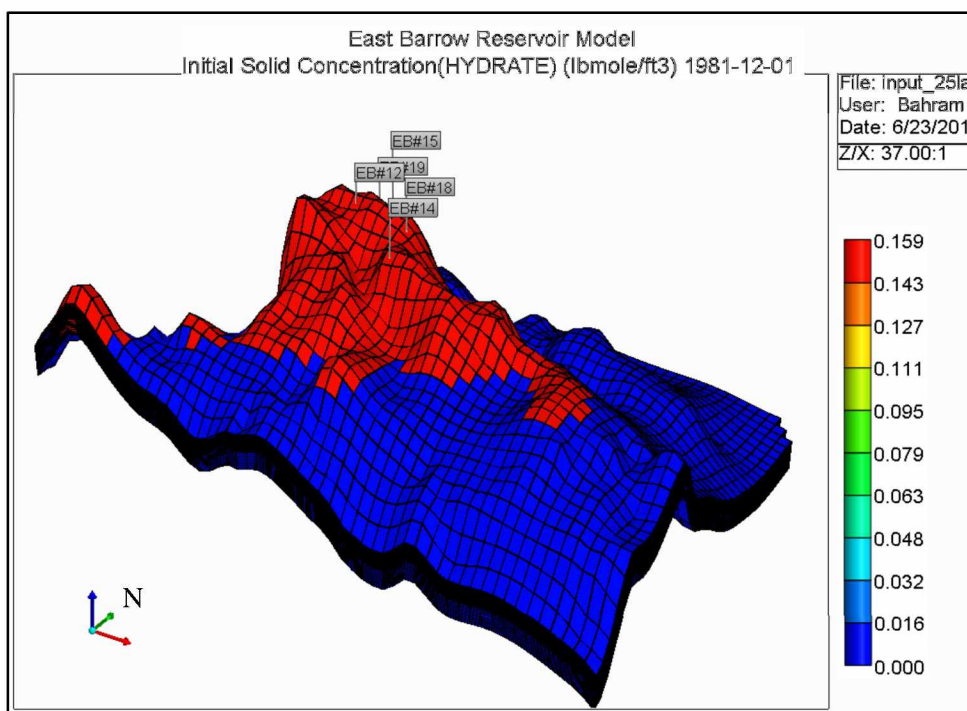


Figure 3.15: Initial Gas Hydrate Saturation, lbmole/ft3 – 3D View

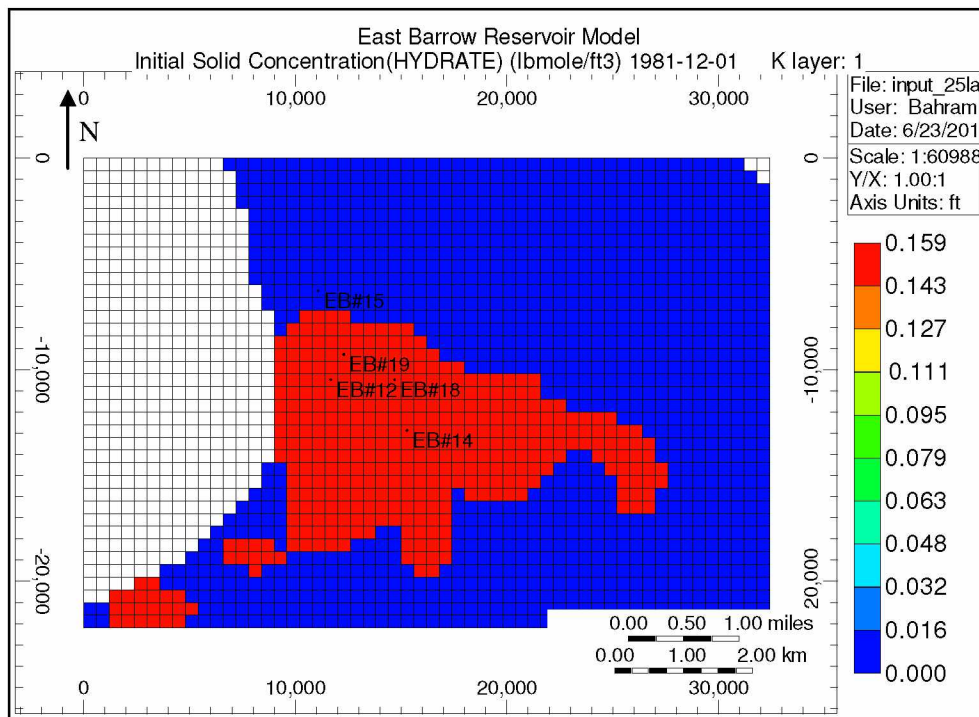


Figure 3.16: Initial Gas Hydrate Saturation (K Layer 1), lbmole/ft3 – IJ Plane View

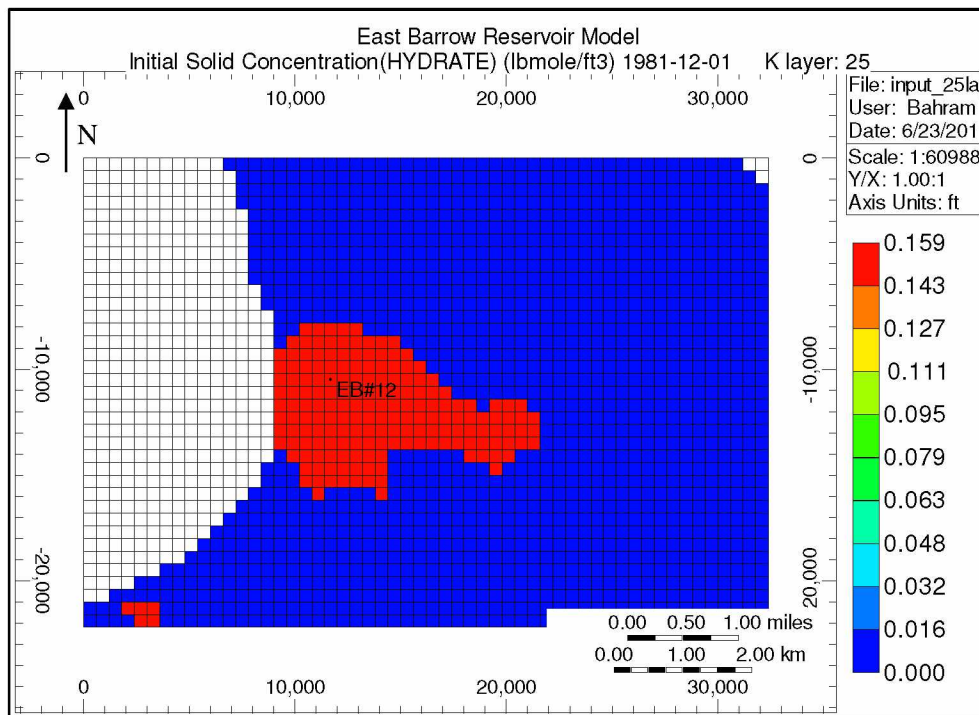


Figure 3.17: Initial Gas Hydrate Saturation (K Layer 25), lbmole/ft3 – IJ Plane View

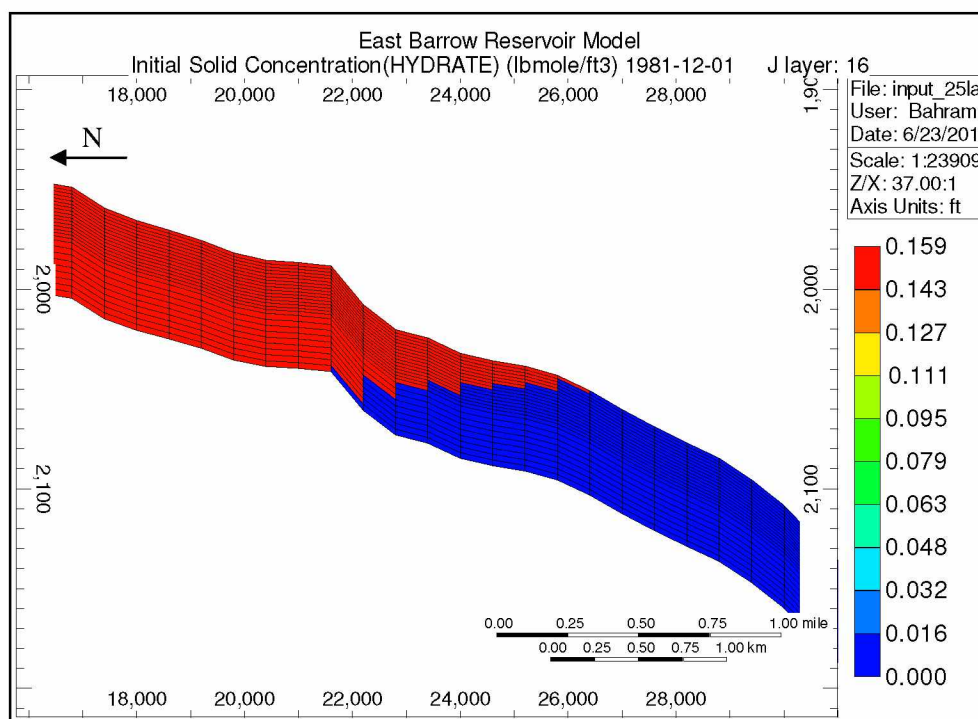


Figure 3.18: Initial Hydrate–Gas Contact– IK Plane View

## 6. Initial Gas Saturation

A gas phase is present in both free gas zone and hydrate zone (Stokes and Walsh, 2007). Initial water saturation in both zones was estimated as 55% from the well logs (Panda and Morahan, 2008). Hence gas saturation in the free gas zone equals 45%. However, in the gas hydrate zone where all three phases are present, free gas saturation is only 14% (Stokes and Walsh, 2007). The free gas zone is located below the gas hydrate zone and above the water leg. Gas–Water Contact (GWC) was estimated to be at 2080 ft.

In order to specify gas saturation in the model, a formula was written in the CMG formula editor (Singh, 2008). As part of this study, the formula was updated according to the newer version of software. In the formula, gas saturation between 1900 ft and 2050 ft (the hydrate zone) is specified as 14%; between 2050 ft and 2080 ft (free gas zone) it is 45%; and in the water leg, below 2080 ft, gas saturation is 0%.

The formula is given as:

$$\text{IF } ((X0 > 1900) \text{ AND } (X0 \leq 2050)) \text{ THEN } ((0.14)) \text{ ELSEIF } ((X0 > 2050) \text{ AND } (X0 \leq 2080)) \text{ THEN } ((0.45)) \text{ ELSE } ((0))$$

where X0 is grid bottom depth, ft (Figure 3.19).

The 3D view of gas saturation of the reservoir is shown in Figure 3.20. Saturation of topmost (K=1) and bottommost (K=25) layers is shown in Figures 3.21 and 3.22, respectively. Figure 3.23 is a magnified 2D view of HGC and GWC.

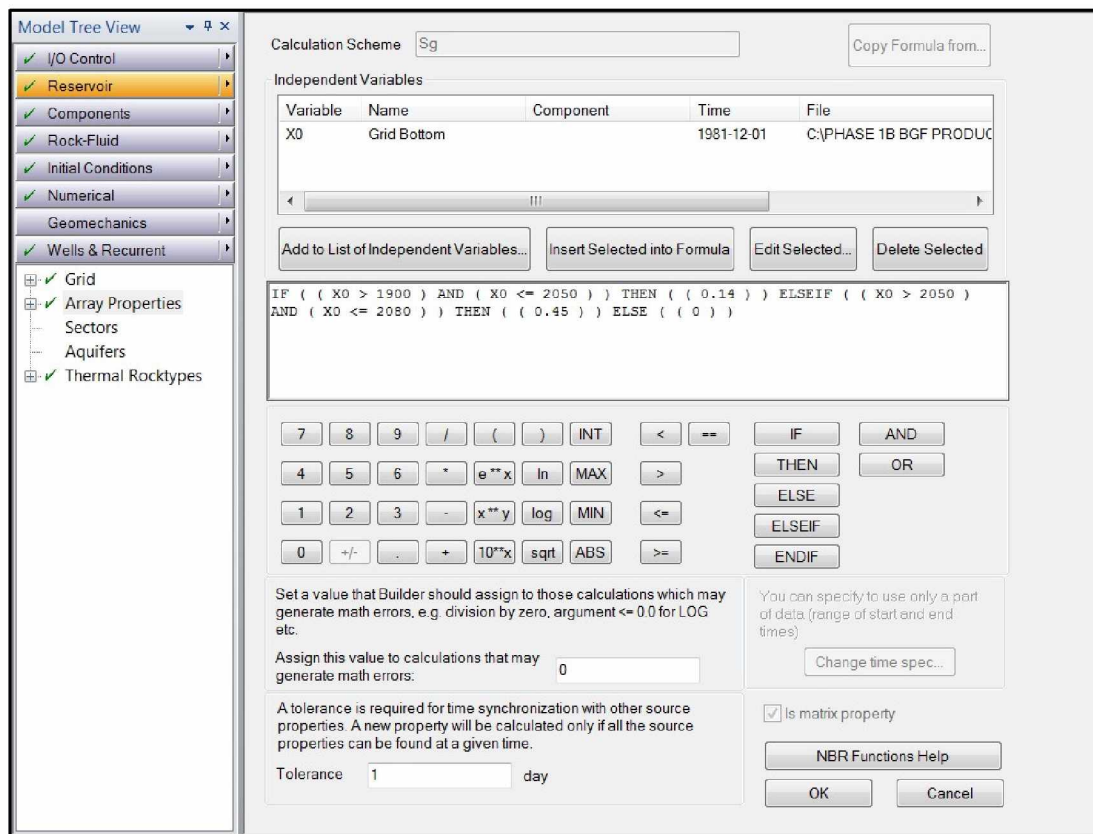


Figure 3.19: Formula Editor – Gas Saturation Initialization

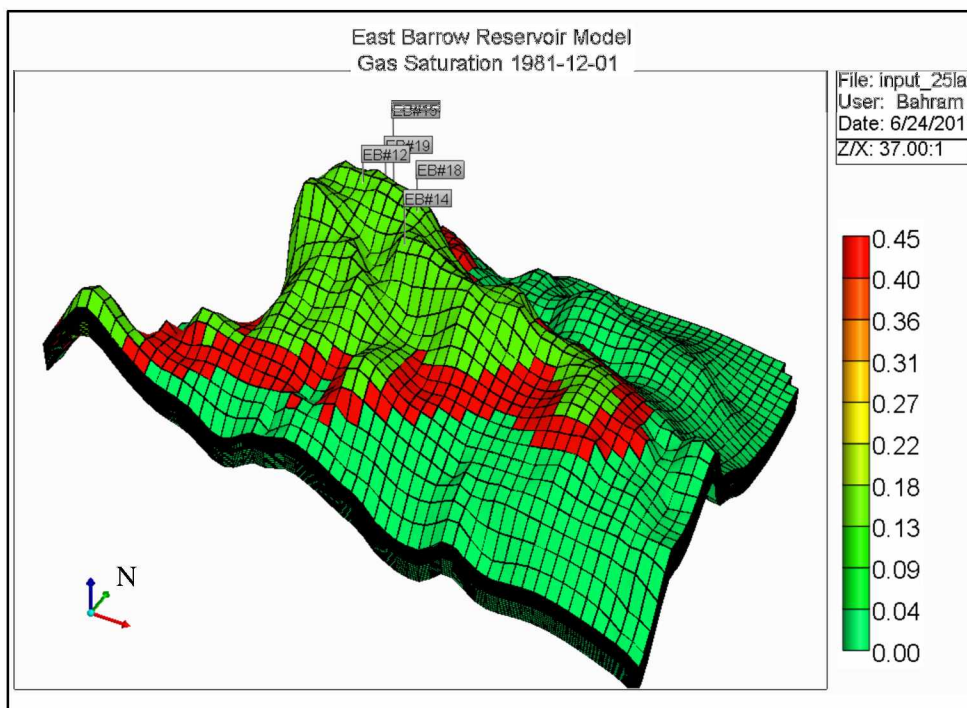


Figure 3.20: Initial Gas Saturation – 3D View

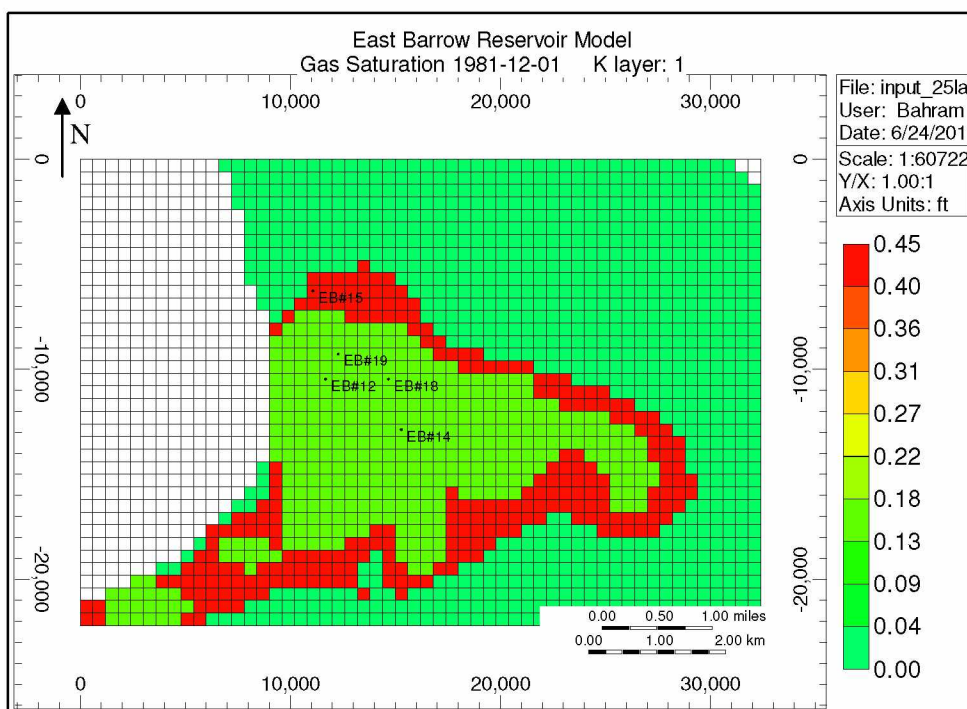


Figure 3.21: Initial Gas Saturation (K Layer 1) – IJ Plane View

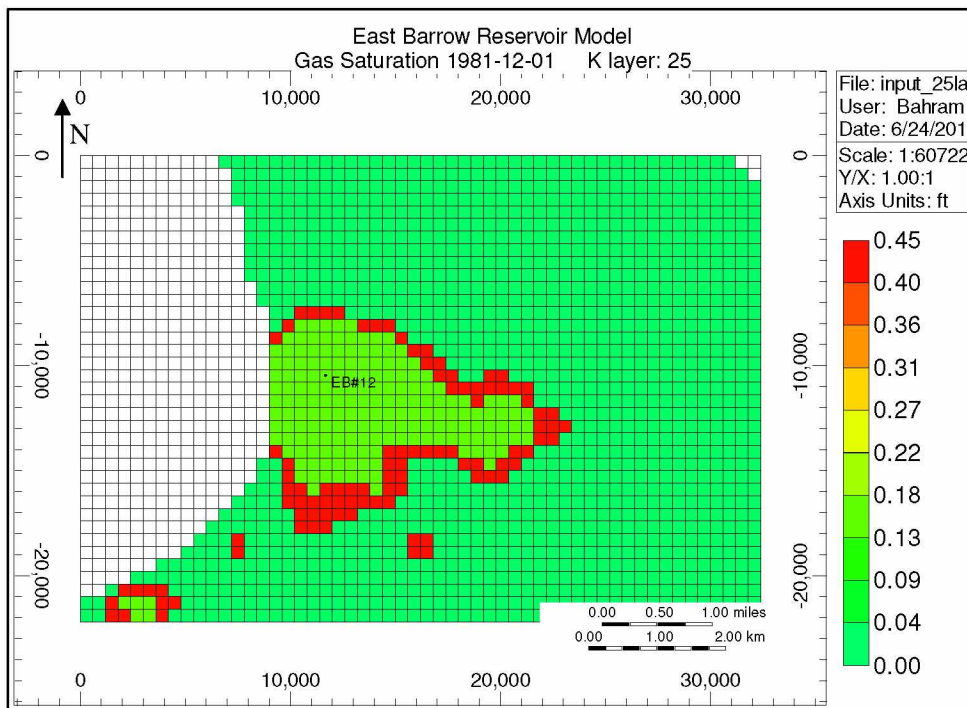


Figure 3.22: Initial Gas Saturation (K Layer 25) – IJ Plane View

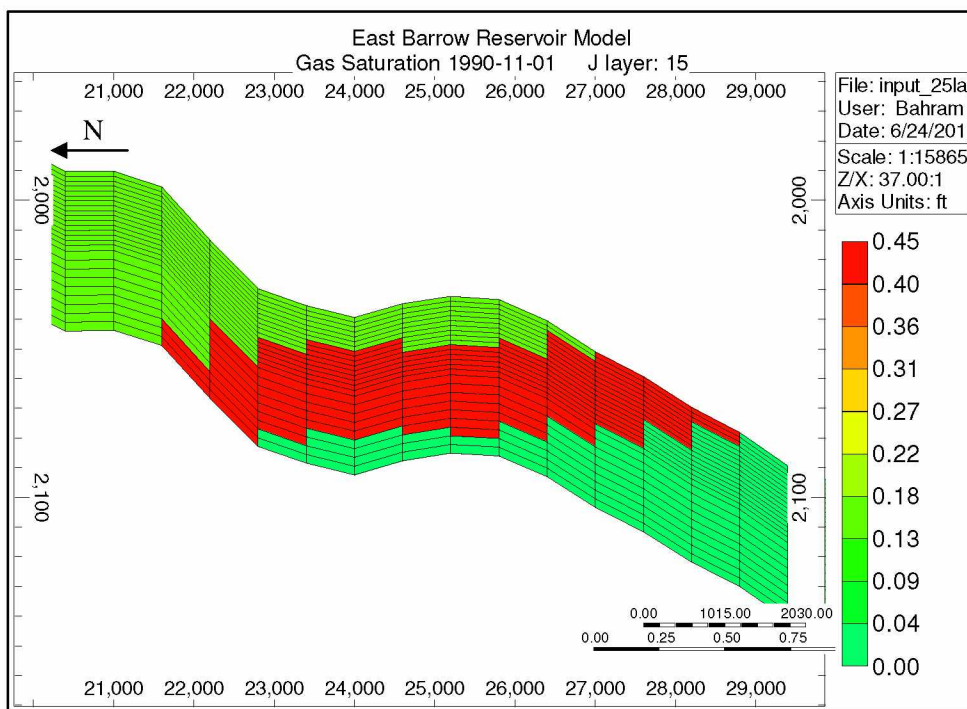


Figure 3.23: Initial HGC and GWC – IK Plane View

## 7. Initial Water Saturation

Previously, water saturation in the EB field model was specified as 55% in gas hydrate and free gas zones, and 100% in the water leg (Singh, 2008). Current CMG STARS hydrate specification procedure requires a gas hydrate saturation value to be added to water saturation, as gas hydrates are initialized as a solid fraction within the water phase.

Hence, as part of the model update, water saturation was altered. A new formula was written using the formula editor and it was initialized as a water saturation property of the field. As a result, according to the formula, water saturation in the hydrate zone was increased to 86% (31% hydrate saturation); in the free gas zone it was kept at 55%; and in the water leg it was at 100%. The three zones were divided by fluid contacts: HGC at 2050 ft and GWC at 2080 ft. The formula is given as

```
IF ((X0 > 2050) AND (X0 <= 2080)) THEN ((0.55)) ELSEIF ((X0 > 1900) AND (X0 <= 2050)) THEN ((0.86)) ELSE ((1))
```

where X0 is grid bottom depth, ft (Figure 3.24).

Figure 3.25 shows a 3D view of water saturation in the reservoir. Figures 3.26 and 3.27 represent the topmost (K=1) and bottommost (K=25) layer water saturation, respectively. A vertical section with magnified fluid contacts is displayed in Figure 3.28.

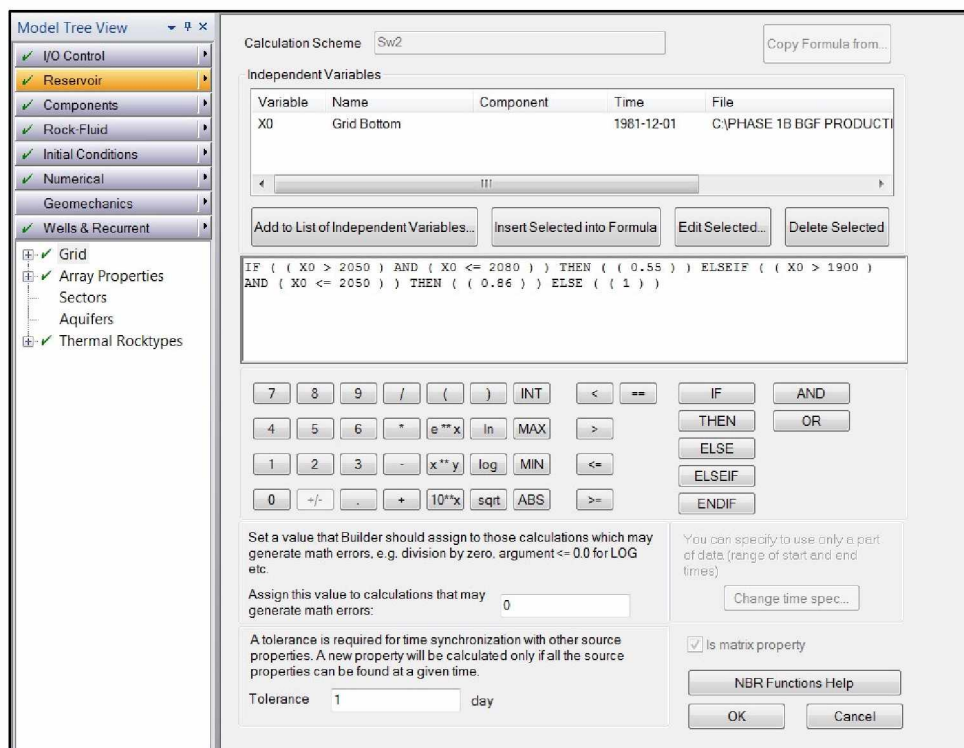


Figure 3.24: Formula Editor – Water Saturation Initialization

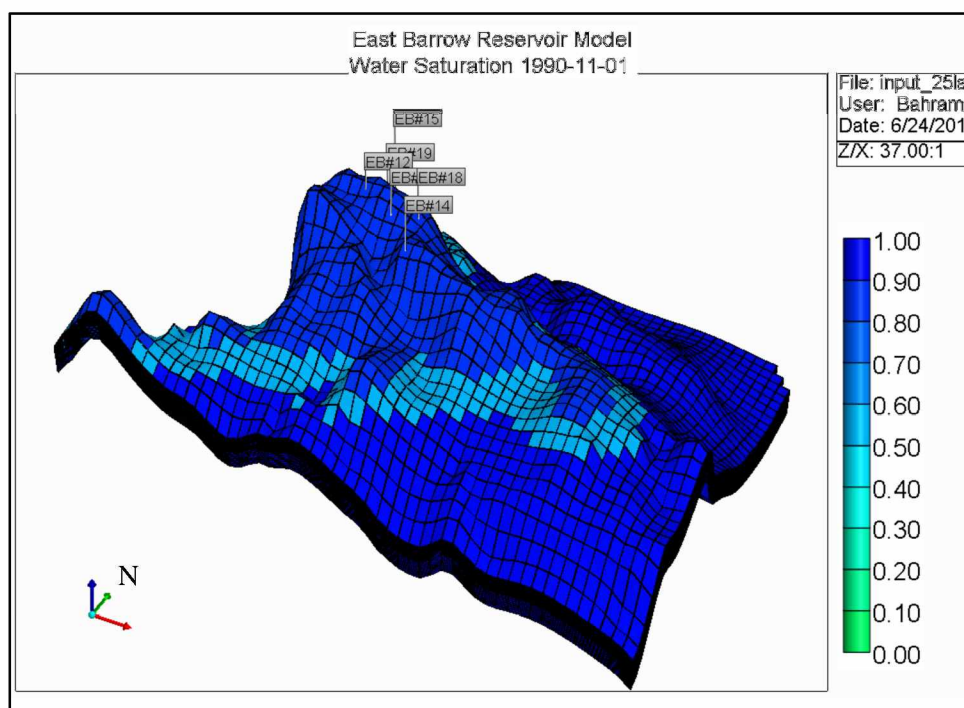


Figure 3.25: Initial Water Saturation – 3D View



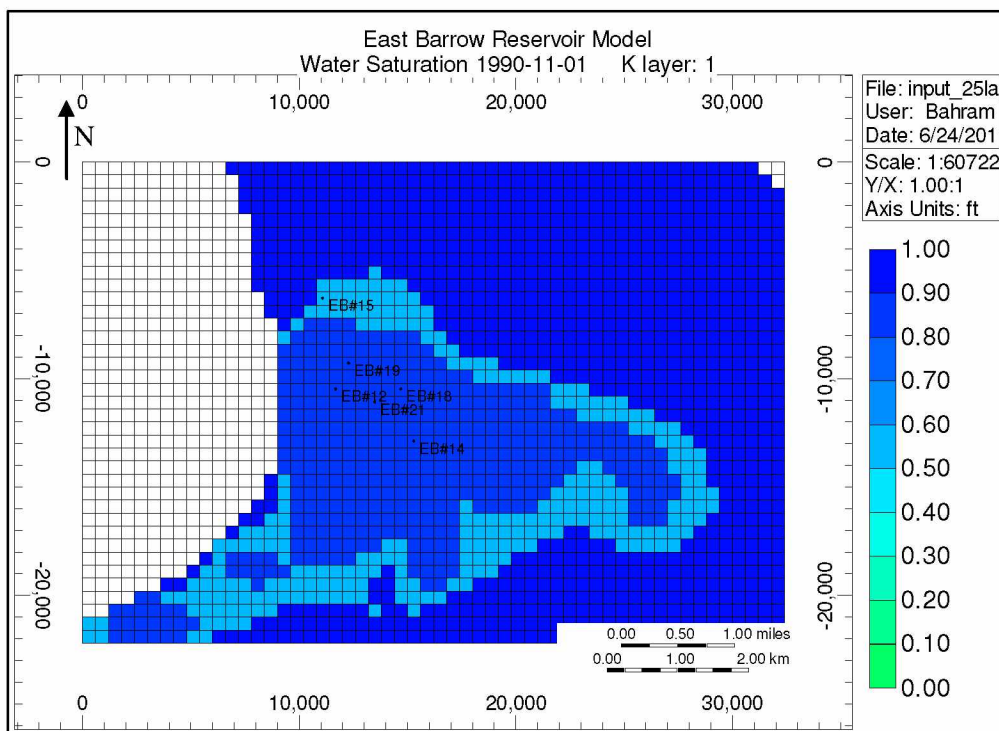


Figure 3.26: Initial Water Saturation (K Layer 1) – IJ Plane View

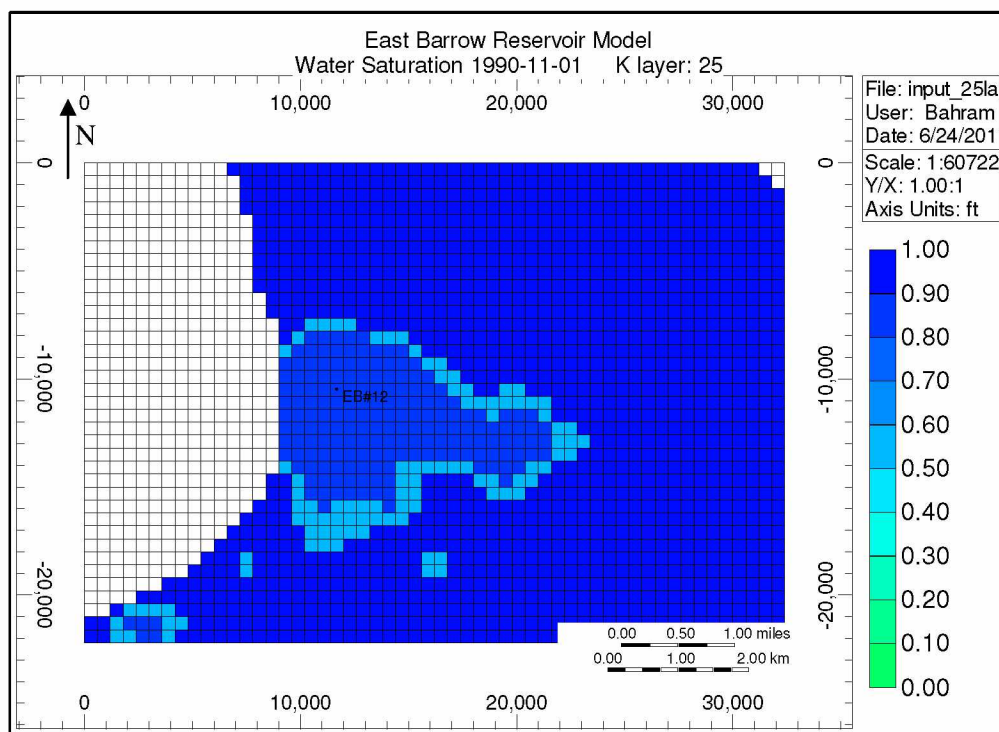


Figure 3.27: Initial Water Saturation (K Layer 25) – IJ Plane View

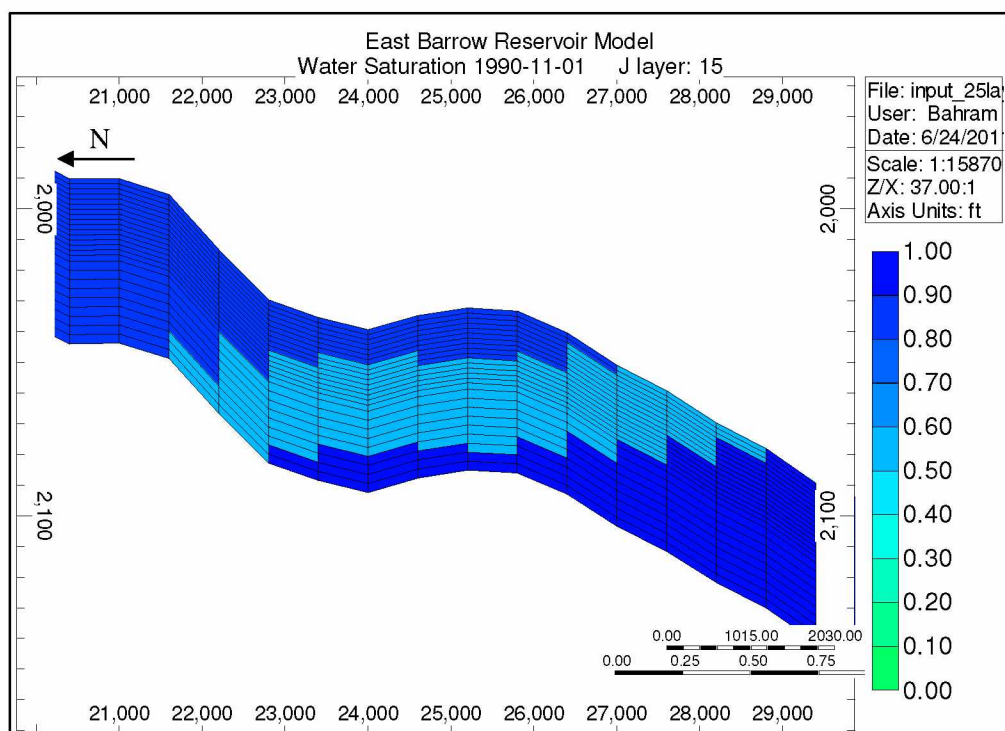


Figure 3.28: Initial HGC and GWC – IK Plane View

#### c. Fluid Component Properties

Gas hydrates were initialized as a solid immobile phase. Two chemical reactions were specified to simulate hydrate dissociation and reformation phenomena. Component properties and reaction details are summarized in Appendix A.

#### d. Well Rates

The EB gas reservoir has 6 producer wells: EB #12, #14, #15, #18, #19, and #21. Wellbore diagrams are displayed in Appendix B. The wells were specified in the model and production rates were imported directly (Singh, 2008). For the purpose of model update, the latest production data were added. Currently, only EB #14 is in production (Walsh, personal communication). Since only a few dates needed to be added, flow rates were specified manually using the ALTER keyword. The ALTER keyword allows change in the primary constraint of the well at a certain selected point of time to match the actual production history.

### 3.1.3.2 Walakpa Gas Field

Like the EB model, the WAL geological model was built in ROXAR RMS (Panda and Morahan, 2008) and then imported into CMG STARS (Singh, 2008). Due to similarity in the model initialization process, the WAL model is discussed briefly.

#### a. Reservoir Grid

The reservoir grid consists of 63,000 grid blocks (Figure 3.29). It has 100 grid blocks in I direction, 63 in J direction, and 10 layers in K direction. Lateral dimensions of a single grid block are 500 ft by 500 ft (IJ Plane). Vertical thickness of the grid block (K direction) varies between 1.6 ft and 4.5 ft. Reservoir depth range is 1879 ft at the top and 3109 ft at the aquifer.

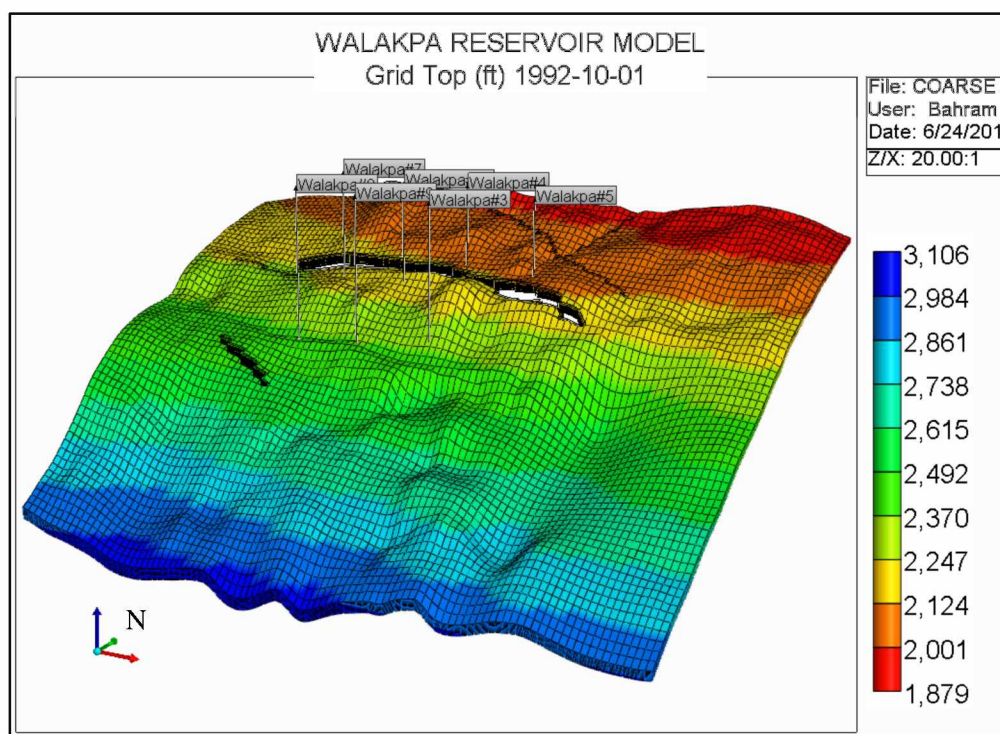


Figure 3.29: Walakpa Reservoir Grid – 3D View

## b. Reservoir Properties

### 1. Porosity

The geological model was populated with porosity data obtained from logs by Panda and Morahan (2008) before being imported to CMG (Singh, 2008). Reservoir porosity ranges between 8.5% and 24.7% (Figure 3.30).

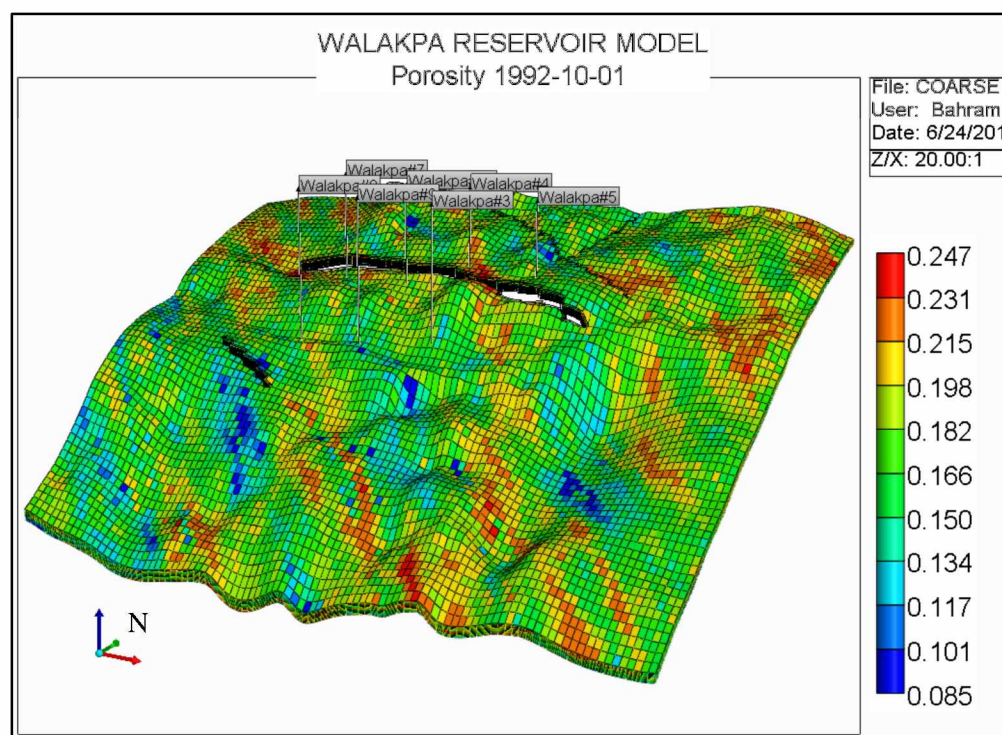


Figure 3.30: Porosity Distribution – 3D View

## 2. Permeability

Similarly to porosity, reservoir permeability was specified in the geological model. It was initially obtained from well logs (Panda and Morahan, 2008). Permeability in each grid block is similar in all three directions (I, J, and K). It varies between 0.1 md and 250 md throughout the field (Figure 3.31).

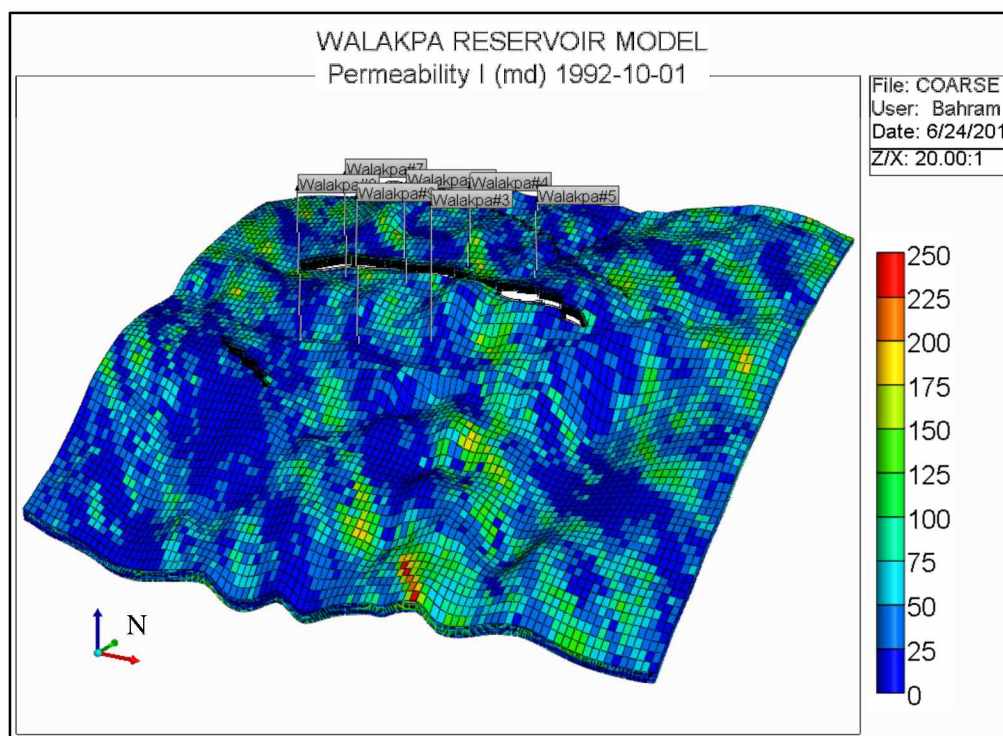


Figure 3.31: Permeability Distribution, md – 3D View

### 3. Temperature

Initial WAL temperature was specified according to reservoir geothermal gradient of 1.88 °F/100 ft (Singh, 2008). Hence, at the top of the reservoir the temperature is 49.6°F, and at the bottom it equals 72.4°F (Figure 3.32). The updated formula of initial reservoir temperature written in the CMG formula editor is given as

$$(X0 - 950) * 0.01888 + 32$$

where X0 is grid top depth, ft.

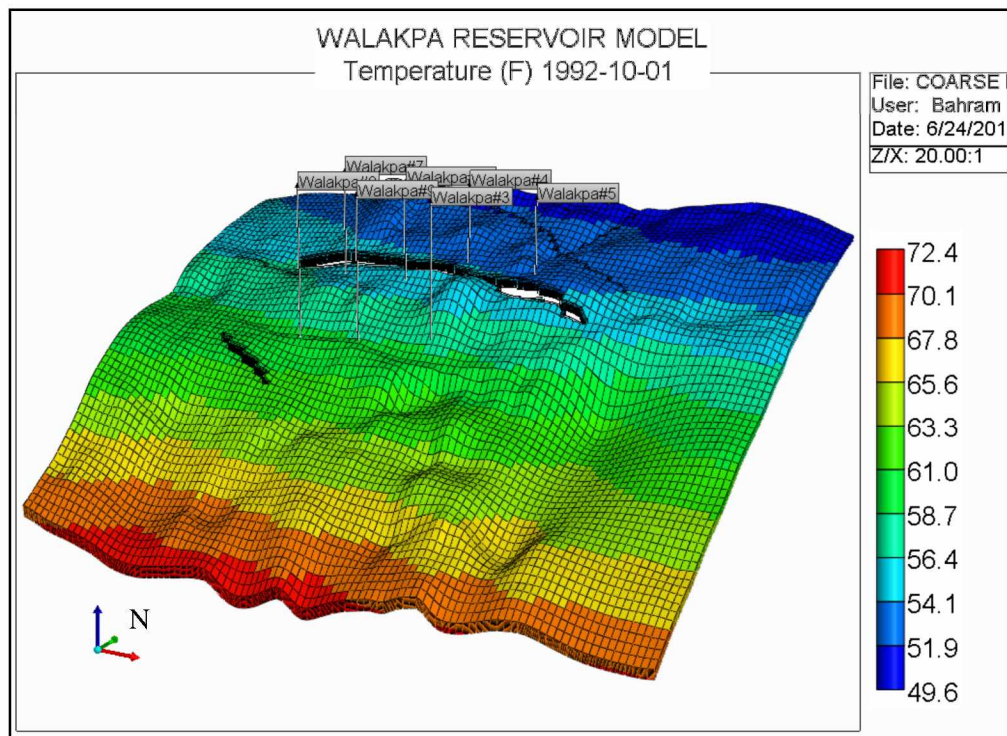


Figure 3.32: Initial Reservoir Temperature Distribution, °F – 3D View

#### 4. Reservoir Pressure

Initial reservoir pressure was 1039 psi (Panda and Morahan, 2008), (Figure 3.33). While specifying the pressure, gas pressure gradient was neglected and water pressure gradient of 0.433 psi/ft was used (Singh, 2008). The formula defining pressure was modified in the formula editor. It is given as

IF ((X0 > 1875) AND (X0 <= 2750)) THEN ((1039)) ELSE ((X0 \* 0.433))

where X0 is grid bottom depth, ft.

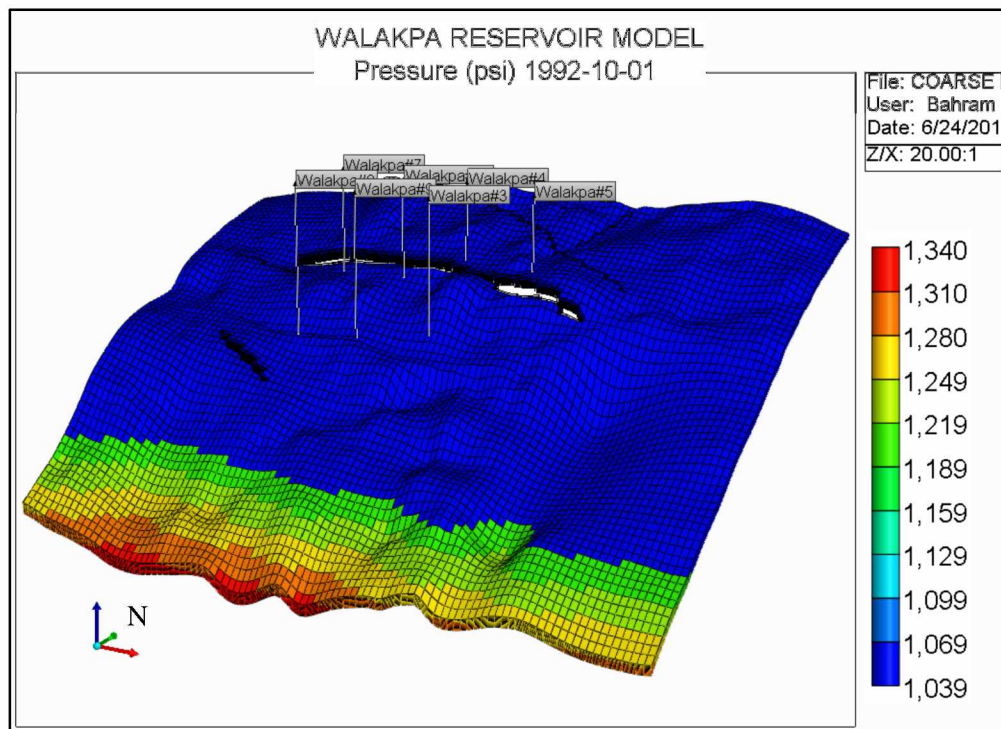


Figure 3.33: Initial Reservoir Pressure, psi – 3D View

## 5. Initial Hydrate Saturation

Like in EB reservoir, all three phases are present in the hydrate zone. Gas hydrate saturation in the hydrate layer was estimated at 30%. HGC depth is 2000 ft (Singh, 2008). For free gas zone and aquifer, gas hydrate saturation was specified as 0%. As explained earlier, solid concentration represents hydrate saturation in the reservoir (SOLCONC keyword). From a sensitivity study (explained later) the concentration was estimated to be equal to  $0.1441 \text{ lbmole/ft}^3$  (Figure 3.34). The formula written in the CMG formula editor in order to specify solid concentration appears as

```
IF (X0 <= 2000) THEN (0.144089) ELSE (0)
```

where X0 is grid bottom depth, ft.

A magnified 2D view of HGC in the JK plane is shown in Figure 3.35.

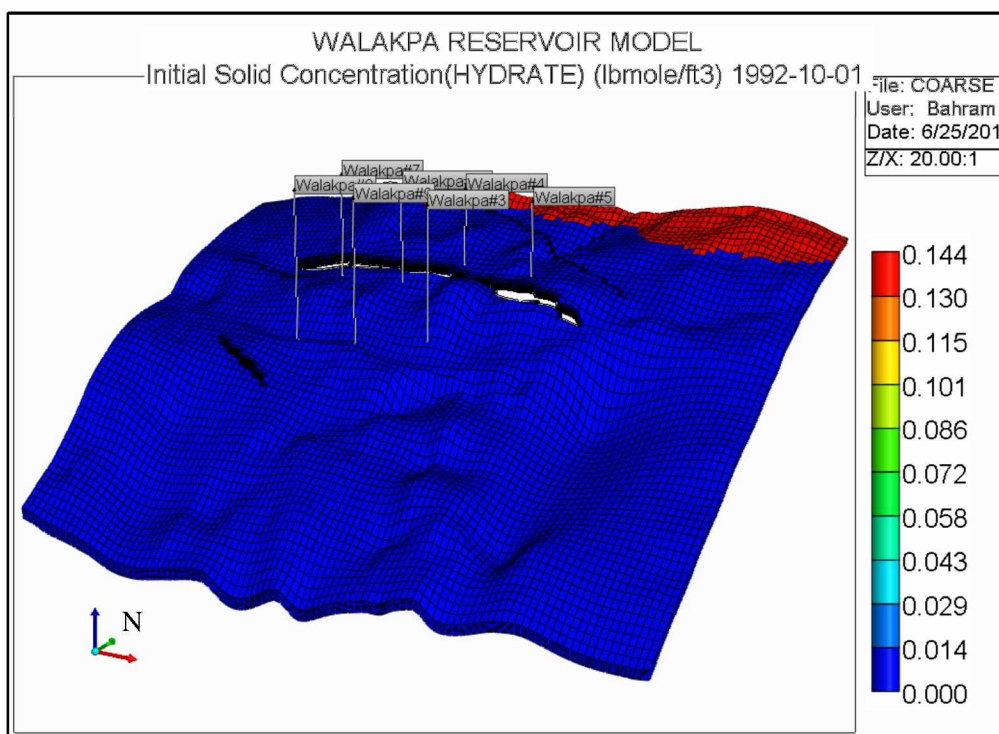


Figure 3.34: Initial Gas Hydrate Saturation,  $\text{lbmole/ft}^3$  – 3D View



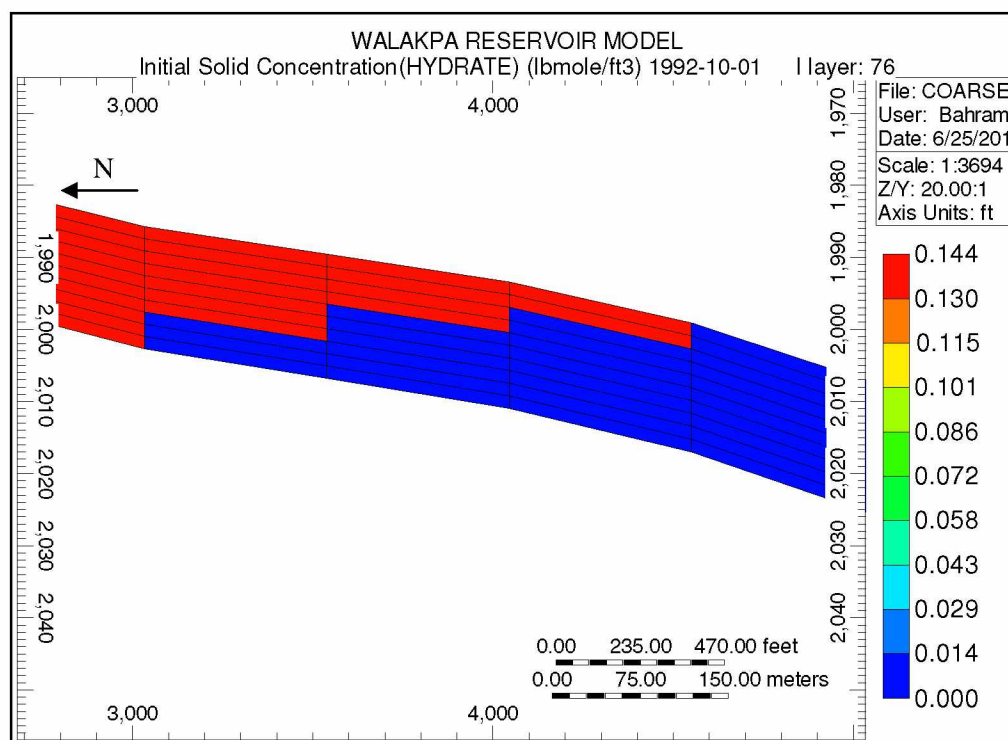


Figure 3.35: Initial HGC – IK Plane View

## 6. Initial Gas Saturation

Gas is present in both the gas hydrate and free gas zones. There is 0% gas saturation in the water leg. Due to 55% connate water saturation, gas saturation in the free gas zone is only 45% (Figure 3.36). In the hydrate layer, gas saturation is equal to 15% (Singh, 2008). A formula was modified using the formula editor to specify hydrate saturation according to HGC at 2000 ft and GWC at 2750 ft. The formula is given as

```
IF ((X0 <= 2000)) THEN (0.15) ELSEIF ((X0 > 2000) AND (X0 <= 2750)) THEN
((0.45)) ELSE ((0))
```

where X0 is grid bottom depth, ft.

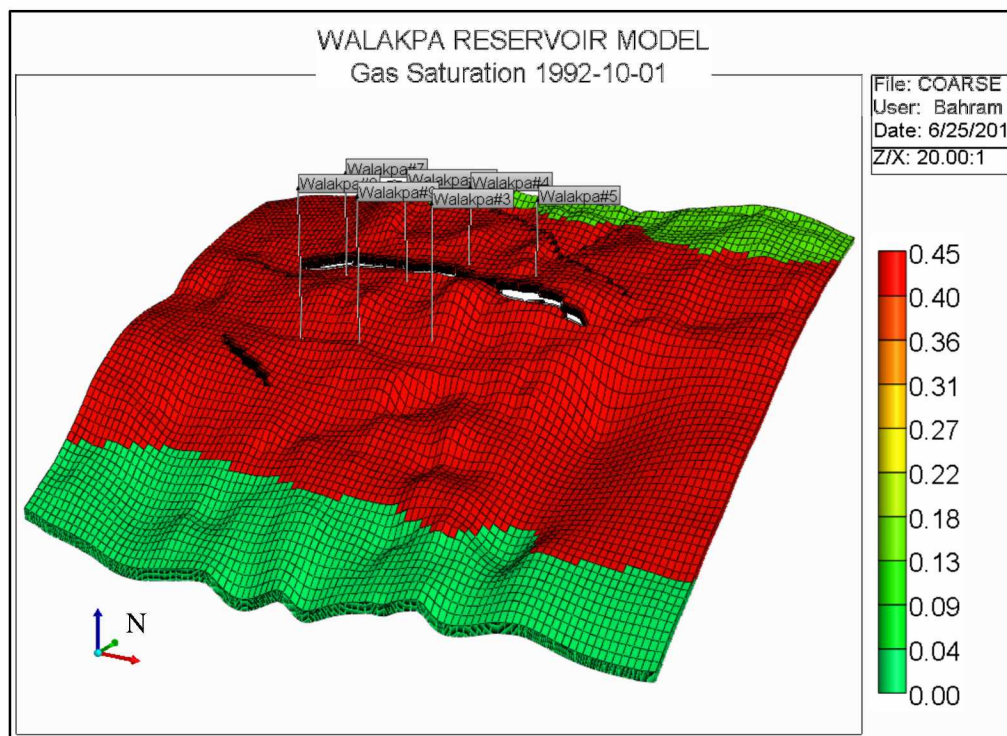


Figure 3.36: Initial Gas Saturation – 3D View

#### 7. Initial Water Saturation

In the free gas and hydrate zones initial water saturation was assigned as 55% (Singh, 2008). Apparently, the aquifer has 100% water saturation. Taking into consideration gas hydrate specification peculiarity, hydrate saturation was added to water saturation in the hydrate zone bringing it to 85% (Figure 3.37). A formula considering saturations and fluid contacts was written and assigned for the water saturation property. It is given as

```
IF ((X0 <= 2000)) THEN ((0.85)) ELSEIF ((X0 > 2000) AND (X0 <= 2750)) THEN
((0.55)) ELSE ((1))
```

where X0 is grid bottom depth, ft.

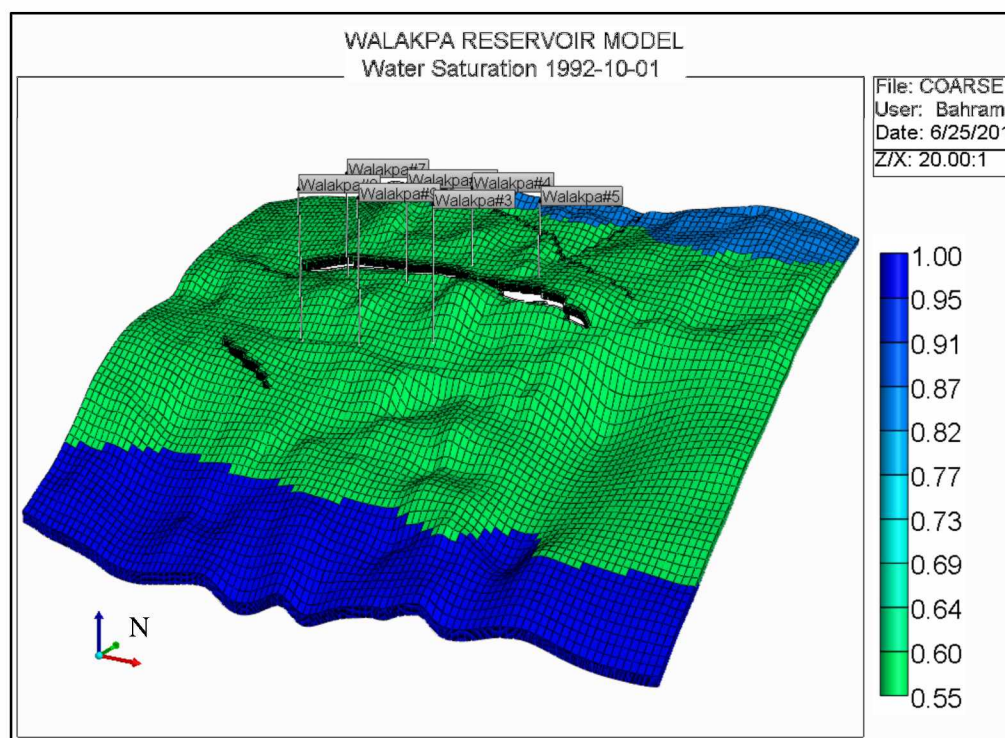


Figure 3.37: Initial Water Saturation – 3D View

#### c. Fluid Component Properties

Gas hydrates were initialized as solid immobile phase. Two chemical reactions were specified to simulate hydrate dissociation and reformation phenomena. Component properties and reaction details are summarized in Appendix A.

#### d. Well Rates

The WAL gas field has nine producer wells: Wal #02, #03, #04, #05, #06, #07, #08, #09, and #10. Well locations are displayed in Figure 3.38. Wellbore diagrams are provided in Appendix C. All of them are vertical wells drilled into the free gas zone. Well locations and production data were specified by Singh (2008) and updated within this study. All of the wells are in production so far. Similar to the EB field, flow rates were updated manually using the ALTER keyword. Afterwards, four new wells planned for drilling were specified. All four of the wells are horizontal with completion length summarized in Table 3.1. Wellbore diagrams are provided in Appendix D.

Table 3.1: Walakpa Horizontal Well Completion Lengths

Well name	Completion length, ft
Walakpa 11	1528.0
Walakpa 12	1505.6
Walakpa 13	1611.6
Walakpa 14	1501.6

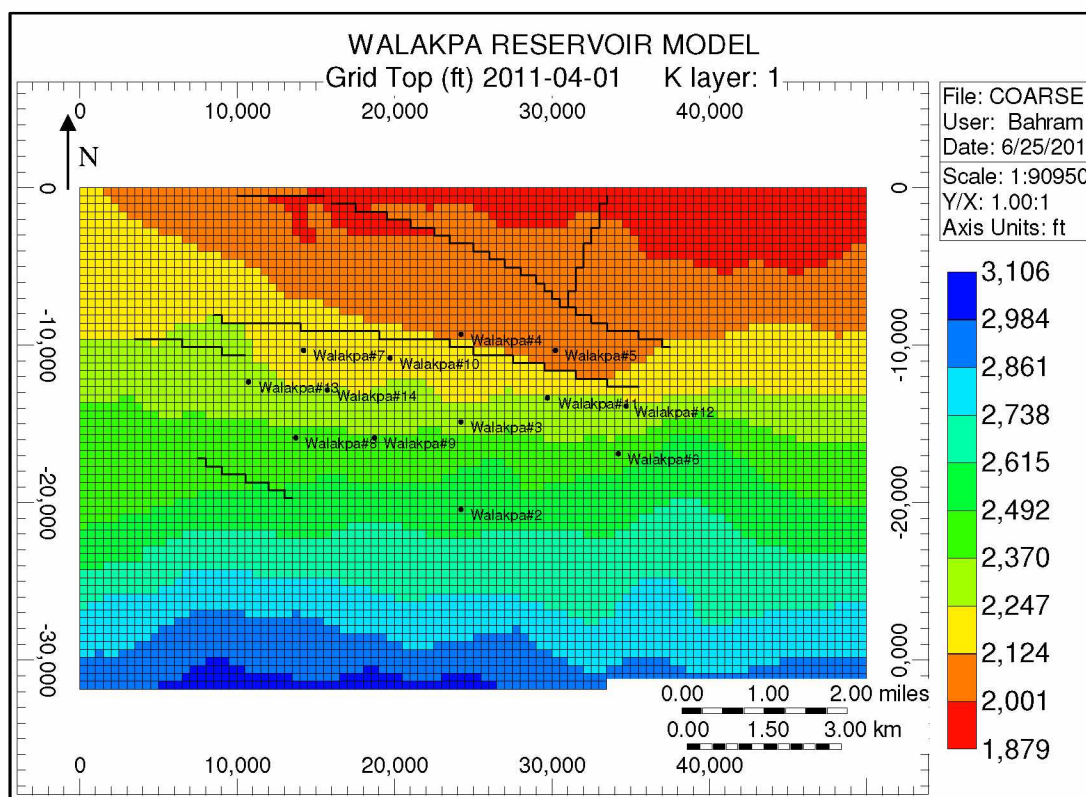


Figure 3.38: Well Locations – IJ Plane View

### 3.1.4 Sensitivity Study

The objective of the sensitivity study, which is critical for gas hydrate initialization, was to calibrate the models and by doing so determine the optimum value of the initial solid concentration (SOLCONC keyword). This optimum value is the one that matches the

initial hydrate saturation and leads to realistic field performance with minimum material balance error.

#### ***3.1.4.1 East Barrow Gas Field***

As stated earlier, gas hydrate saturation in the hydrate zone of EB field was equal to 31%. Singh (2008) models were rebuilt for hydrate specification. Then several simulation runs were performed to attain the required output. The five different scenarios attempted were:

- a. Initial Solid Concentration = 0.1000 lbmole/ft<sup>3</sup>
- b. Initial Solid Concentration = 0.1500 lbmole/ft<sup>3</sup>
- c. Initial Solid Concentration = 0.1586 lbmole/ft<sup>3</sup> (best-case model)
- d. Initial Solid Concentration = 0.2000 lbmole/ft<sup>3</sup>
- e. Initial Solid Concentration = 0.3000 lbmole/ft<sup>3</sup>

#### ***3.1.4.2 Walakpa Gas Field***

Similar to EB field, a gas hydrate saturation sensitivity study was performed for the rebuilt WAL field. Initial gas hydrate saturation in the hydrate layer of WAL field was 30%. Numerous simulation runs allowed identification of the optimum initial solid concentration value. The five different scenarios attempted were:

- a. Initial Solid Concentration = 0.1400 lbmole/ft<sup>3</sup>
- b. Initial Solid Concentration = 0.1441 lbmole/ft<sup>3</sup> (best-case model)
- c. Initial Solid Concentration = 0.1450 lbmole/ft<sup>3</sup>
- d. Initial Solid Concentration = 0.1535 lbmole/ft<sup>3</sup>
- e. Initial Solid Concentration = 0.1586 lbmole/ft<sup>3</sup>

#### **3.1.5 Forecasting Study**

A forecasting study was performed for WAL field based on a logical well production limit of 0.5 MMscfd for vertical wells. Higher production rates are not recommended for current wells because of the well-choking possibility (Stokes and Walsh, 2007). Two forecasting cases were studied: field production with existing wells only and production of existing wells along with four new horizontal wells. For new horizontal wells, a limit

of 0.7 MMscfd was assumed. Both cases were run for 20 years. Table 3.2 summarizes the forecasting simulation study.

Table 3.2: Forecasting Summary

Forecasting Period	20 Years (01-Jun-2011 to 01-Jun-2031)	
Wells Produced	9 Existing Wells	9 Existing and 4 New Wells
Production Rate	0.5 MMscfd/Well (Vertical)	0.5 MMscfd/Well (Vertical), 0.7 MMscfd/Well (Horizontal)

### 3.2 Well Choking Study

In conditions similar to ones in the BGF, the possibility of well choking is a big concern (Stokes and Walsh, 2007). It was noticed that at a higher initial production rate, well performance tended to worsen faster (Stokes and Walsh, 2007). Such a phenomenon is probably happening on a pore scale. Possibly observing it in models developed as part of this work is unlikely.

In order to investigate this problem, a simplistic simulation model was built in CMG STARS. The model was assigned reservoir properties equal or similar to those of the EB gas field. Reservoir performance at various well rates was studied. The model is briefly described below:

#### 3.2.1 Model Initialization

##### a. Reservoir Grid

A simple radial grid of 500 ft diameter was created in STARS (Figure 3.39). Grid depth ranged from 1900 ft (top) to 2330 ft (bottom). The reservoir grid consisted of 1200 blocks: 60 layers (K direction) and 60 blocks in radial direction.

## b. Reservoir Properties

### 1. Porosity

Uniform porosity of 20% was assigned for the entire model.

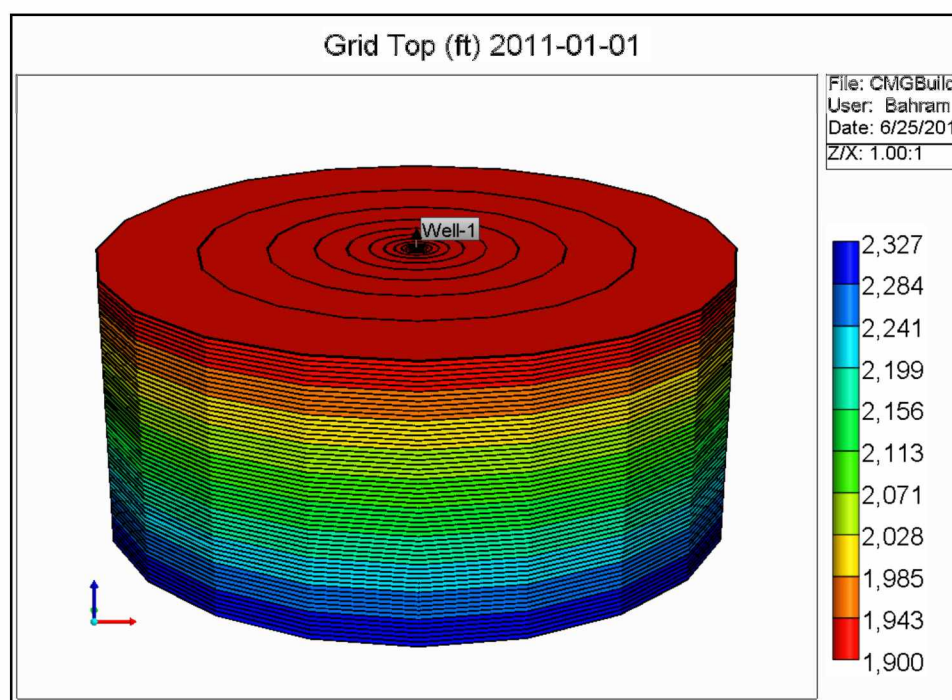


Figure 3.39: Simplistic Radial Grid – 3D View

### 2. Permeability

Permeability in horizontal (I and J) directions was defined as 50 md, 10 md in vertical (K) direction.

### 3. Temperature

The EB gas pool initial temperature conditions were used in the simplistic model. The temperature at the top of the formation was 41°F. At bottom it was 47.8°F (Figure 3.40).

### 4. Reservoir Pressure

Initial reservoir pressure equaled to 975 psi at the top of the reservoir.

### 5. Initial Hydrate Saturation

Gas hydrate saturation of 31% was specified for the hydrate zone. HGC depth was 2050 ft, similar to EB field.

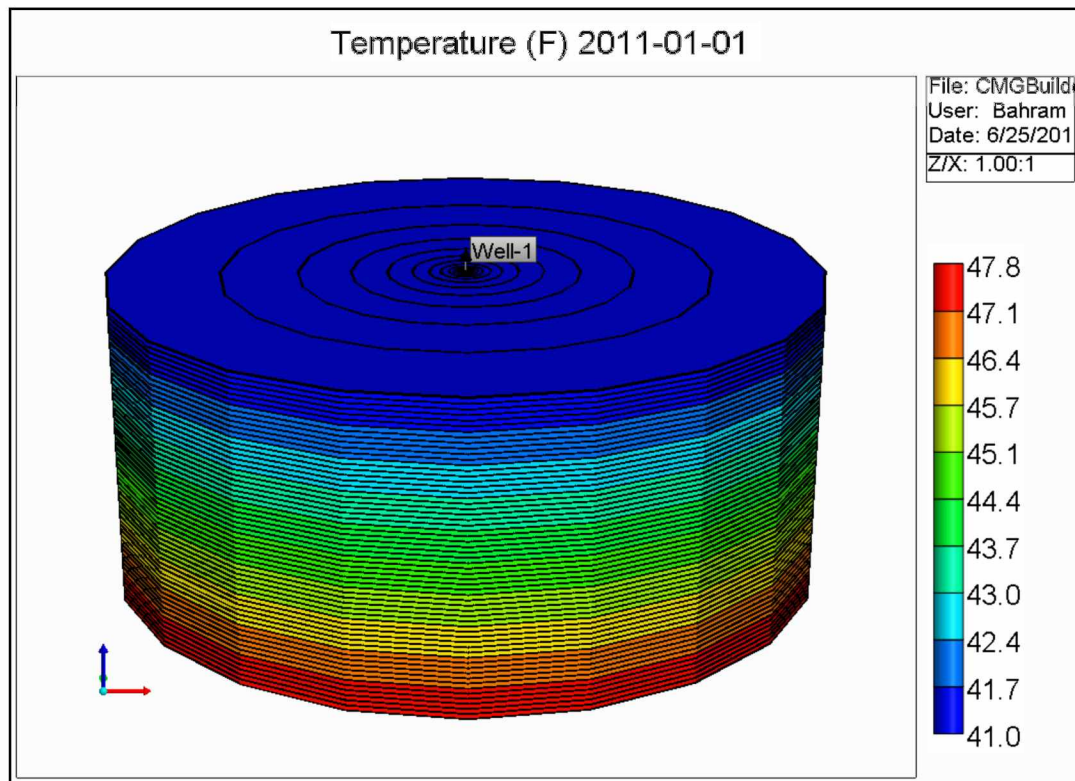


Figure 3.40: Initial Temperature Distribution, °F – 3D View

### 6. Initial Gas Saturation

Gas saturation values chosen were the same as in EB field: 14% in gas hydrate zone and 45% in free gas zone. In the water leg, gas saturation was 0% (Figure 3.41). GWC was located at a depth of 2080 ft.

### 7. Initial Water Saturation

Water saturation, similar to that of EB field, was specified as 100% in the water leg and 55% in free gas and hydrate zones.

### 8. Component Properties



Refer to Appendix A.

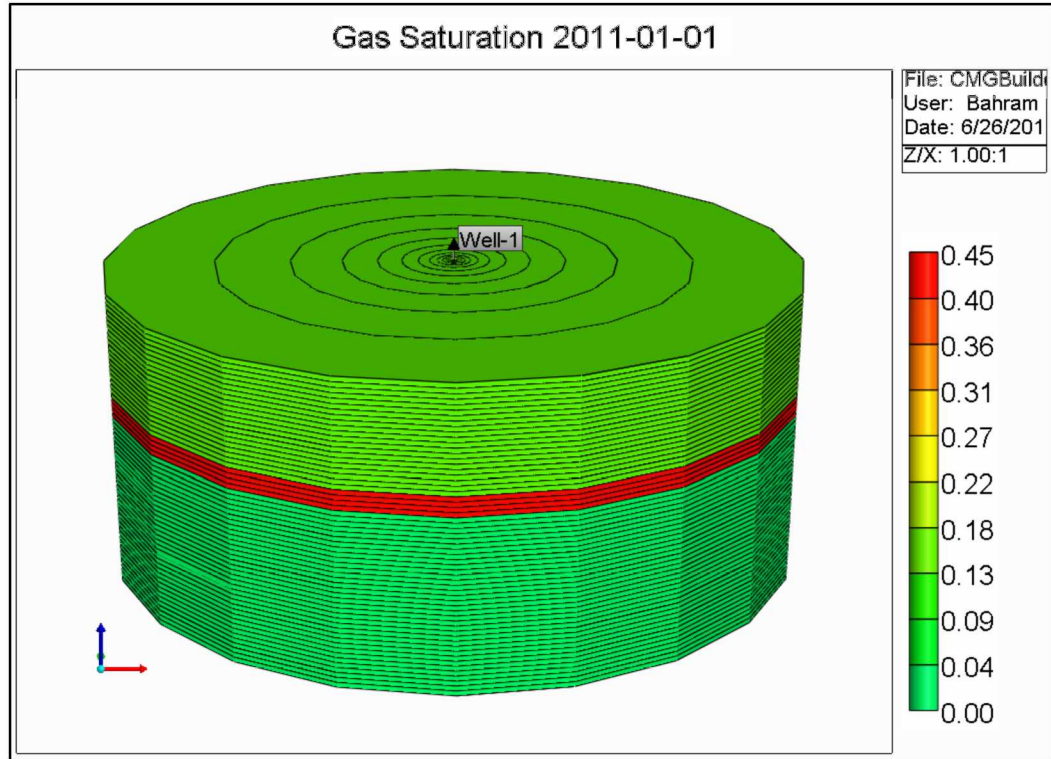


Figure 3.41: Initial Gas Saturation – 3D View

### 9. Production Well

A single production well was placed in the center of the radial grid. It was completed in the hydrate zone (K layers 7 and 8).

#### 3.2.2 Study Procedures

The simulation model was run in order to assess well-reservoir system performance in the hydrate reservoir. The three scenarios studied were:

- a. Well produces at 10 Mscfd
- b. Well produces at 30 Mscfd
- c. Well produces at 100 Mscfd

For all three scenarios, the model was run for 25 years.

## 4. RESULTS AND DISCUSSION

### 4.1 BGF Reservoir Simulation Study

In order to incorporate hydrates, both of the models were subjected to detailed revision. Most of the reservoir properties, reactions, and components were changed and redefined. These included gas hydrate dissociation and formation reactions input with respective coefficients and k-values. As a result of performed modifications both models became complete, full-fledged gas hydrate reservoir simulation models.

#### 4.1.1 Sensitivity Study

As mentioned earlier, five different scenarios were simulated for each field in order to obtain the optimum value of initial solid concentration (SOLCONC keyword). Upon successful simulation, each scenario was thoroughly studied and compared to the others. Resulting hydrate saturation errors obtained from the first several runs were used to calculate precisely the actual concentration value.

##### 4.1.1.1 East Barrow Gas Field

As a result of the sensitivity study, an initial solid concentration of 0.1586 lbmole/ft<sup>3</sup> was specified for the entire gas hydrate zone. The outcome of applying this particular value was not only precise hydrate saturation (31%), but also minimum material balance error (around 1%) among all simulation scenarios. The results are summarized in Table 4.1.

Table 4.1: East Barrow field sensitivity study summary

Solid concentration, lbmole/ft <sup>3</sup>	Hydrate saturation, %	Material balance error, %
0.1000	17.4	8.7
0.1500	29.3	2.9
0.1586	31.0	0.8
0.2000	34.8	5.2
0.3000	52.2	12.5

### ***4.1.1.2 Walakpa Gas Field***

Five simulation scenarios attempted for the sensitivity study in WAL field denoted one best-case model that matched actual hydrate saturation (30%) and led to the least material balance error (between 2% and 3.5% depending on simulation ending date). In the case of the WAL field, to narrow the window of possible values, the solid concentration value obtained in EB field was used for the first run. That value seemed too high and was reduced in subsequent scenarios to the optimum of 0.1441 lbmole/ft<sup>3</sup>. The sensitivity study results for Walakpa field are summarized in Table 4.2.

Table 4.2: Walakpa field sensitivity study summary

Solid concentration, lbmole/ft <sup>3</sup>	Hydrate saturation, %	Material balance error, %
0.1400	26.2	1.8
0.1441	30.0	0.7
0.1450	30.3	1.2
0.1535	38.1	2.4
0.1586	39.6	2.7

## **4.1.2 Reservoir Simulation Results**

### ***4.1.2.1 East Barrow Gas Field***

East Barrow field has been in production since 1981. Reservoir production was simulated till 1-Mar-2011. Within the almost 30 years of its life, the pool has produced almost 9 Bcf of natural gas (Figure 4.1). The shaly layer has absolutely no impact on production. It can be noticed by comparing the two models. Moreover, permeability of 5 md is more than enough for an unrestricted gas flow.

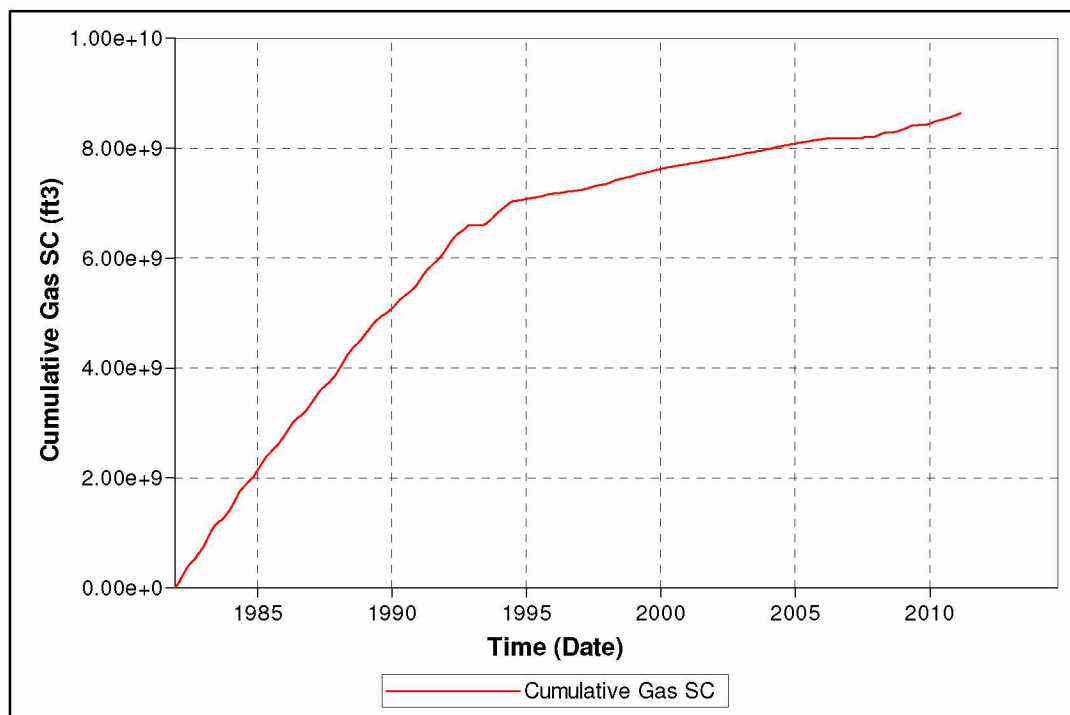


Figure 4.1: East Barrow Cumulative Gas Production, ft<sup>3</sup>

In order to monitor fluid dynamics in the hydrate zone a representative location was selected (I=19, J=19) and saturation values were monitored at various depths (K=1; 5; 10; 15; 20; 25) within that location (Figure 4.2). Gas hydrate saturation variation within the location is shown in Figure 4.3. The Figure clearly shows gas hydrate saturation decrease with time in the top and bottom parts of the pay zone. In the middle part, however, hydrate saturation stays fairly constant with only slight variations.

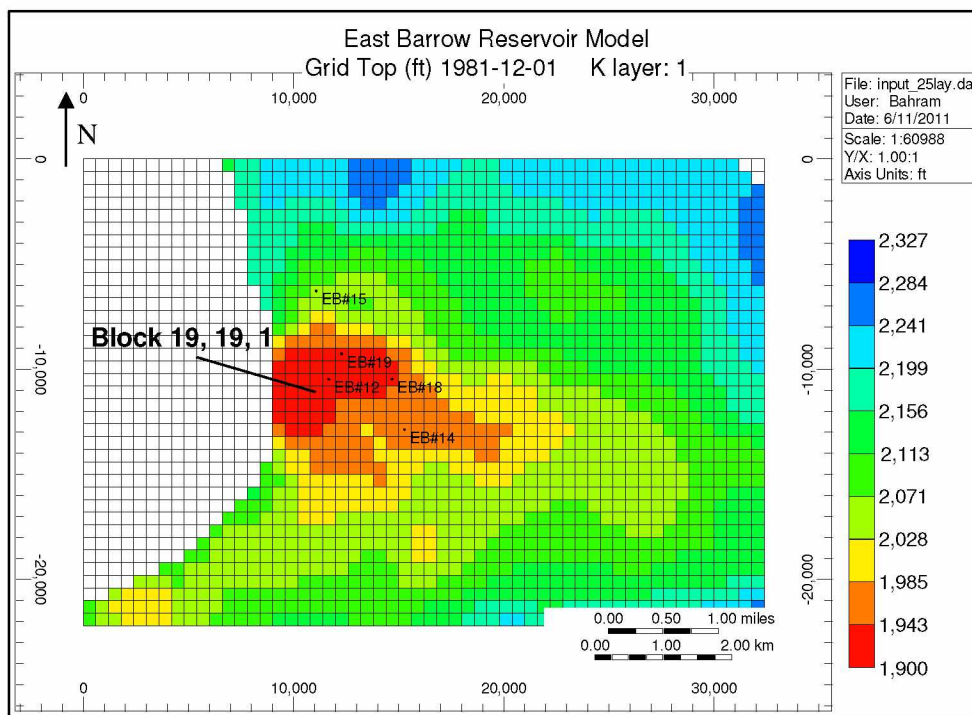


Figure 4.2: Representative Grid Block Location

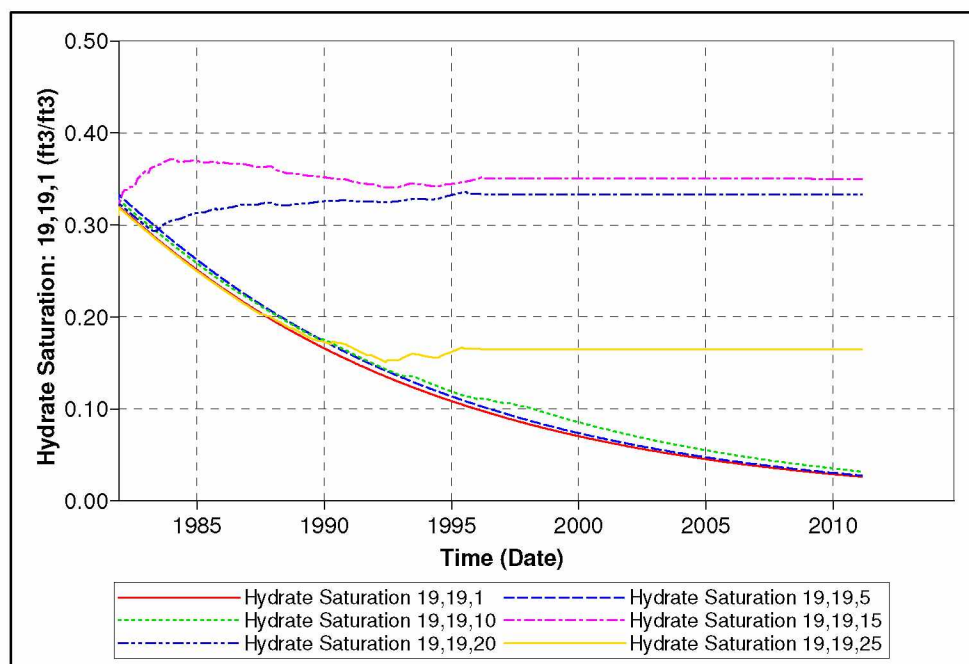


Figure 4.3: Gas Hydrate Saturation Profile at Grid Block 19,19,1

Gas saturation trends over time in the representative location are shown in Figure 4.4. This plot shows a very slight decrease in gas saturation in the top part of the pay zone after a quick increase in the beginning (note 14% of initial gas saturation in the hydrate zone). On the other hand, gas saturation in the bottom part decreases with time. Comparing K layers 5 and 10, it can be concluded that greater depth tends to show larger decrease in gas saturation.

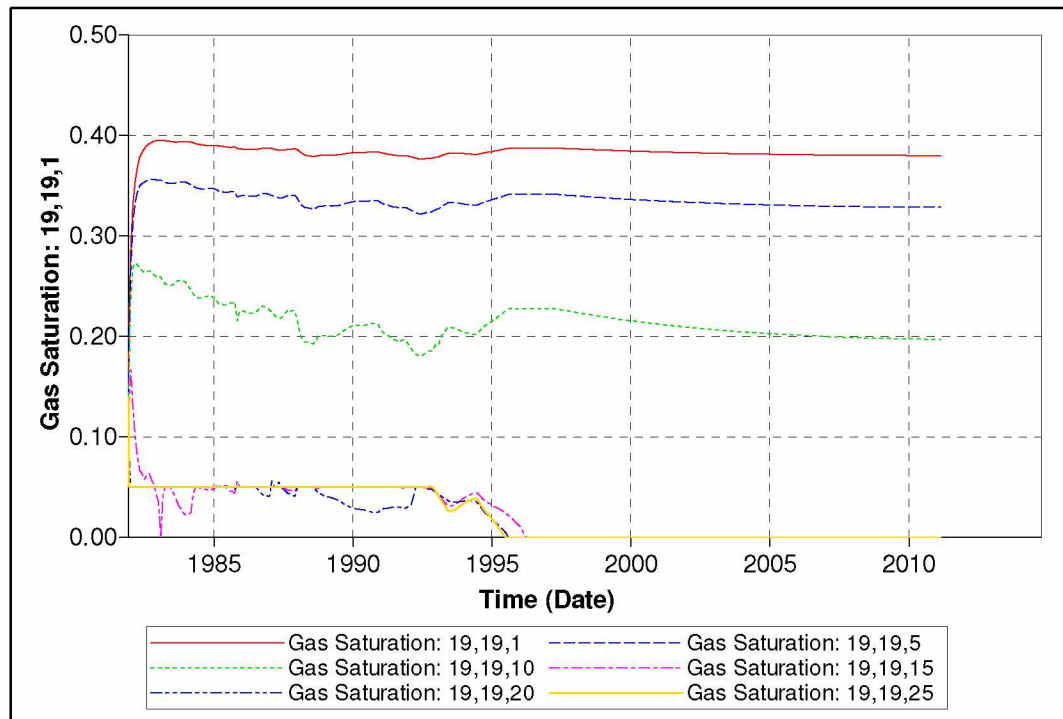


Figure 4.4: Gas Saturation Profile

Variation in water saturation with time is shown in Figure 4.5. Even though water saturation increases in all layers, one can clearly see that in the lower pay zone it increases to 100% fairly quickly.

Comparison of this plot with that of gas saturation in Figure 4.4, leads to the conclusion that hydrate dissociation is accompanied by large water dropout. Due to gravity segregation, gas freed from hydrates tends to flow upward, and water tends to settle towards the bottommost layer.

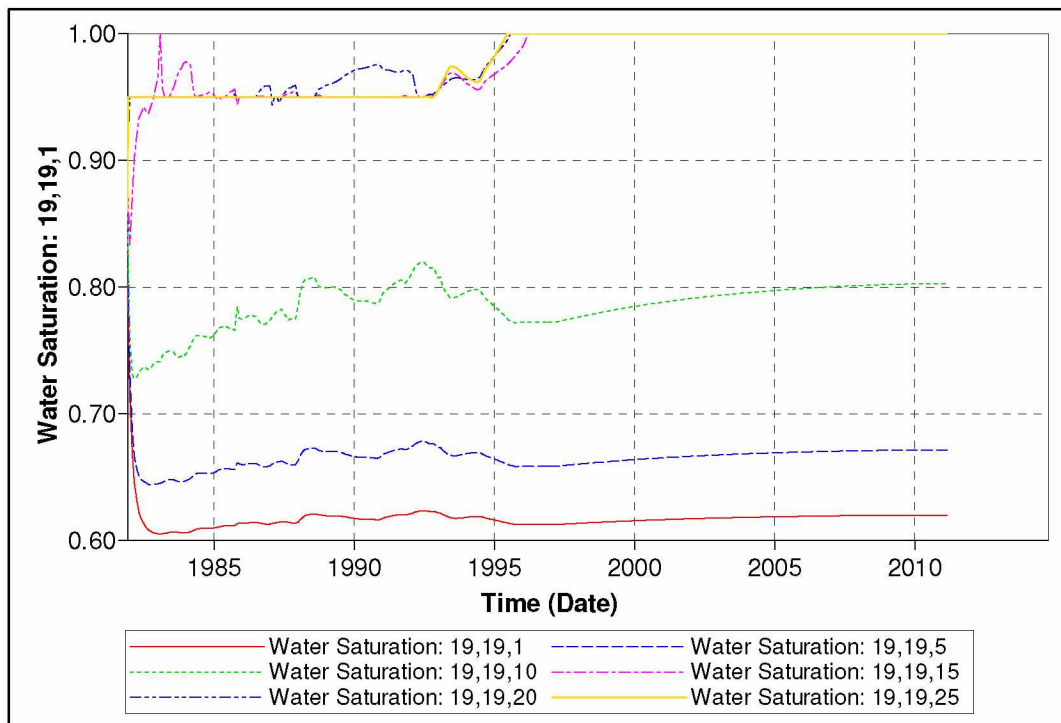


Figure 4.5: Water Saturation Profile

A 3D view of hydrate saturation at the end of simulation is provided in Figure 4.6. Even though it can be thought that the hydrate has completely dissociated, this is not the case. Most of initial hydrate saturation has dropped to 5% (out of the color scale). However, in the lower layers (K=13 to 25) gas hydrate saturation is still significant (Figure 4.7). Some grid blocks even show an increase in hydrate saturation.

Such a fluid saturations change is likely happening due to water dropout from the upper layers and gas penetration from the free gas zone located downdip.

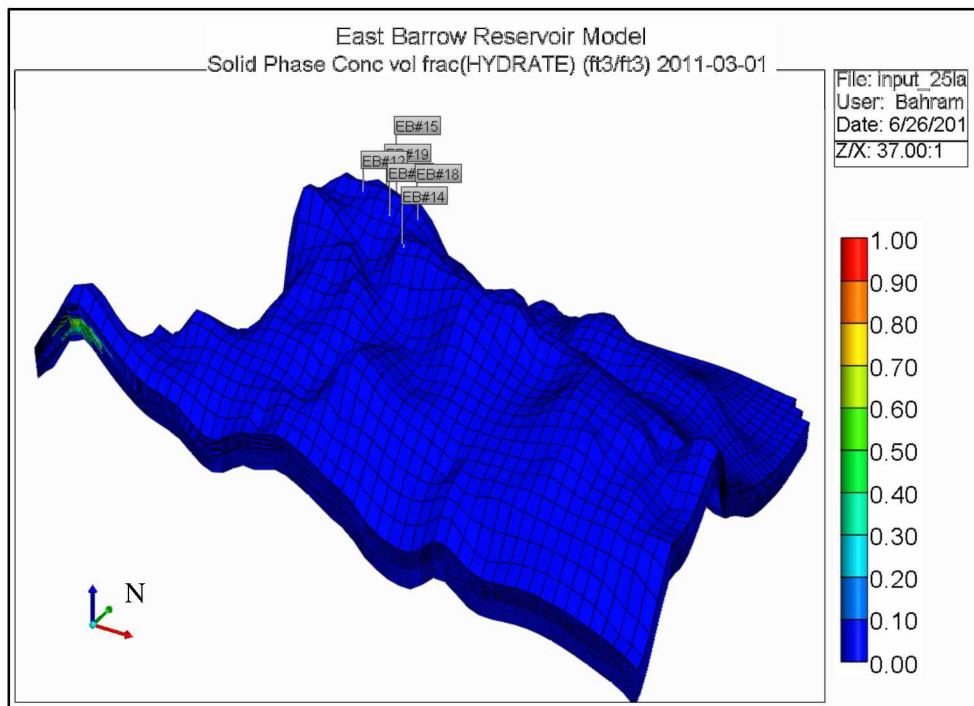


Figure 4.6: Hydrate Saturation at Simulation End – 3D View

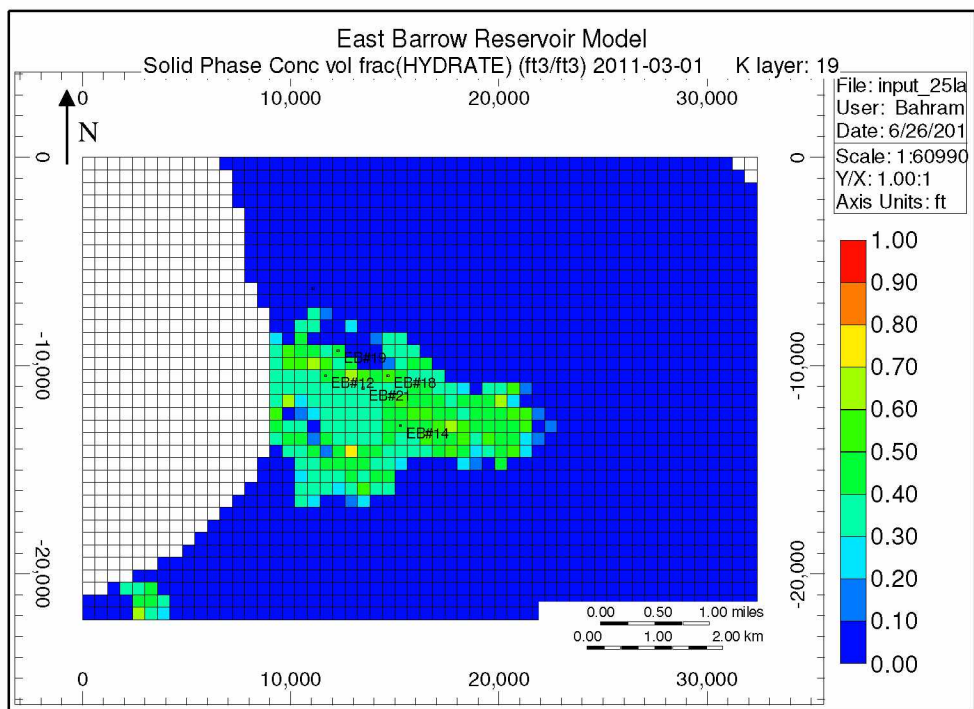


Figure 4.7: Hydrate Saturation at Simulation End (K Layer 19) – IJ Plane View



Gas saturation distribution has dramatically changed by the end of simulation, as is displayed in Figure 4.8. However, in the lower layers (K=20 to 25), gas saturation is insignificant (Figure 4.9).

This pattern can be interpreted as due to the accumulation of gas freed from hydrates by hydrate dissociation in the top portion of the reservoir, with a significant amount of gas hydrates remaining in the lower layers. This remaining gas hydrate could still contribute considerably to gas production.

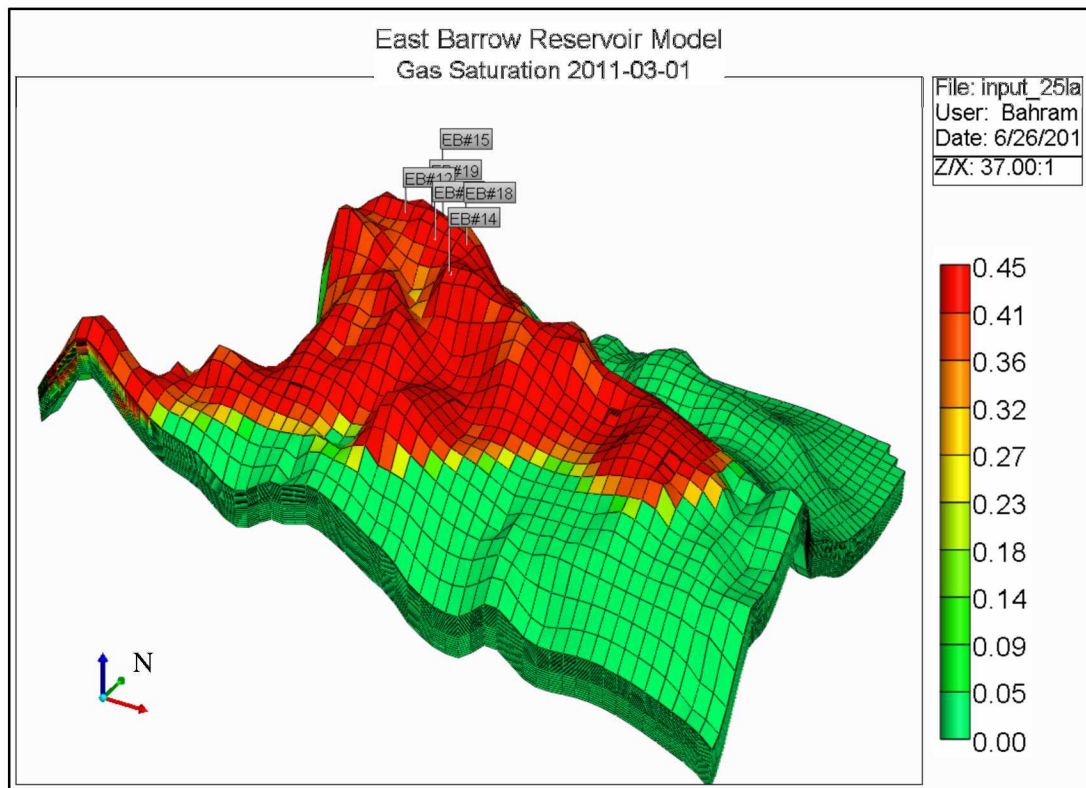


Figure 4.8: Gas Saturation at Simulation End – 3D View

Water saturation shown in Figure 4.10 decreases in the hydrate zone due to water migration downward. The bottommost layers (K= 23 to 25) have water saturation of 100% almost everywhere (Figure 4.11).

Some portion of the free gas zone is swept by the aquifer. Hydrates are most likely still present in the bottommost layers, but no free gas.

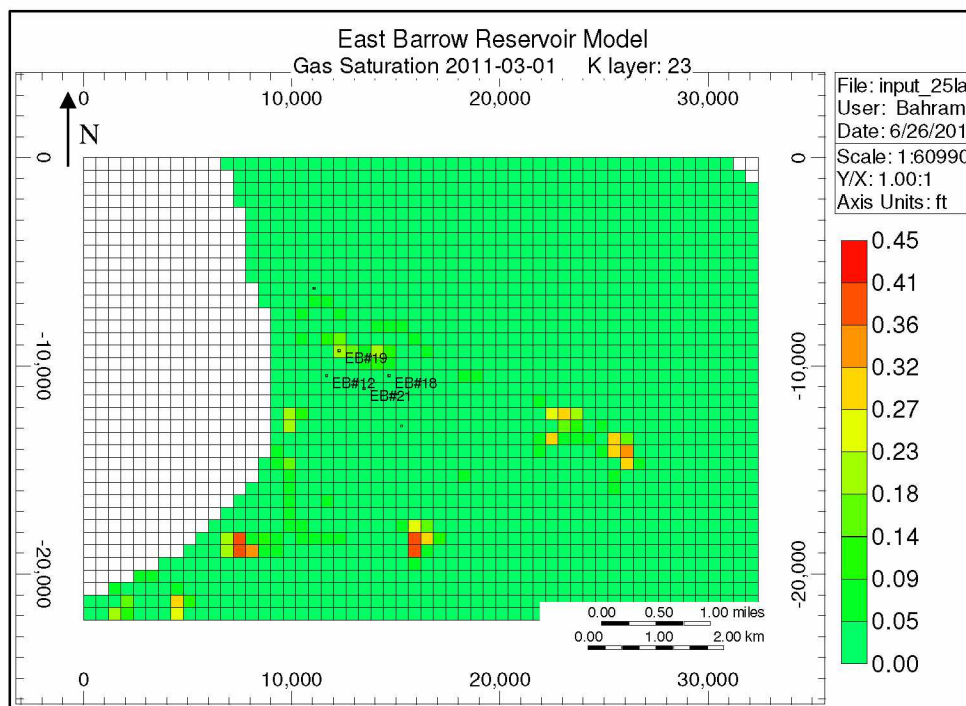


Figure 4.9: Gas Saturation at Simulation End (K Layer 23) – IJ Plane View

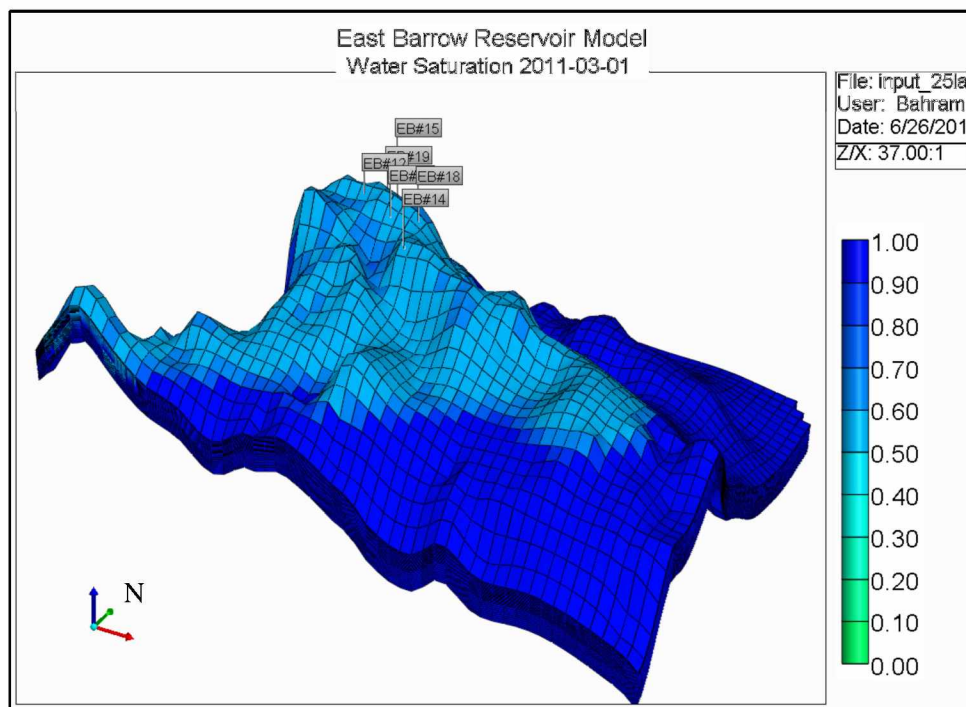


Figure 4.10: Water Saturation at Simulation End – 3D View

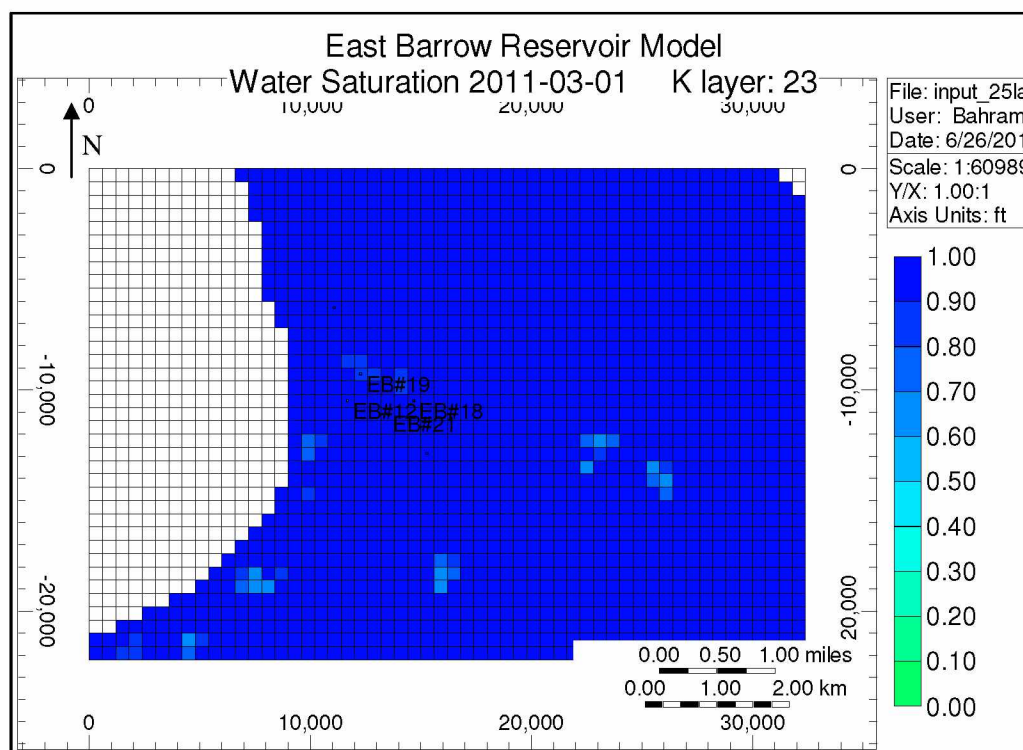


Figure 4.11: Water Saturation at Simulation End (K Layer 23) – IJ Plane View

Reservoir temperature increases with production throughout the field (Figure 4.12). Average increase of 4–5°F is observed in the gas hydrate zone. In the water leg, the temperature increment is around 2°F.

The temperature increase could be happening likely due to warm aquifer flux. Overall increase in temperature should contribute to hydrate dissociation.

Reservoir pressure generally decreases with time reaching as low as 885 psi in the hydrate cap (Figure 4.13). Hence, pressure drop in the top of the hydrate layer is around 90 psi, whereas at the lowest layer (K=25) it is only 70 psi. In the water leg, pressure mostly stays constant at 975 psi. Some regions at the edges of reservoir show a slight increase of 5–20 psi.

The dynamics of fluid contacts are presented in Figures 4.14 to 4.19. Figures 4.14 and 4.15 are colored with respect to gas saturation, Figures 4.16 and 4.17 denote hydrate saturation and Figures 4.18 and 4.19 represent water saturation.

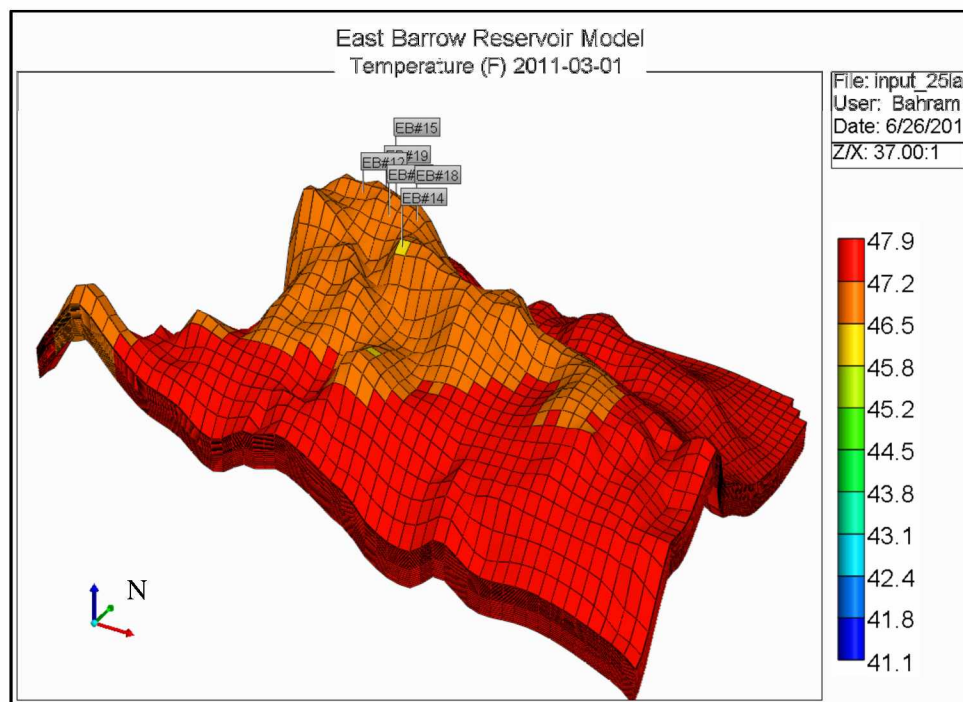


Figure 4.12: Temperature Distribution at Simulation End – 3D View

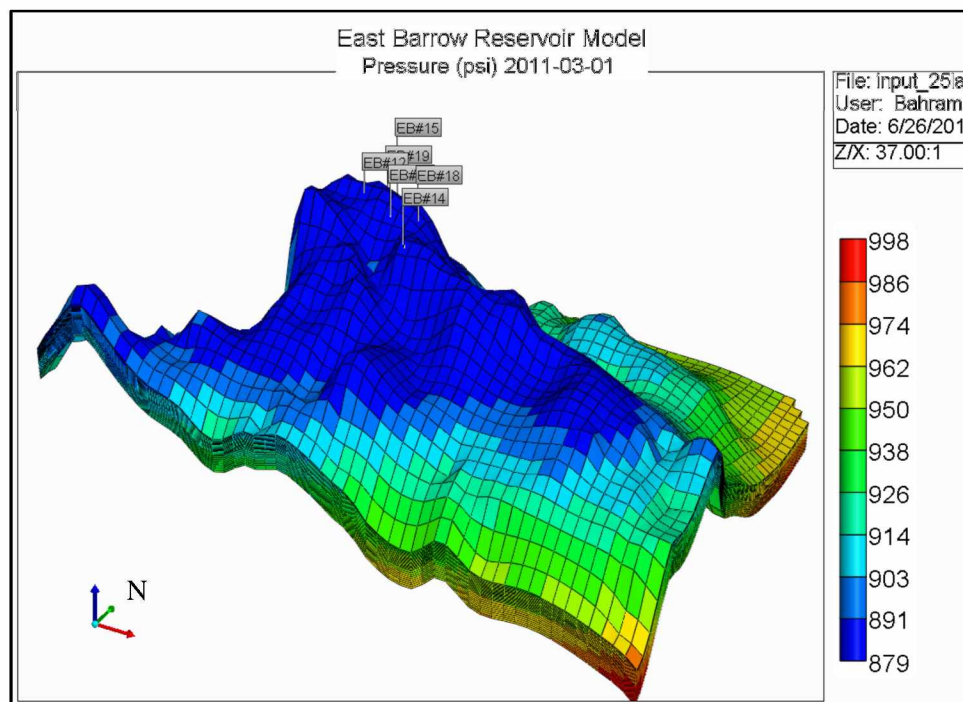


Figure 4.13: Pressure Distribution at Simulation End – 3D View

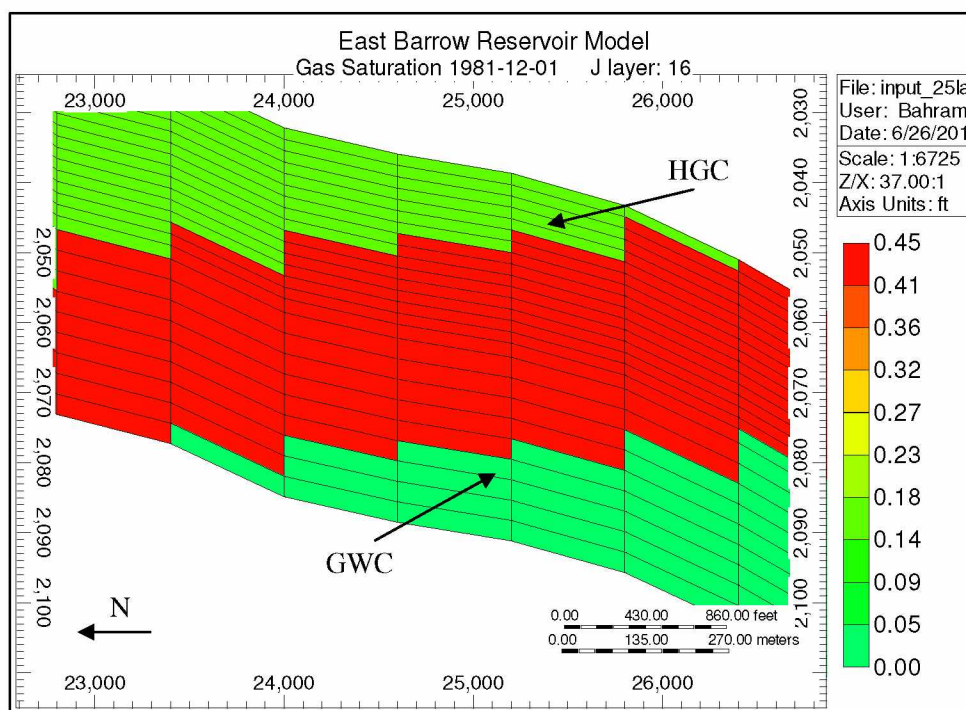


Figure 4.14: Initial HGC and GWC – IK Plane View

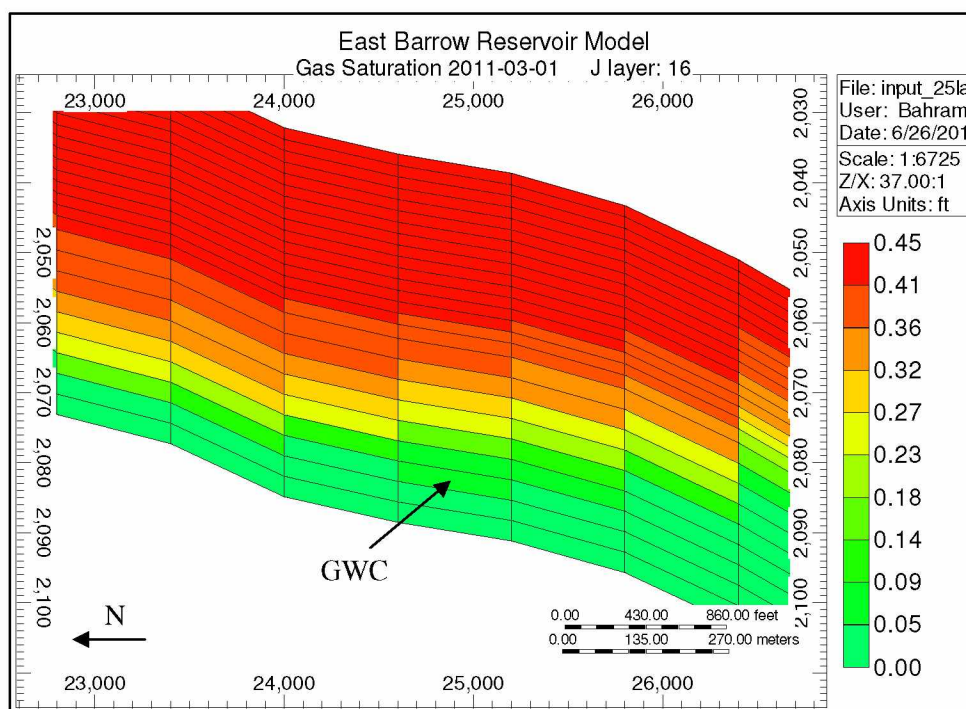


Figure 4.15: GWC at Simulation End– IK Plane View

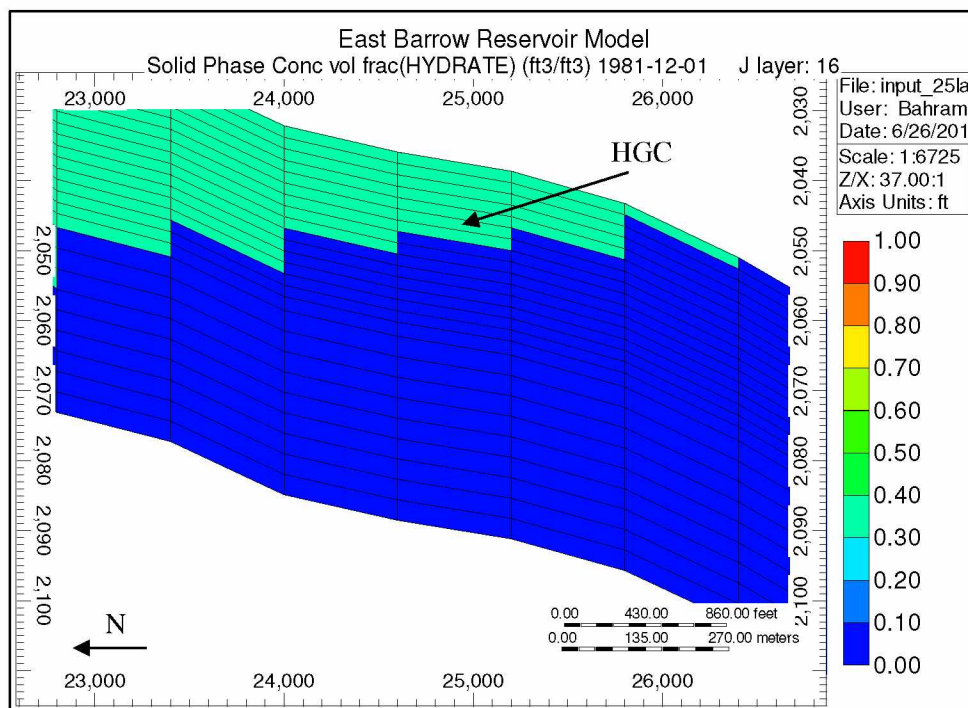


Figure 4.16: Initial HGC – IK Plane View

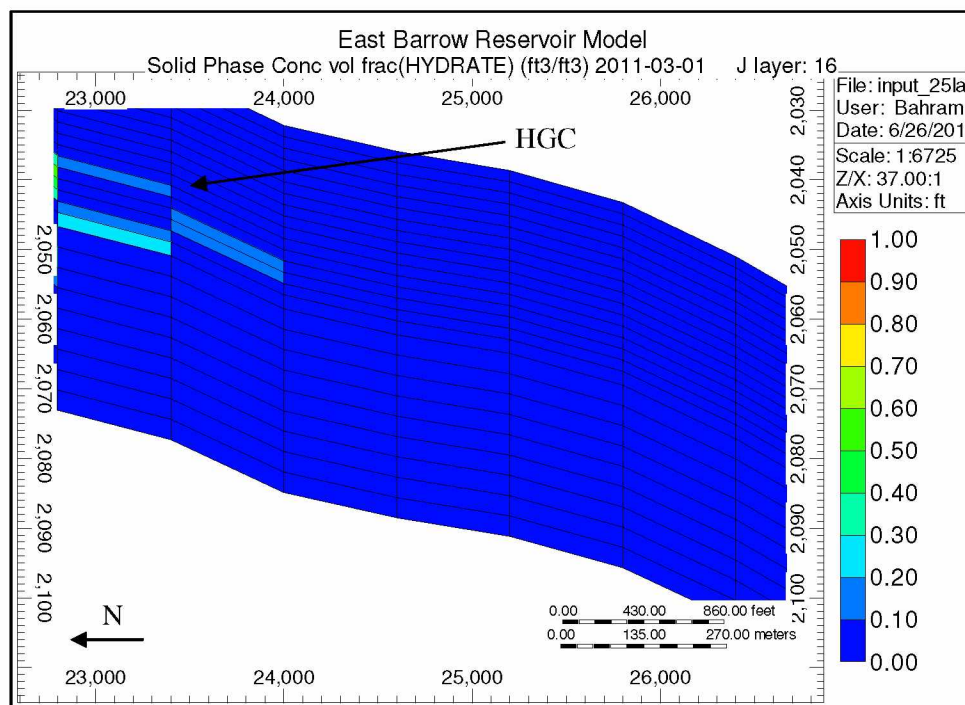


Figure 4.17: HGC at Simulation End – IK Plane View

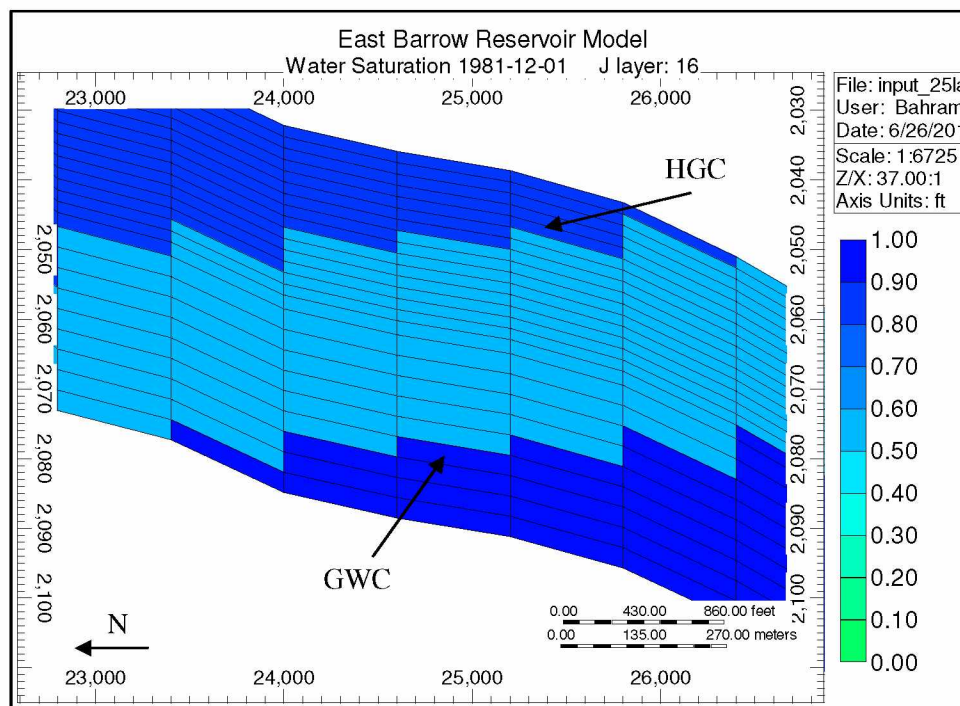


Figure 4.18: Initial HGC and GWC – IK Plane View

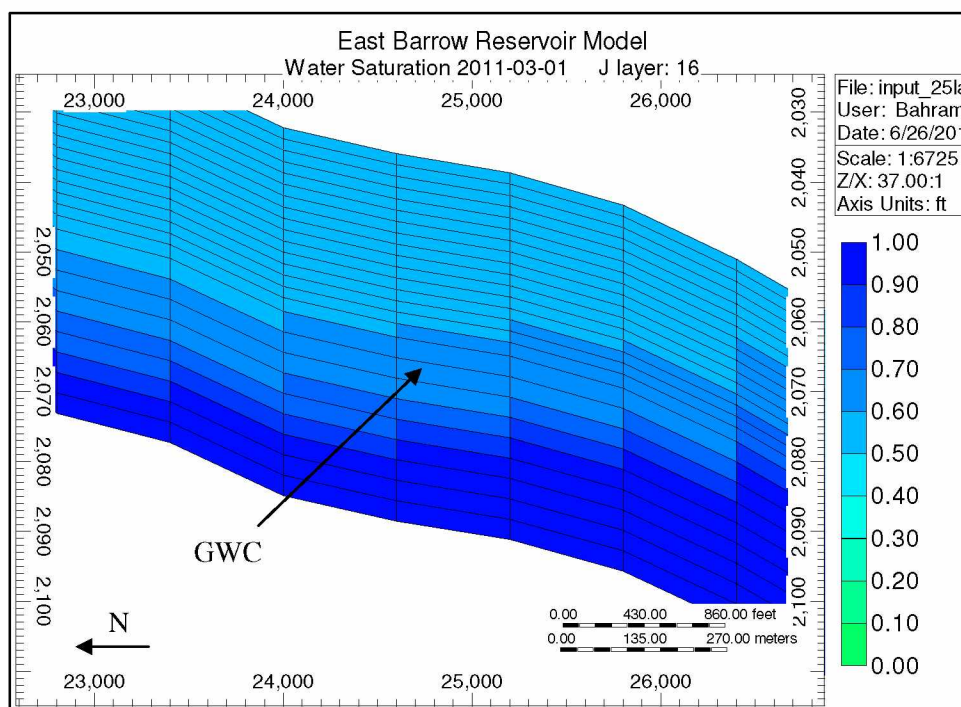


Figure 4.19: GWC at Simulation End – IK Plane View

Changes in Figures 4.14, 4.15, 4.18, and 4.19 demonstrate GWC movement and prove water sweep. The GWC shifted from 2080 ft to 2070 ft (about 10 ft). Figures 4.16 and 4.17 indicate clear hydrate dissociation. More dissociation happened at the top layer of the pay zone. This can be likely explained by fluid segregation and water dropout reforming hydrates in the layers located beneath.

#### 4.1.2.2 Walakpa Gas Field

The Walakpa gas field has been producing natural gas since October 1992. In almost 19 years of operation it has produced 22 Bcf of gas (Figure 4.20). Field production was simulated till 1-Jun-2011.

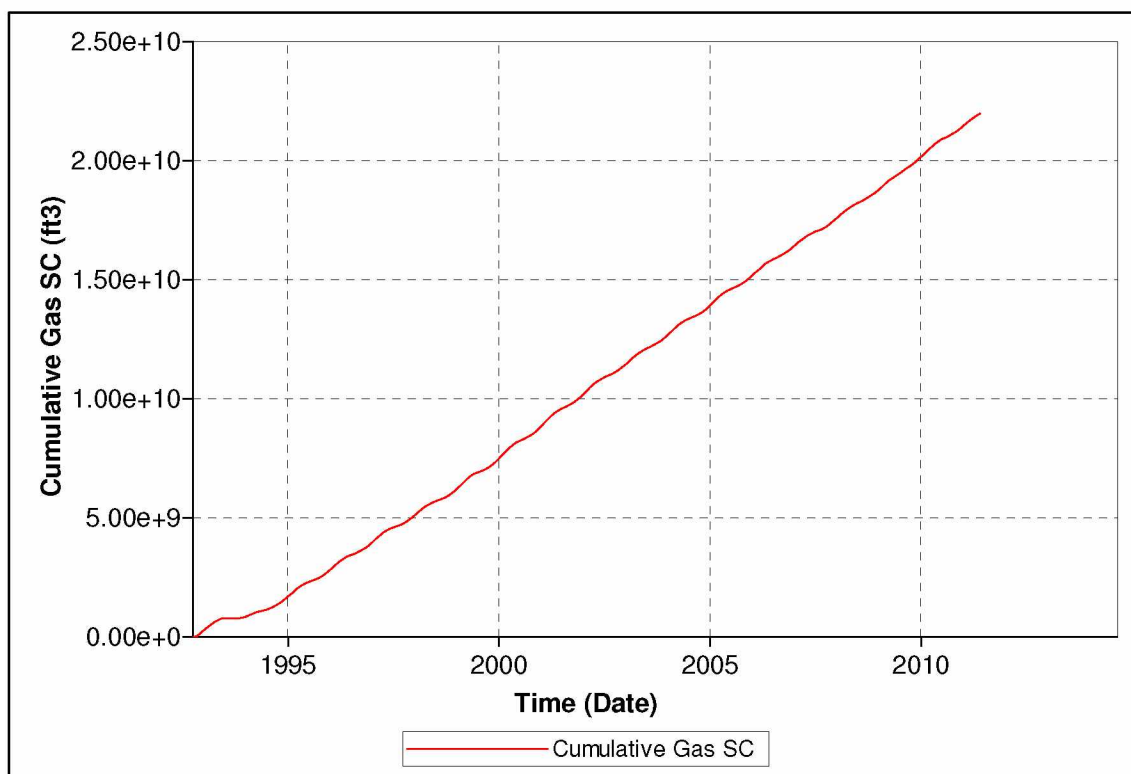


Figure 4.20: Walakpa Cumulative Gas Production, ft<sup>3</sup>

Gas hydrate saturation at the end of the simulation period is shown in Figure 4.21. Even though almost no hydrate is observed in the topmost layer, like EB field, significant hydrate saturation remains within lower layers (K=5 to 8) (Figure 4.22).



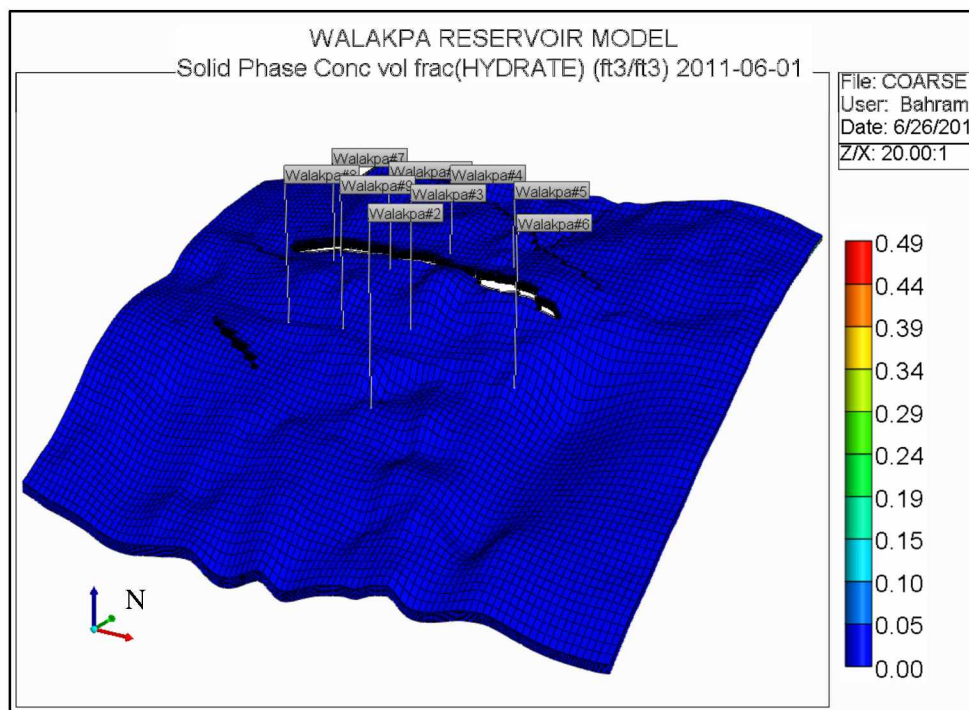


Figure 4.21: Hydrate Saturation at Simulation End – 3D View

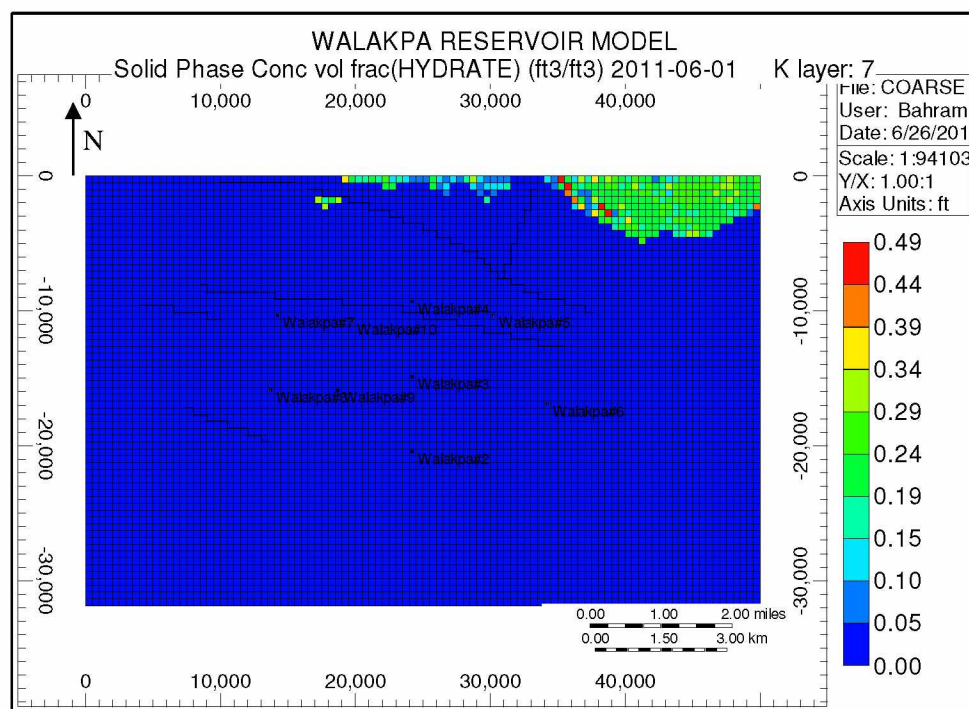


Figure 4.22: Hydrate Saturation at Simulation End (K Layer 7) – IJ Plane View

Changes in water saturation have two trends: gas zone sweep due to aquifer support and hydrate dissociation. A 3D view of water saturation distribution is presented in Figure 4.23. Water saturation in the lowest layer (K=10) of the hydrate portion increased to about 95–100% (Figure 4.24). Also observed was that hydrate saturation in the same portion of reservoir had decreased to almost 0%. Most likely water released from hydrates settles in the lowest layer as a result of gravity.

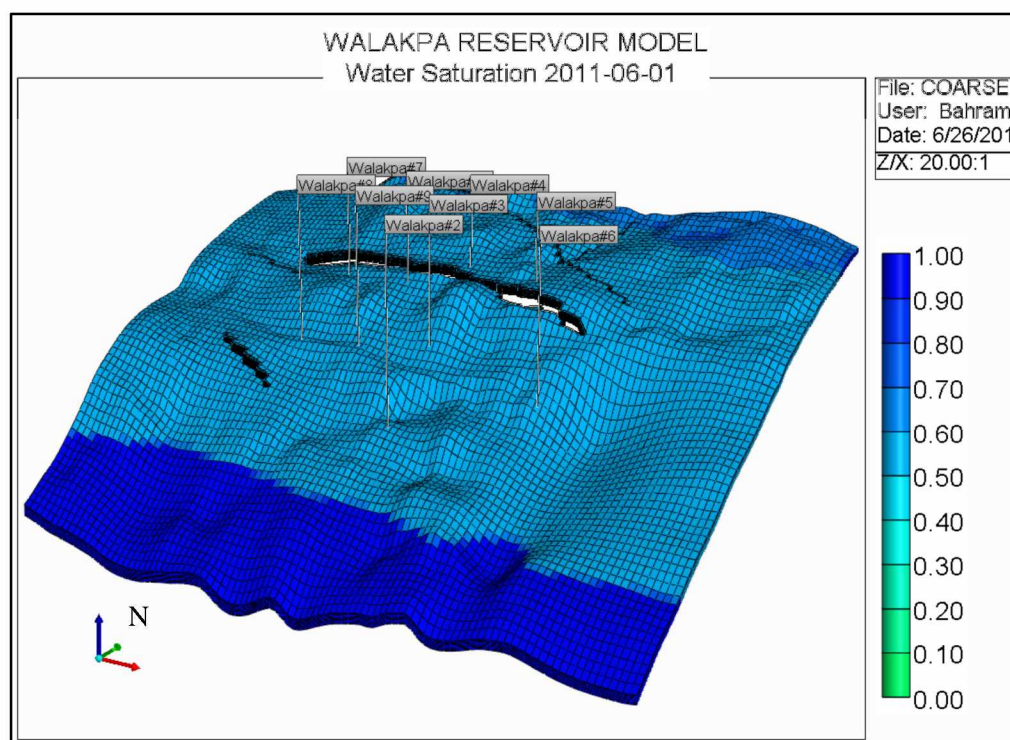


Figure 4.23: Water Saturation at Simulation End – 3D View

Reservoir temperature decreases with production throughout the field. Close to the hydrate zone, the temperature drop is about 2°F, whereas around the producers the drop reaches 5°F. The temperature distribution at the end of simulation is shown in Figure 4.25.

The difference in temperature behavior between Walakpa and East Barrow fields could be due to different well placement: wells are drilled into hydrate zone in East Barrow field, whereas in Walakpa field all the wells are in free gas zone.

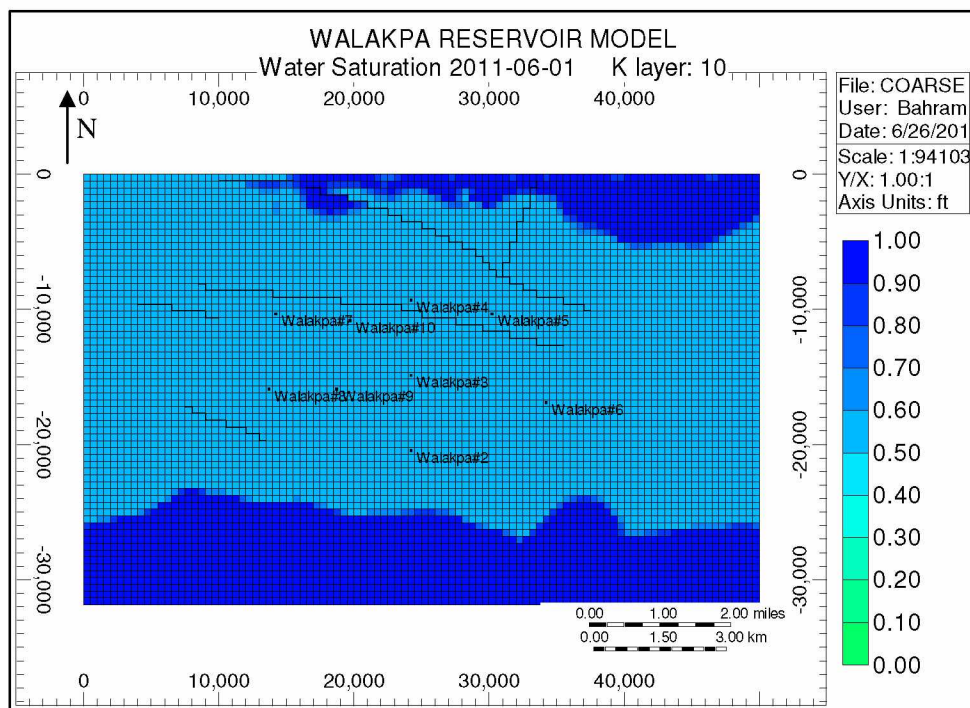


Figure 4.24: Water Saturation at Simulation End (K Layer 10) – IJ Plane View

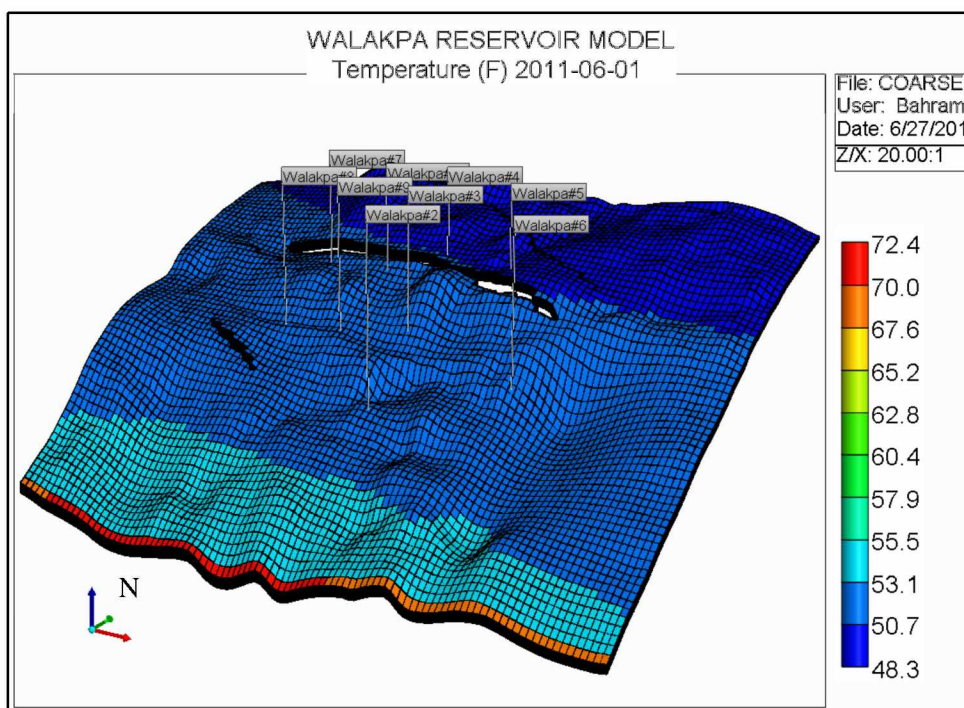


Figure 4.25: Temperature Distribution at Simulation End – 3D View

In 19 years of production, reservoir pressure has decreased only slightly. This is most likely due to the strong aquifer specified properly in the model. Average pressure drop throughout the reservoir is between 50 and 100 psi. In the regions adjacent to producers it reaches 200 psi. Pressure distribution at the end of simulation is shown in Figure 4.26.

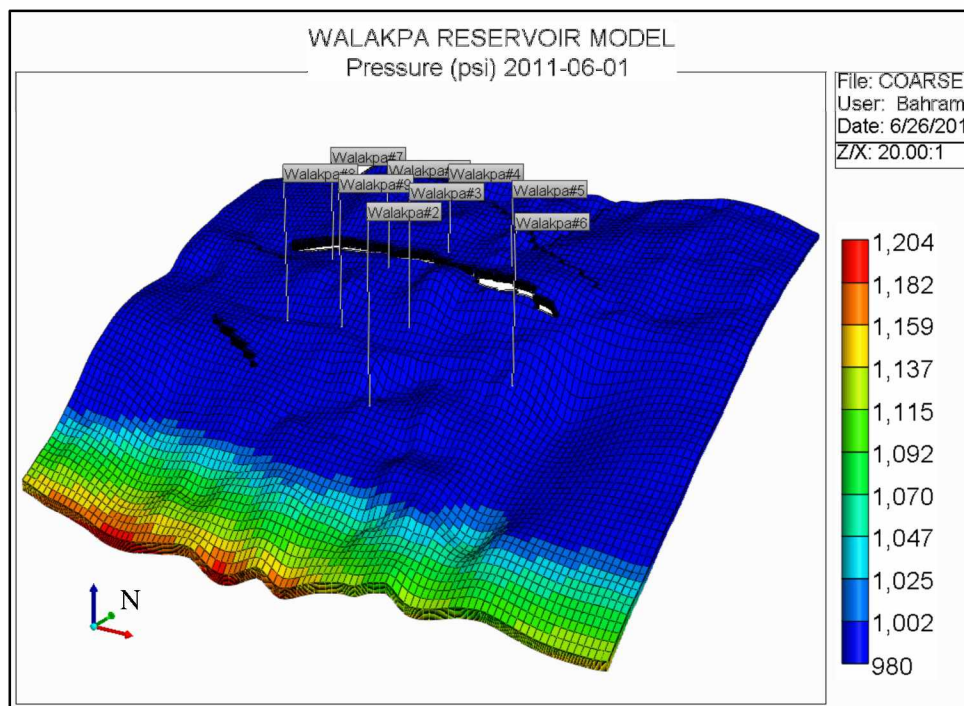


Figure 4.26: Pressure Distribution at Simulation End – 3D View

Figures 4.27 and 4.28 display initial and current (end of simulation) gas saturations and the resulting HGC, respectively. The gas saturation has increased in the upper layers of hydrate, whereas it has decreased in the lower layers. This can be explained by hydrate dissociation phenomena. Overall, HGC rose for about 10 ft in depth.

Initial and final hydrate saturation variation at the HGC is displayed in Figures 4.29 and 4.30. Hydrates gradually dissociate with time, which indicates proper specification of hydrates and reaction parameters. Water saturation also changes with simulated production, resulting in a change in the GWC depth. This can be observed from Figures 4.31 and 4.32. Total rise of GWC is about 8 ft.

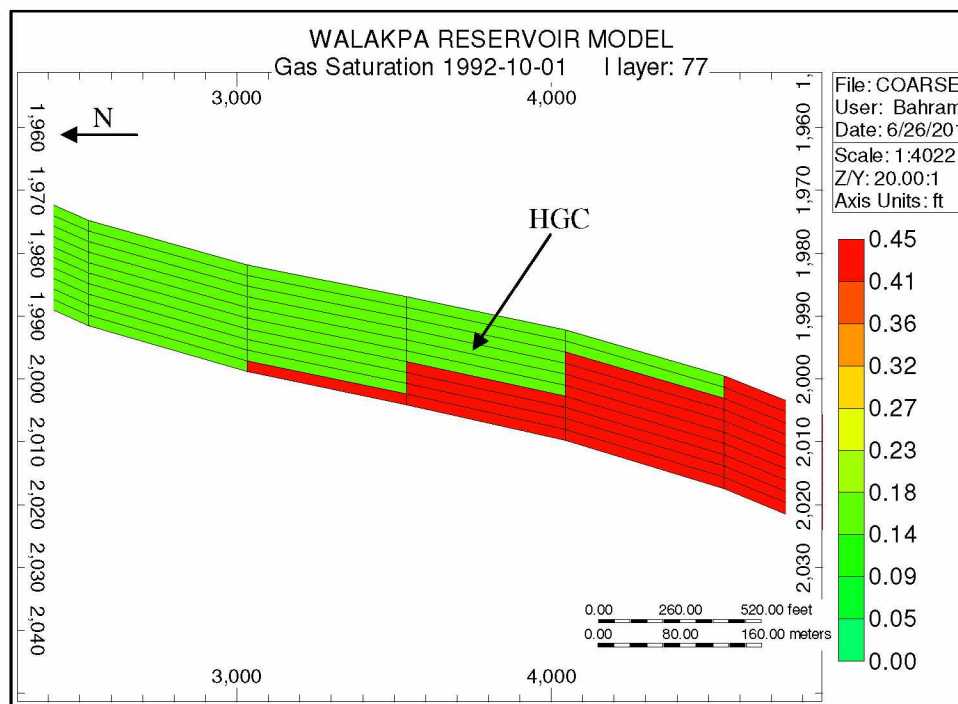


Figure 4.27: Initial HGC and Gas Saturation – JK Plane View

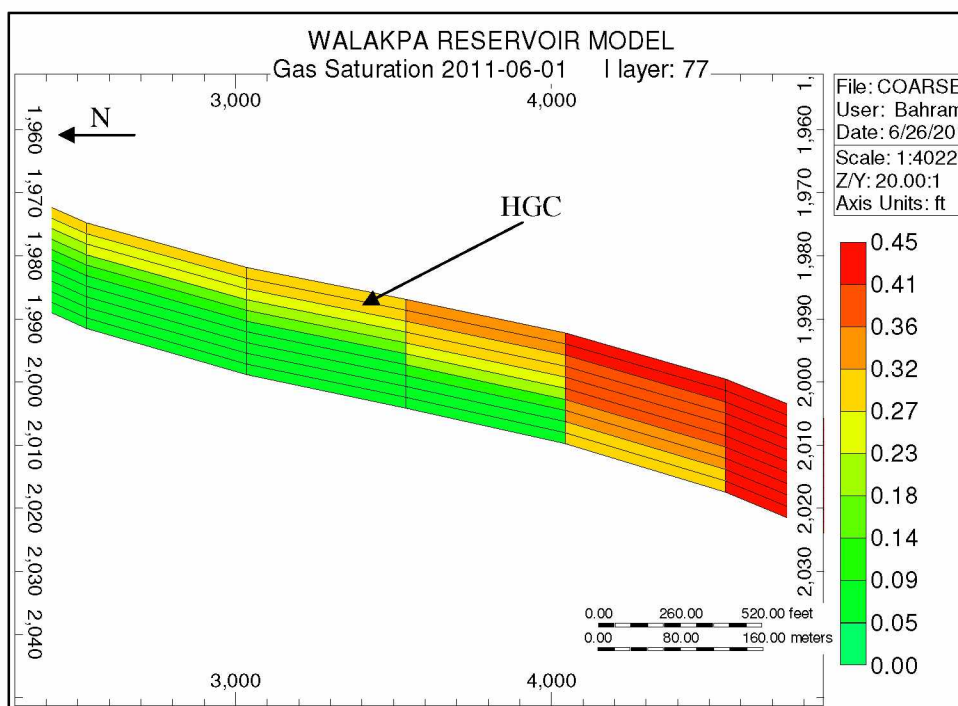


Figure 4.28: Current HGC and Gas Saturation – JK Plane View

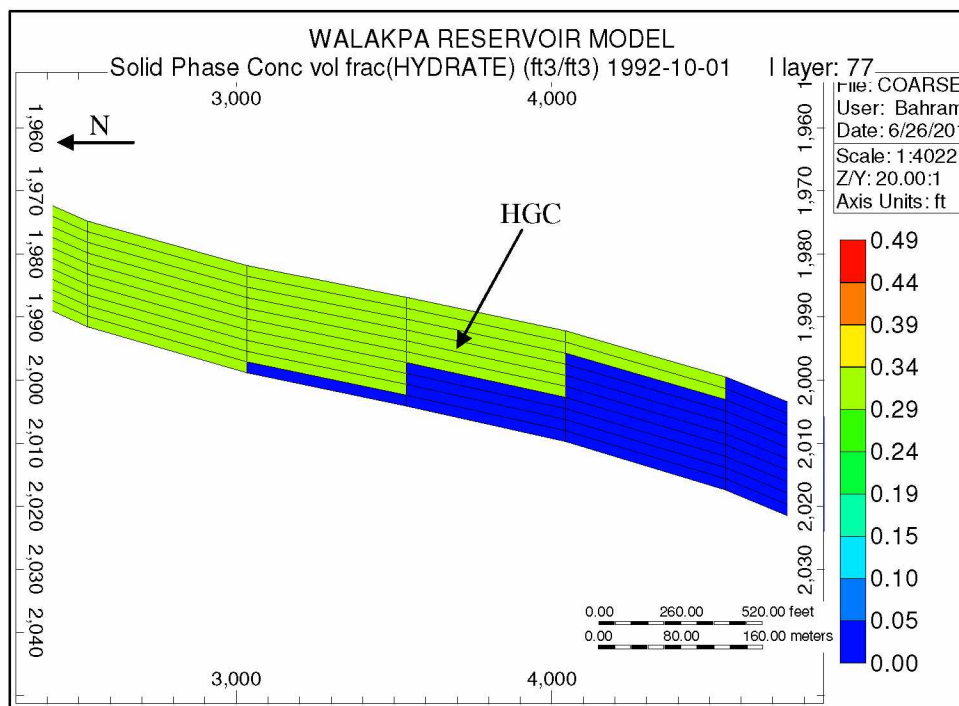


Figure 4.29: Initial HGC and Hydrate Saturation – JK Plane View

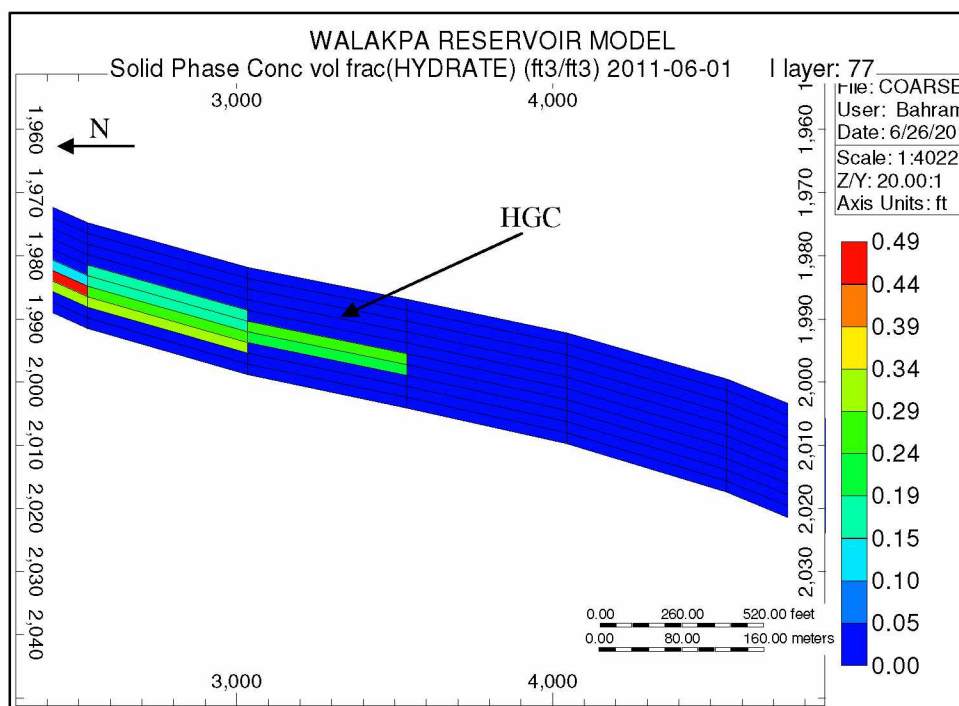


Figure 4.30: Current HGC and Hydrate Saturation – JK Plane View

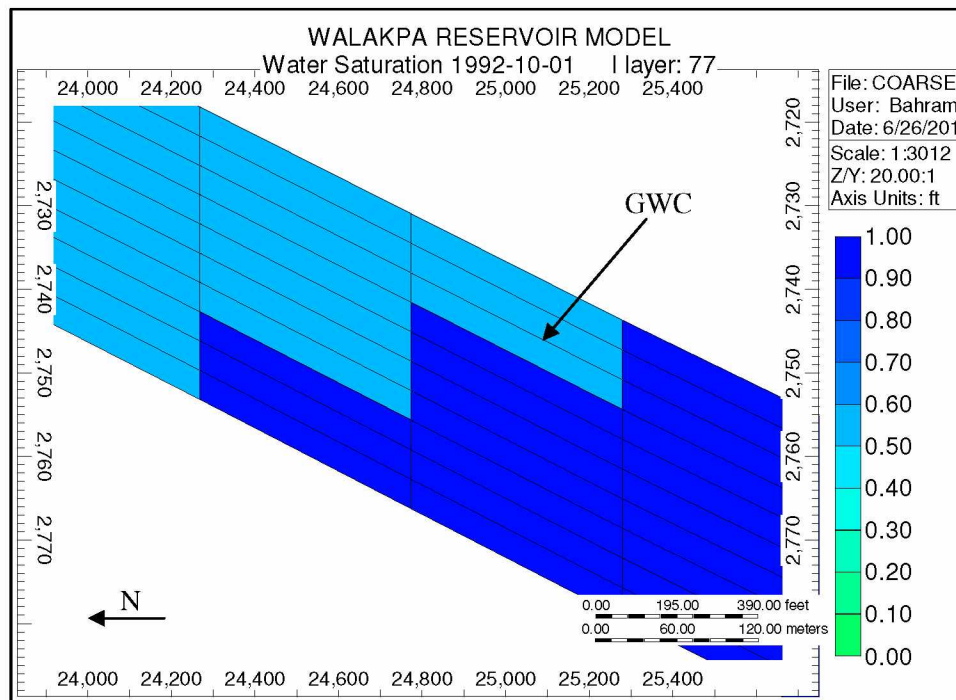


Figure 4.31: Initial GWC and Water Saturation – JK Plane View

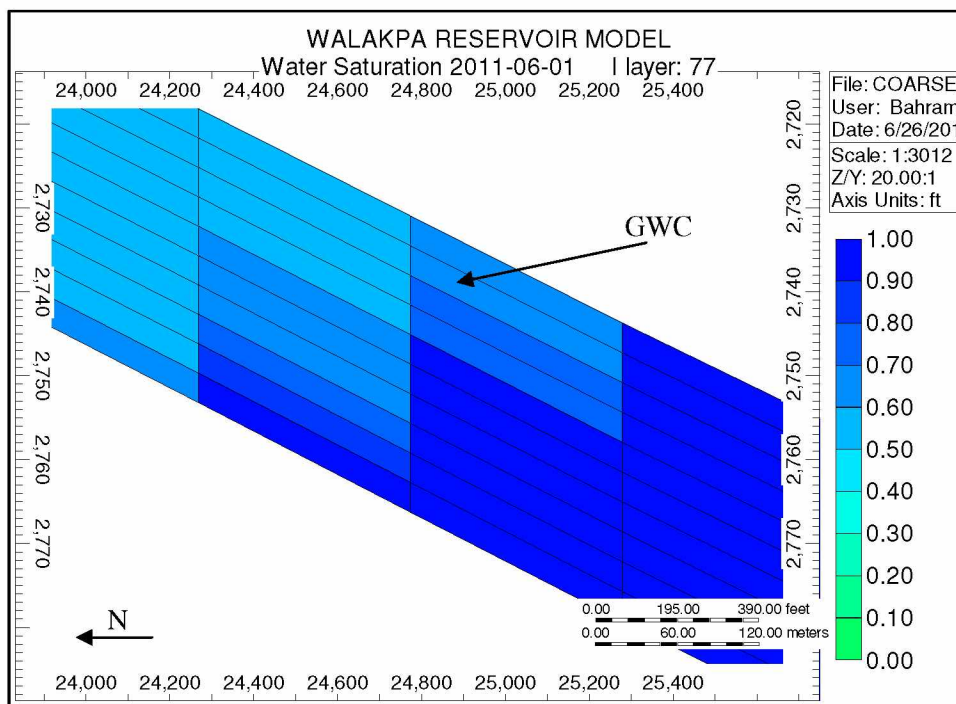


Figure 4.32: Current GWC and Water Saturation – JK Plane View

### 4.1.3 New Walakpa Wells

Four planned horizontal wells were incorporated to the model successfully. Well locations were recalculated from given X and Y coordinates into the CMG grid block system. All wells were completed according to the well plans taking into consideration the appropriate completion lengths. A snapshot of the reservoir with new wells is provided in Figure 4.33. In order to display the completion, reservoir transparency was set to 30% and gridlines were switched off.

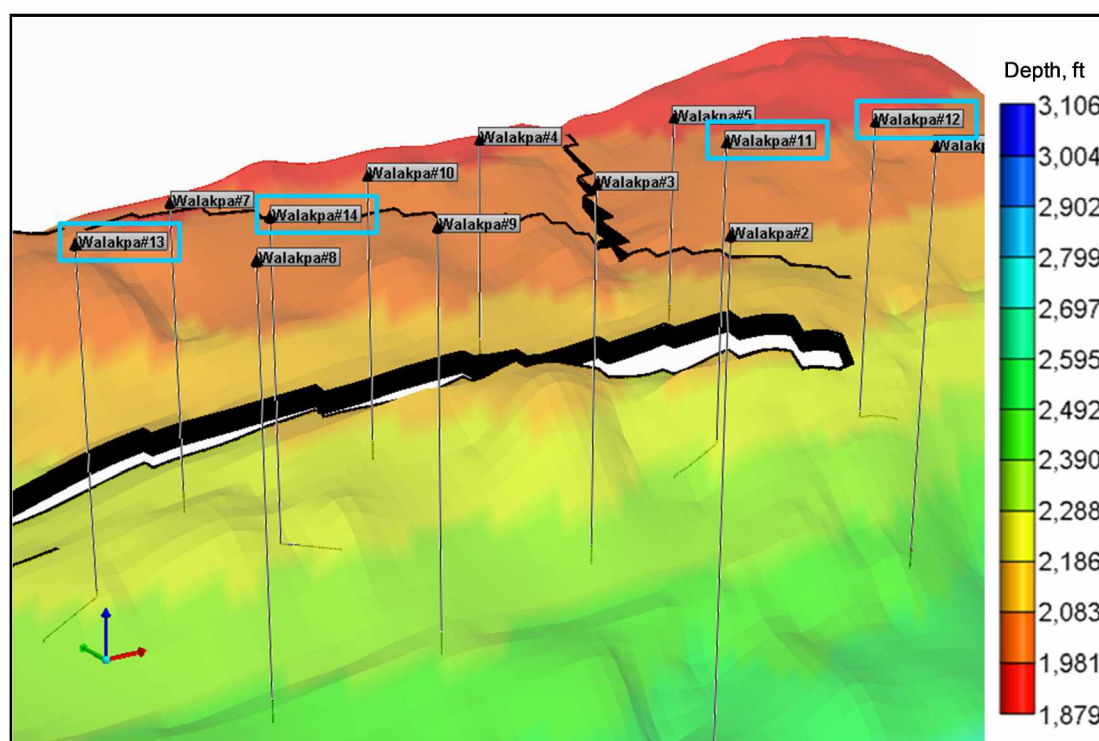


Figure 4.33: New Horizontal Wells in Walakpa Reservoir (Outlined in Blue)



#### 4.1.4 Forecasting Study

Production forecasting was performed for two cases. Both cases were run for 20 years, from present day to 1-Jun-2031. The first case involved only the existing vertical wells. A cumulative production profile for this case was obtained from the simulation and is displayed in Figure 4.34. It shows ultimate production of 54.85 Bcf.

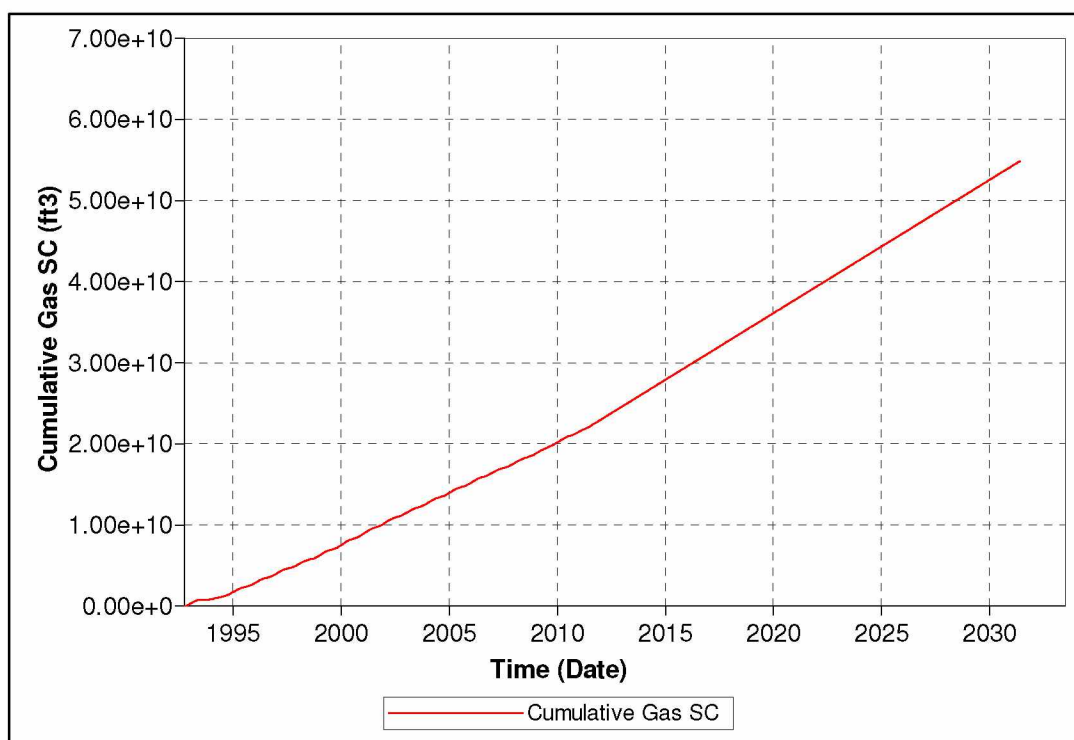


Figure 4.34: First Case Cumulative Gas Production (only existing wells), ft<sup>3</sup>

The second forecasting case involved existing vertical wells and four new horizontal wells. Since a start date for production from the new wells is unknown, the wells were modeled as starting production on 1-Sep-2011. This case was also run till 1-Jun-2031. A production rate of 0.7 MMscfd was assumed for each horizontal well. Resulting ultimate production for the second case comprised 74.60 Bcf (Figure 4.35).

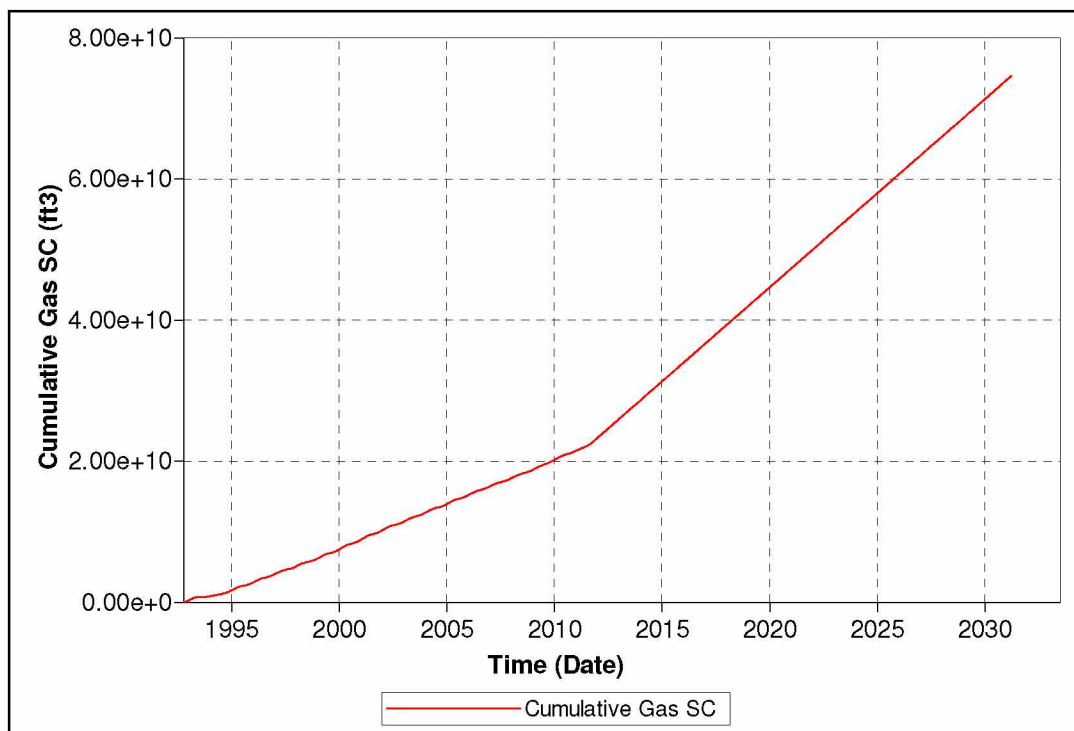


Figure 4.35: Second Case Cumulative Gas Production incorporating all existing wells and four planned wells, ft<sup>3</sup>

Forecasting simulation runs are summarized and compared with production to date (1-Jun-2011) in Table 4.1.

Table 4.1: Summary of Production Simulation for Walakpa Field

	Cumulative Gas Production, Bcf	Gas Recovery, %	Cumulative Water Production, bbl
Production to date (until 1-Jun-2011)	21.98	3.78	84
9 Wells Forecast (until 1-Jun-2031)	54.85	9.42	212
With New Wells (until 1-Jun-2031)	74.60	12.82	297

#### 4.1.5 Horizontal Permeability

Vertical permeability ( $k_v$ ) was assumed equal to horizontal permeability ( $k_h$ ) in both models ( $k_v = k_h$ ), (Singh, 2008). However, such assumption was made due to limited amount of well data. Vertical permeability ( $k_v$ ) tends to be lower than horizontal due to depositional phenomena. The difference can be quite significant. To assess the impact of aforementioned assumption several runs of East Barrow field simulation model were performed varying the value of  $k_v/k_h$ . Six values of  $k_v/k_h$  were assumed.

The impact of difference in  $k_v/k_h$  on cumulative production is displayed in Figure 4.36. The difference between the highest cumulative production at  $k_v/k_h = 1$  and the lowest one at  $k_v/k_h = 0.1$  is equal to 35.26 MMscf. Taking into consideration almost 30 years of production, this difference can be regarded as fairly insignificant.

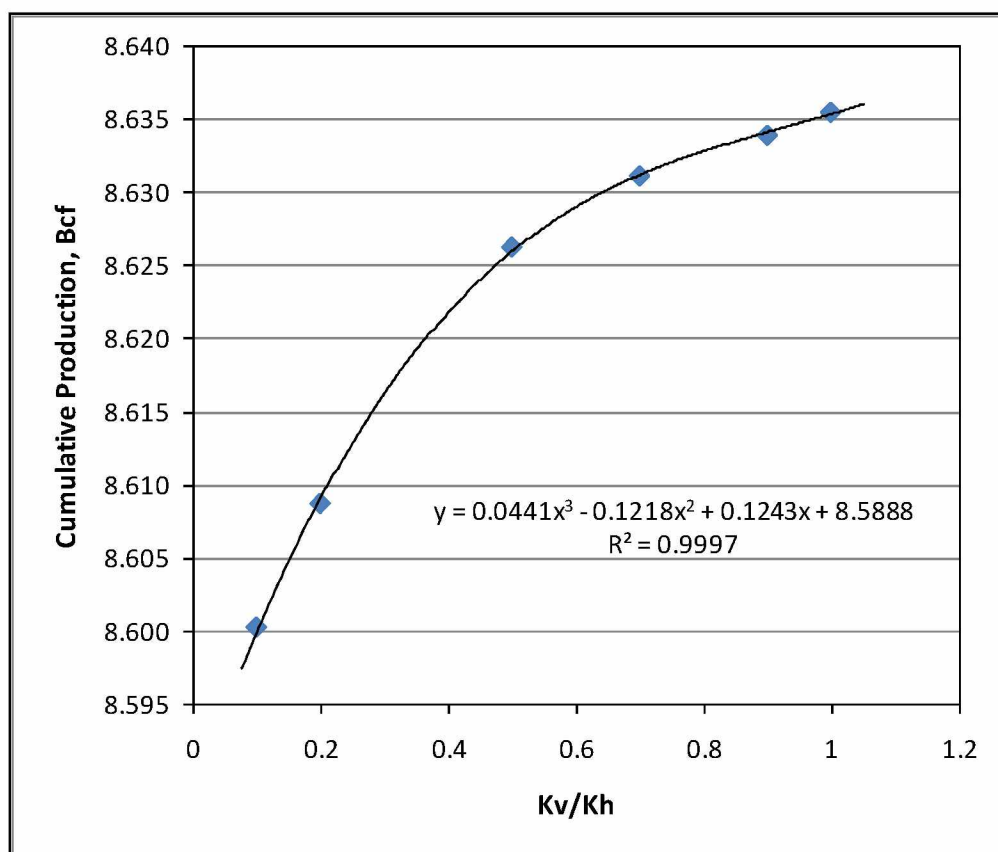


Figure 4.36: Dependence of Cumulative Production on  $k_v/k_h$

## 4.2 Well Choking Study

Well choking study was performed to assess production decline phenomena. The study is of key importance since higher production rates lead to sooner rate drop. Several scenarios were simulated and examined, of which three representative ones were selected and displayed in detail. Well production rates were the only difference between the scenarios.

In the first case, the well was producing constantly at a specified rate of 10 Mscfd for about 9.8 years when the rate dropped to as low as 80 scfd (Figure 4.37). Since no actions were assigned for the well in case of production drop, the well was kept open and the production rate gradually increased with time. The rate reached 5.7 Mscfd by the end of simulation (15 years).

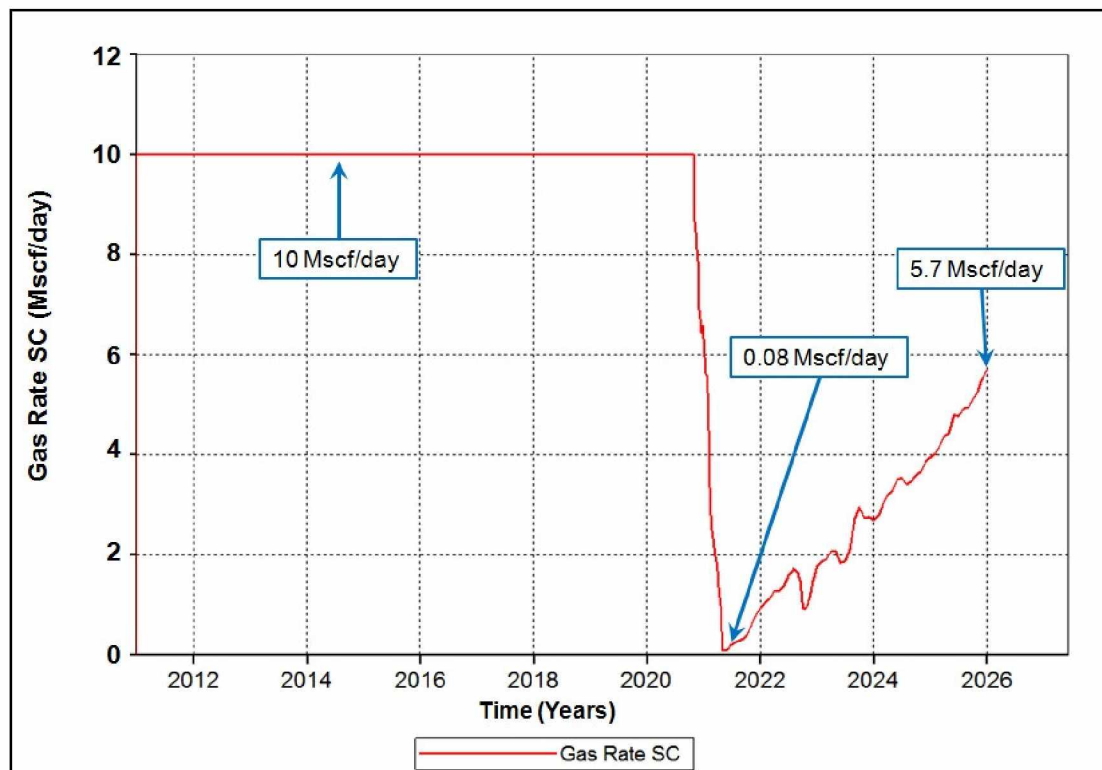


Figure 4.37: Production Profile for the First Case (10 Mscfd)

At the time of rate drop, an increase in hydrate saturation around the wellbore was observed (Figure 4.38). At first, hydrates started forming above the perforations, consistently occupying more pore space in a downward direction. At the moment of rate drop hydrates most likely obstruct fluid flow all around the wellbore. The distance from perforations to hydrate bond ranges between 5 ft and 10 ft.

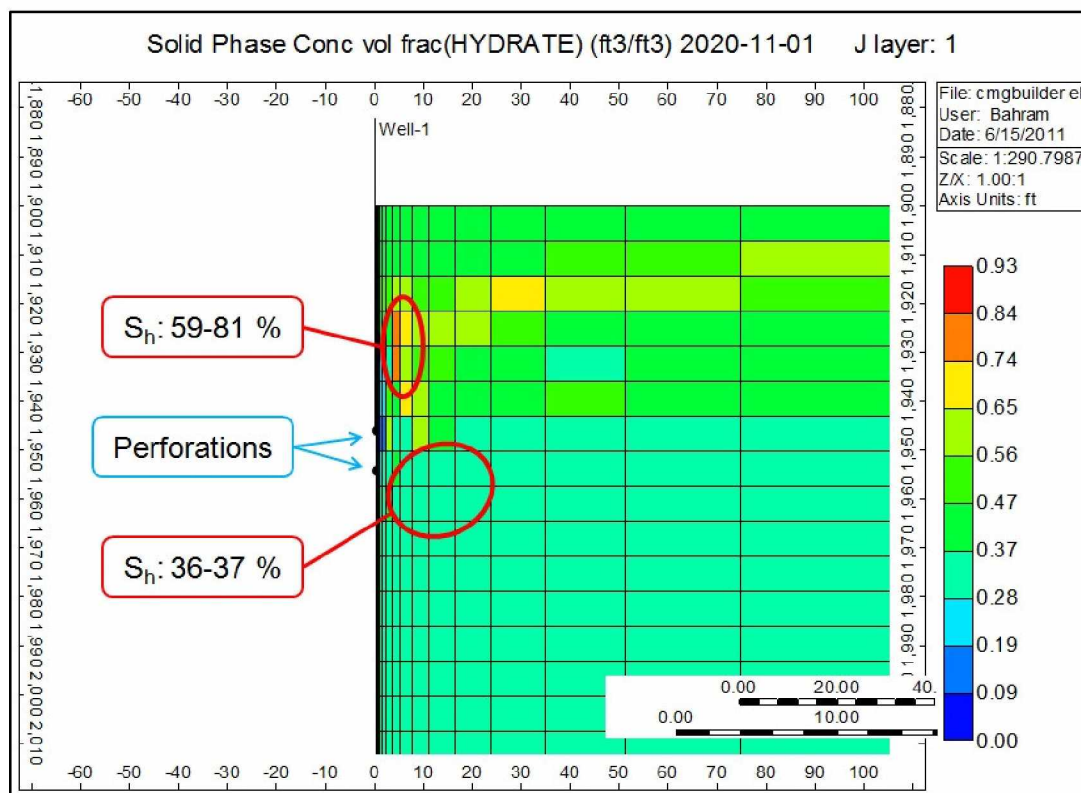


Figure 4.38: Hydrate Saturation ( $S_h$ ) After 9.8 Years of Production at 10 Mscfd

For the second case, gas production rate was increased threefold to 30 Mscfd. In this case the well died faster after 5.8 years of constant production at the specified rate (Figure 4.39). The rate dropped first to 1.6 Mscfd, and in several months to even 0.7 Mscfd. In this case as well as in the previous one, the well was kept open. The rate started to increase gradually, ending up at a value of 13.1 Mscfd by the end of simulation (15 years).

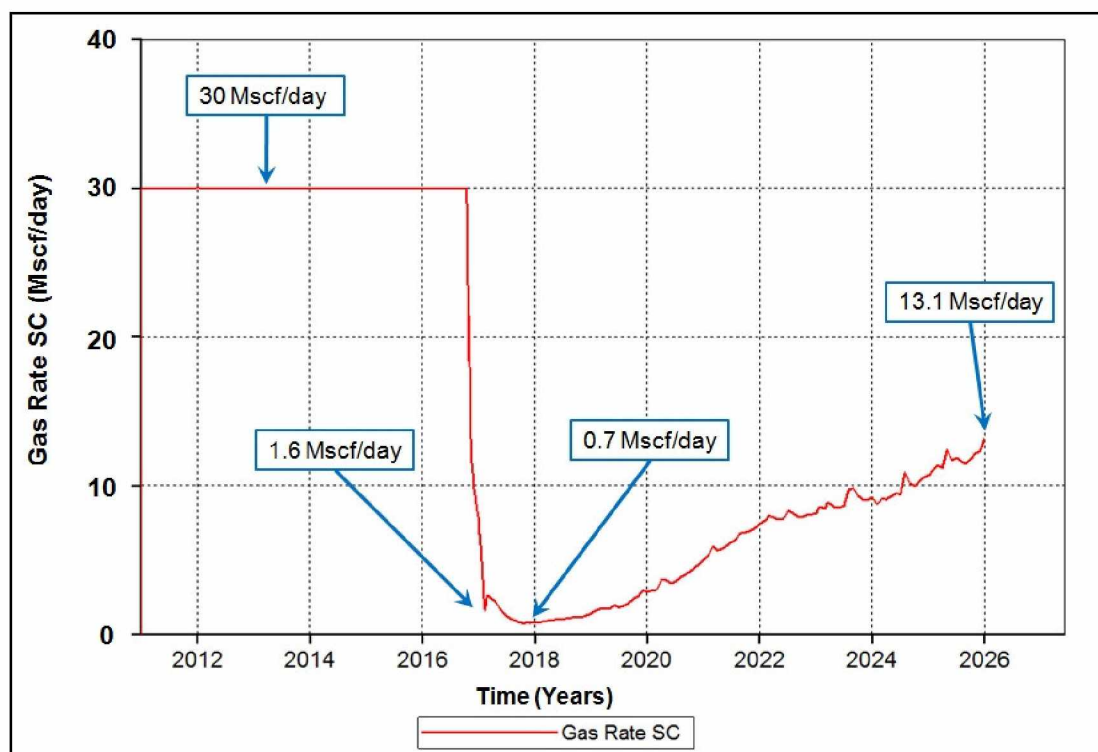


Figure 4.39: Production Profile for the Second Case (30 Mscfd)

The gas hydrate bond around the well formed faster in the second case (Figure 4.40), which could possibly be explained by the Joule-Thompson effect taking place more intensively due to faster dissociation. The bond also formed around the wellbore more uniformly than in the first case.

In the third scenario, well rate was increased to 100 Mscfd which led to even more rapid choking. The well produced at initial rate for 3.2 years before production rate declined to 0.17 Mscfd (Figure 4.41). Similar to previous cases, the well remained open and kept producing at low rate with only slight increase. By the end of simulation the production rate reached 11.3 Mscfd.

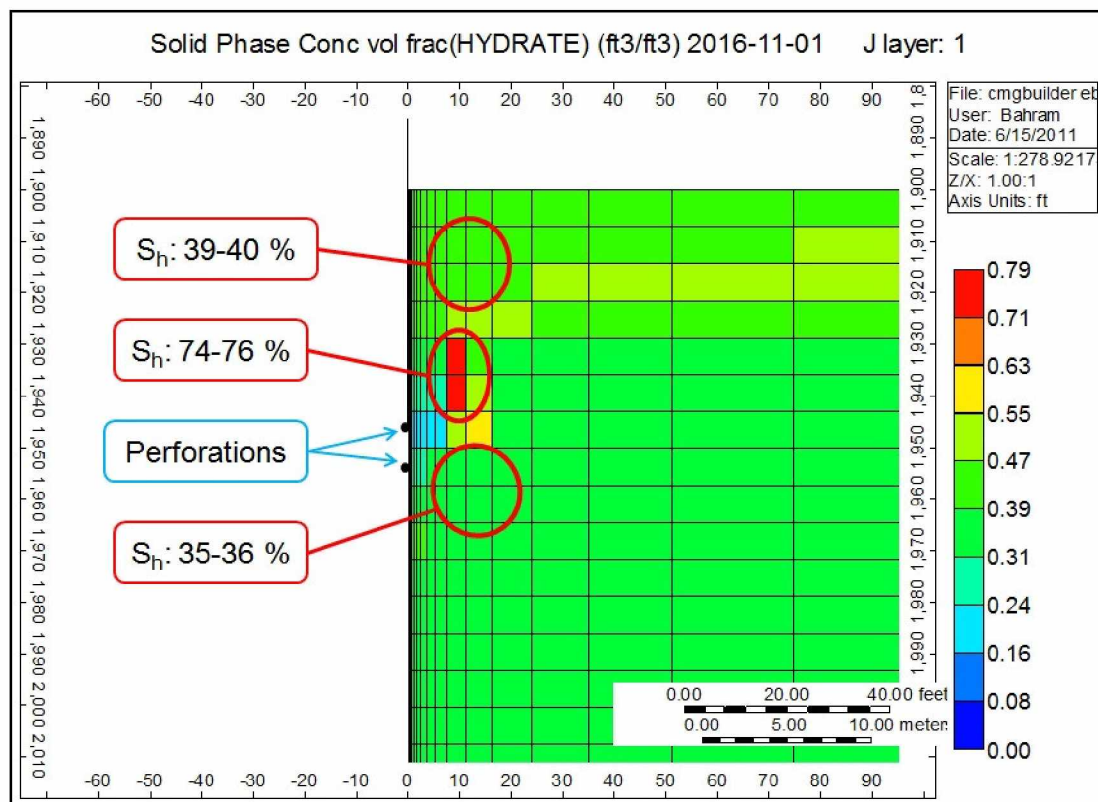


Figure 4.40: Hydrate Saturation ( $S_h$ ) After 5.8 Years of Production at 30 Mscfd

In this case hydrates formed around perforations had the most uniform distribution (Figure 4.42). A conclusion was made that the hydrate bond distribution around the wellbore is rate-controlled. Hydrate bond distance from the well was close to 10 ft, analogous to other cases.

Generally all three cases showed hydrate reformation around the wellbore. Longer production at constant rate required smallest rate value. However, it surely impacted the cumulative gas production. At higher flow rate substantially more gas is being produced, even though the well rate declines earlier.

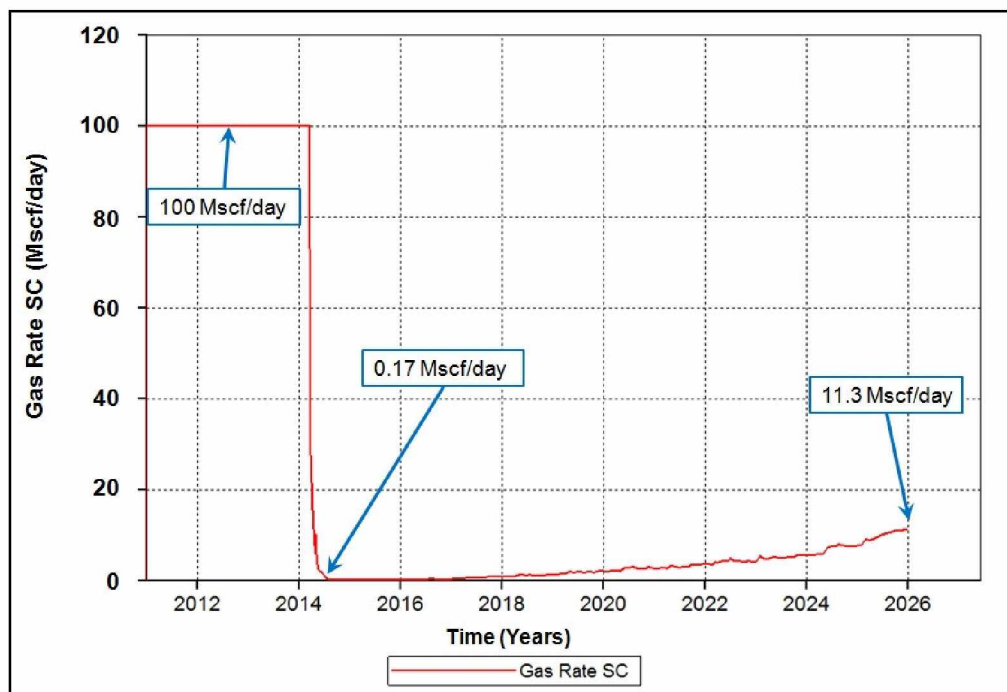


Figure 4.41: Production Profile for the Third Case (100 Mscfd)

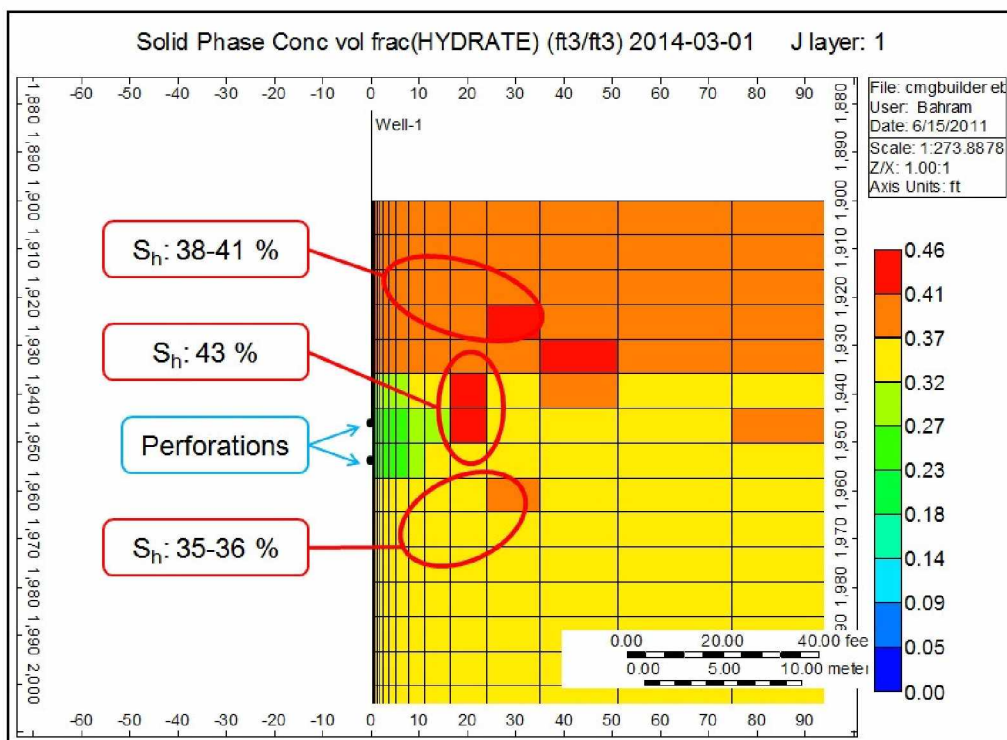


Figure 4.42: Hydrate Saturation ( $S_h$ ) After 3.2 Years of Production at 100 Mscfd



In all cases after production rate drops with choking, it starts to increase gradually. It is likely happening as a result of reformed gas hydrate dissociation taking place in radial direction around the completed interval. Radial direction of dissociation front could explain the progressive flow rate growth. Gas flow rate could possibly approach some optimum value at which the well produces steadily.

Cumulative production of the three cases plotted on Figure 4.43 clearly shows that the third case before the choking produces more gas than the other two throughout the simulation time (15 years).

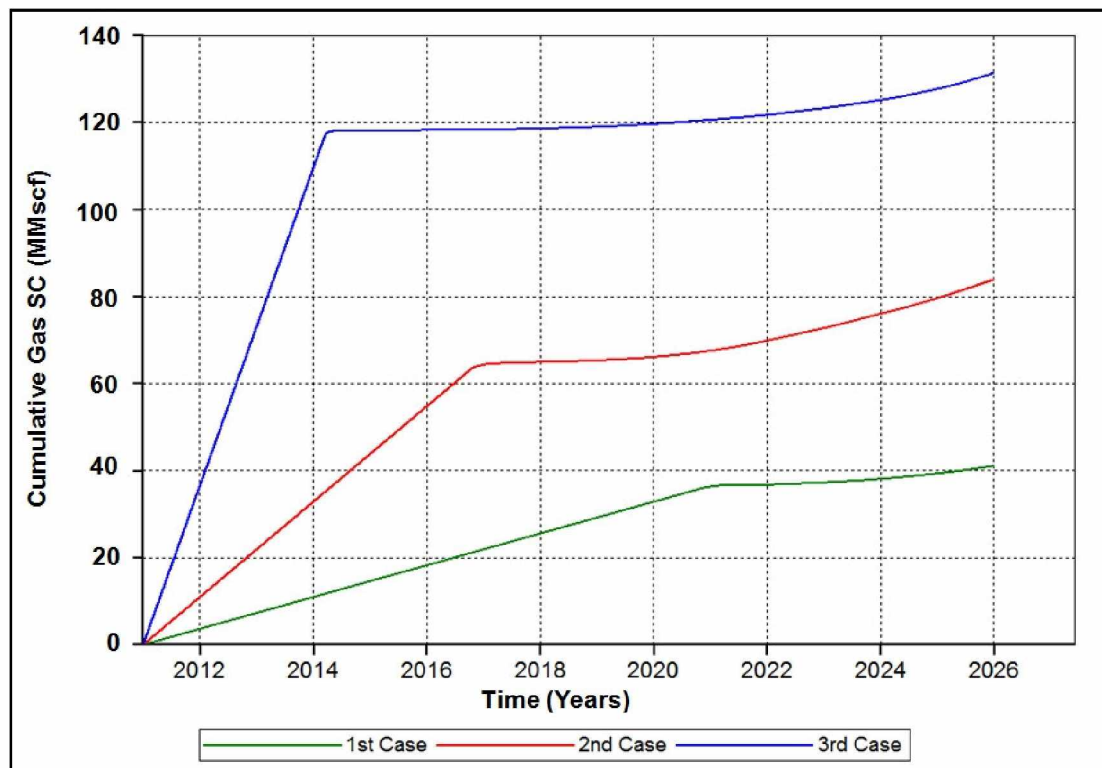


Figure 4.43: Cumulative Production Comparison of All Three Cases

A representative grid block (10, 1, 7) adjacent to the wellbore was selected to assess gas hydrate stability according to pressure and temperature (Figure 4.44). Five well rates were selected: 1, 10, 30, 60, and 100 Mscfd respectively. The rates of 1 and 60 Mscfd were selected in addition to previously described rates to get the better picture and fill possible gaps. Pressure and temperature in the representative grid block were recorded

for all the cases at the moment of the highest rate case choking (3.2 years). Obtained points were plotted on the chart along with hydrate equilibrium curve developed by Singh (2008) (Figure 4.45).

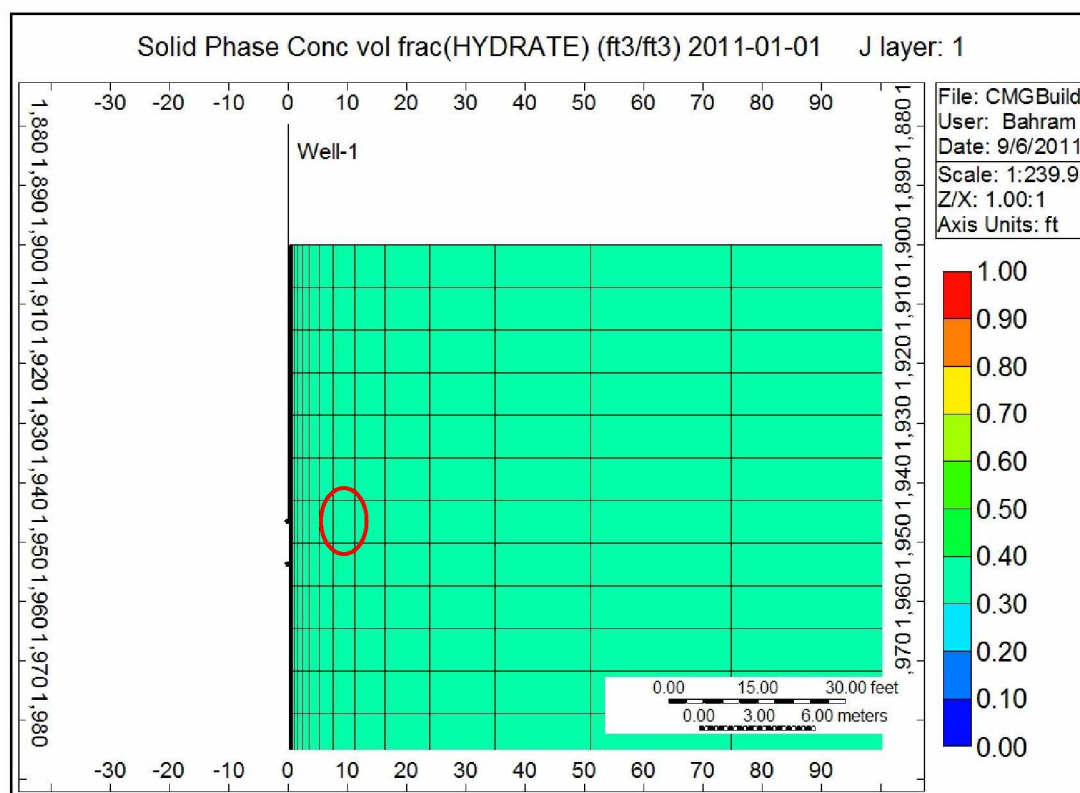


Figure 4.44: Representative Grid Block (10, 1, 7)

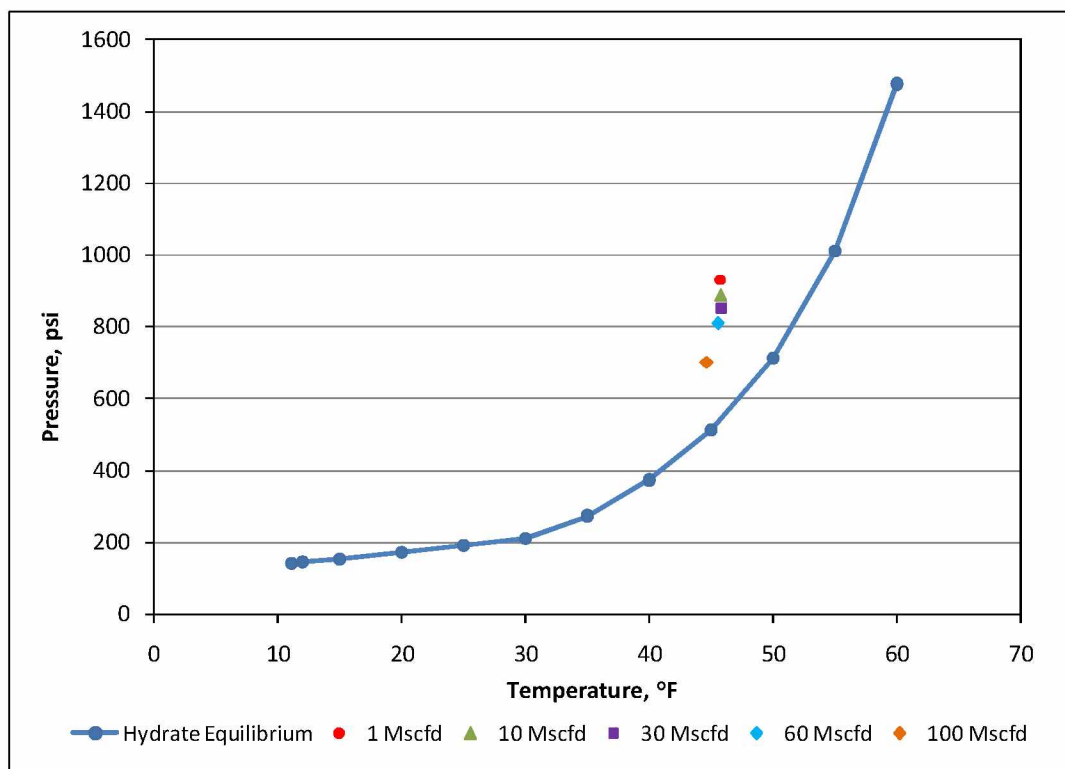


Figure 4.45: Hydrate Equilibrium Curve

According to Figure 4.45, all the points fall into hydrate stability region. It means that gas hydrates should be present in all of the cases which is consistent with the study results.

This study was performed to assess the reason of production decline in the BGF. The simplest way to overcome well choking is further depressurization. Well stimulation could be another, yet more expensive solution.

## 5. CONCLUSIONS AND RECOMMENDATIONS

### 5.1 Conclusions

#### 5.1.1 BGF Reservoir Simulation

Existing gas hydrate reservoir simulation models were successfully rebuilt and modified according to hydrate specification procedures. Reactions were specified with all required coefficients and appropriate parameters. Some reservoir property initializing formulas were redefined. Hydrate specification adequacy was properly tuned up via sensitivity studies for both models. They were updated with the latest production data, and production was simulated. It was observed that with gas hydrate dissociation, released water tends to drop off whereas gas occupies the upper portion of the pore space.

##### *5.1.1.1 East Barrow Gas Field*

Some portion of hydrates initially existing within the field dissociated with production, however, hydrates were still present in considerable amounts, especially in the middle layers of the field. Gas being released from hydrates accumulated in the upper layers of the field. Swept gas–water contact moved about 10 ft in vertical direction displacing free gas. Temperature increasing across the field implies further hydrate dissociation and gas release. Pressure in the upper portion of the field has decreased which is also favorable for hydrate dissociation.

##### *5.1.1.2 Walakpa Gas Field*

Having large gas reserves, the Walakpa field is capable of long-term production and extensive development. Due to this fact the field requires detailed study. The field has a very strong aquifer that caused reservoir pressure decline to be quite low, even after 19 years of production. The forecasting study for the Walakpa field showed negligible rate decline. Fluid contacts, both hydrate–gas contact and gas–water contact, shifted by 10 ft in vertical direction. Preliminary runs estimated reserves to be sufficient for another 100 years. However, there were limited data available while building the model. Drilling the new wells could contribute significantly to model improvement. Four horizontal wells to

be drilled in the field were successfully initialized. Since logical limitations of new horizontal well flow rates are still unknown, they were assigned to produce at 0.7 MMscfd. They were also accounted for in the production forecasting.

### **5.1.2 Well Choking Study**

A simplistic simulation model was built for the study. The three cases considered for the test showed hydrates forming in the near-wellbore zone. With a higher production rate, hydrates appeared to form more uniformly and faster around the perforations. After the blockage, wells continued low production with gradual increase in flow rate. In all of the cases, the rate did not stabilize by the end of simulation, probably because it was approaching a certain rate value adequate for the model. Volumetric limitations of the model likely prevented rate stabilization to be observed.

## **5.2 Recommendations**

- a. BGF simulation models could be updated with more precise relative permeability data. This would require detailed laboratory experiments on field core samples.
- b. East Barrow field gas production could be increased by bringing the existing wells online. This could be performed in stepwise well-by-well manner, letting gas hydrates which previously reformed around the wellbores gradually dissociate. This proposal is supported by the results of well choking study. It is likely the most economical way to obtain incremental gas production.
- c. In order to achieve more realistic simulation and improve history matching, more data would be required for the Walakpa simulation model. This could be accomplished by using data from the new horizontal wells. Reservoir properties that require adjustment would be absolute permeability and fluid saturations. Temperature data obtained from the new wells would also help to understand thermal dynamics of the field.

- d. Assessment of horizontal well capabilities is important for improved production forecasting. Actual flow rates of the new horizontal wells would give a better picture in general.
- e. Short-term well shut-ins could prevent hydrate formation in the near-wellbore zone by letting formation pressure and temperature stabilize. If shut-ins are not possible, reductions of rate could delay the choking effect substantially.
- f. Well choking, including the possibility of horizontal well choking, should be studied in more detail. Various reservoir properties should be considered in order for researchers to understand the process deeply, beyond the limitations of the used model.

## REFERENCES

- Collett, T. S. and Ehlig-Economides, C. A. Detection and Evaluation of the In-Situ Natural Gas Hydrates in the North Slope Region, Alaska. SPE Paper No. 11673, [www.onepetro.org](http://www.onepetro.org), 1983.
- Evernos, A. I., Heathman, J., Ralstin, J. Impermeation of Porous Media by Forming Hydrates In Situ. SPE Paper No. 2881, [www.onepetro.org](http://www.onepetro.org), September 1971.
- Glenn, R.K. and Allen, W.W. Geology, Reservoir Engineering and Methane Hydrate Resource Potential of the Walakpa Gas Field, North Slope Alaska. Final Technical Report (Under Grant DE-FG21-91MC28131) Submitted to the USDOE, Morgantown Energy Technology Center, Morgantown, WV, 1991, 26p.
- Godbole, S. P., Kamath, V. A., Ehlig-Economides, C. A. Natural Gas Hydrates in the Alaskan Arctic. SPE Paper No. 13593, [www.onepetro.org](http://www.onepetro.org), 1988.
- Jaiswal, N. Measurement of Gas-Water Relative Permeabilities in Hydrate Systems. M.S. Thesis, University of Alaska Fairbanks, Fairbanks, Alaska, August 2004.
- Katz, D. L. Depths to Which Frozen Gas Fields (Gas Hydrates) May Be Expected. SPE Paper No. 3061, [www.onepetro.org](http://www.onepetro.org), April 1971.
- Klauda, J. B. and Sandler, S. I. Global Distribution of Methane Hydrate in Ocean Sediment. *Energy & Fuels*, vol. 19, 2005, pp. 459-470.
- Kvenvolden, K. A. Gas Hydrates – Geological Perspective and Global Change. *Reviews of Geophysics*, vol. 31, 2, May 1993, 173-187 pp.

- Maekawa, T. Equilibrium Conditions for Gas Hydrates of Methane and Ethane Mixtures in Pure Water and Sodium Chloride Solutions. *Geochemical Journal*, Vol. 35, 2001, pp. 59-66.
- Makogon, Y. F., Holditch, S. A., Makogon, T. Y. Natural Gas-Hydrates – A Potential Energy Source for the 21st Century. *Journal of Petroleum Science and Engineering*, vol. 56, 2007, pp. 14-31.
- Makogon, Y. F. Perspectives for the Development of Gas-Hydrate Deposits. 4th Canadian Permafrost Conference, 1982, pp 299-304.
- Makogon, Y. F. "Razmeshenie Zalezhei, Soderzhashih Prirodnii Gaz v Plaste v Vide Gidratov" [Location of the Deposits Containing Natural Gas in Hydrate State within the Formations], "Tsentr Nauchno-Tehnicheskoi Informatsii Ministerstva Gazovoi Promishlennosti" [Scientific-Technical Information Center of the Ministry of Gas Industry], Moscow, 1966.
- Mehta, A. P. and Sloan, E. D. Structure H Hydrates: Implications for the Petroleum Industry. *SPE Journal*, Vol. 4, No. 1, 1999, pp. 3-8.
- Milkov, A. V. Global Estimates of Hydrate-Bound Gas in Marine Sediments: How Much Is Really Out There? *Earth-Science Reviews*, vol. 66, 2004, pp. 183-197.
- Miller, S. L. The Occurrence of Gas Hydrates in the Solar System. *Proceedings of the National Academy of Sciences*, Vol. 47, 1961, pp. 1798-1808.
- Moridis, G. J. and Collett, T. S. Gas Production from Class 1 Hydrate Accumulations. *Recent Advances in the Study of Gas Hydrates*. Taylor, C. and Qwan, J., Eds, Kluwer Academic New York, 2004, pp. 75-88.



- Moridis, G. J., Collett, T. S., Boswell, R., Kurihara, M., Reagan, M. T., Koh, C., Sloan, E. D. Toward Production From Gas Hydrates: Current Status, Assessment of Resources, and Simulation-Based Evaluation of Technology and Potential. SPE Paper No. 114163, [www.onepetro.org](http://www.onepetro.org), 2008.
- Panda, M. N. and Morahan, G. T. An Integrated Reservoir Model Description for East Barrow and Walakpa Gas Fields. Topical Report prepared under DoE Project No. DE-FC26-06NT42962 submitted to the USDOE, Morgantown, WV, [www.netl.doe.gov](http://www.netl.doe.gov), June 2008.
- Schulz, H. D. and Zabel, M. Marine Geochemistry, 2nd edition. Textbook, 2006, pp. 482-484.
- Singh, P. K. An Engineering Study to Investigate the Methane Hydrate Resource Potential Associated with the Barrow Gas Fields in Alaska. M.S. Thesis, University of Alaska Fairbanks, Fairbanks, Alaska, 2008.
- Stokes, P.J., Walsh, T.P., Walsh, C. Walakpa Field Reserve Study. Technical Report Submitted to the NSB, Barrow, Alaska, June 2005, 90p.
- Stokes, P.J. and Walsh, T.P. South and East Barrow Gas Fields Reserves Study. Technical Report Submitted to the NSB, Barrow, Alaska, July 2007, 36p.
- Worthington, P. F. Petrophysical Evaluation of Gas Hydrate Formations. SPE Paper No. IPTC 12610, [www.onepetro.org](http://www.onepetro.org), 2008.

## APPENDIX A. Fluid Component Properties

Three components were initialized in both EB and WAL simulation models: methane gas, water, and gas hydrate. Figure A.1 displays the component specification tool.

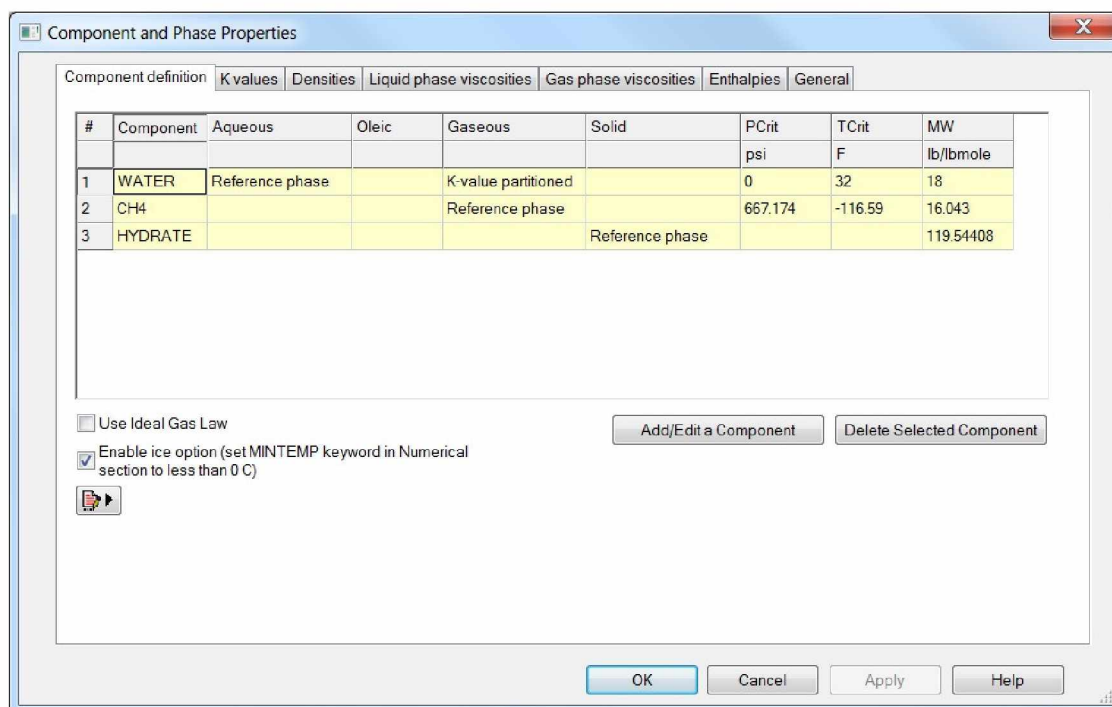


Figure A.1: Component Initialization

Hydrate dissociation (forward) reaction:  $1Hydrate \Rightarrow 5.75H_2O + 1CH_4$

Hydrate formation (backward) reaction:  $5.75H_2O + 1CH_4 \Rightarrow 1Hydrate$

Gas hydrate dissociation and formation reaction parameters are provided in Figures A.2 and A.3 respectively.

Reactions

Reaction: 1

Item	Default	Value
Reaction frequency factor (...)		1.097058e+13
Enthalpy (negative for end...)	0 Btu/lbmole	-22295.1255 Btu/lbmole
Activation energy (EACT)	0 Btu/lbmole	38546.9 Btu/lbmole
Burning zone temperature l...	44.6 F	
Burning zone temperature u...	3140.6 F	

Advanced

Reaction Rate

Deviation from Equilibrium...

Item	WATER	CH4	HYDRATE
	Aqueous	Gas	Solid
Reactant stoichiometry...	0	0	1
Product stoichiometry...	5.7501	1	0
Component reactants...	0	0	1
Reacting in phase ...	Not set/appli...	Not set/app...	Solid phase
Concentration fact...	<input type="checkbox"/>	<input type="checkbox"/>	<input type="checkbox"/>
Critical value of co...			

1 HYDRATE ==> 5.7501 WATER + 1 CH4  
 Reaction 1 has a mass balance error of 0.000301143 percent. To reduce positive error, increase reactant coefficients. To reduce negative error, increase product coefficients.

OK Cancel Apply Help

Figure A.2: Forward Reaction Initialization

Reactions

Reaction: 2

Item	Default	Value
Reaction frequency factor (...)		1.097058e+13
Enthalpy (negative for end...)	0 Btu/lbmole	22294.9 Btu/lbmole
Activation energy (EACT)	0 Btu/lbmole	38546.9 Btu/lbmole
Burning zone temperature l...	44.6 F	
Burning zone temperature u...	3140.6 F	

Advanced

Reaction Rate

Deviation from Equilibrium...

Item	WATER	CH4	HYDRATE
	Aqueous	Gas	Solid
Reactant stoichiometry...	5.75	1	0
Product stoichiometry...	0	0	1
Component reactants...	1	1	0
Reacting in phase ...	Water ph...	Gas pha...	Not set/a...
Concentration fact...	<input type="checkbox"/>	<input type="checkbox"/>	<input type="checkbox"/>
Critical value of co...			

5.75 WATER + 1 CH4 ==> 1 HYDRATE  
 Reaction 2 has a mass balance error of 0.000451718 percent. To reduce positive error, increase reactant coefficients. To reduce negative error, increase product coefficients.

OK Cancel Apply Help

Figure A.3: Backward Reaction Initialization

### APPENDIX B. Wellbore Diagrams of the Existing EB Wells

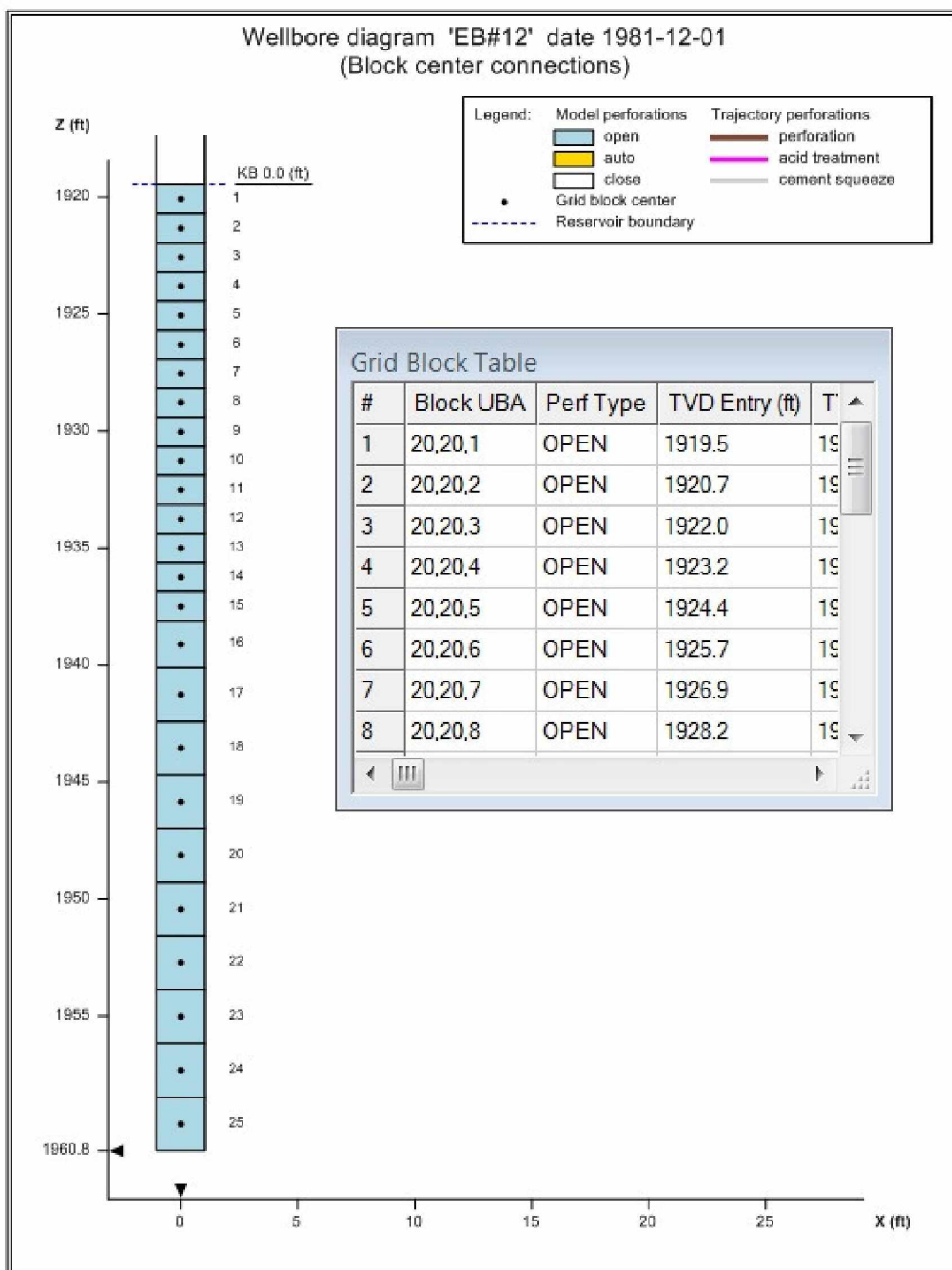


Figure B.1: Wellbore Diagram of EB #12

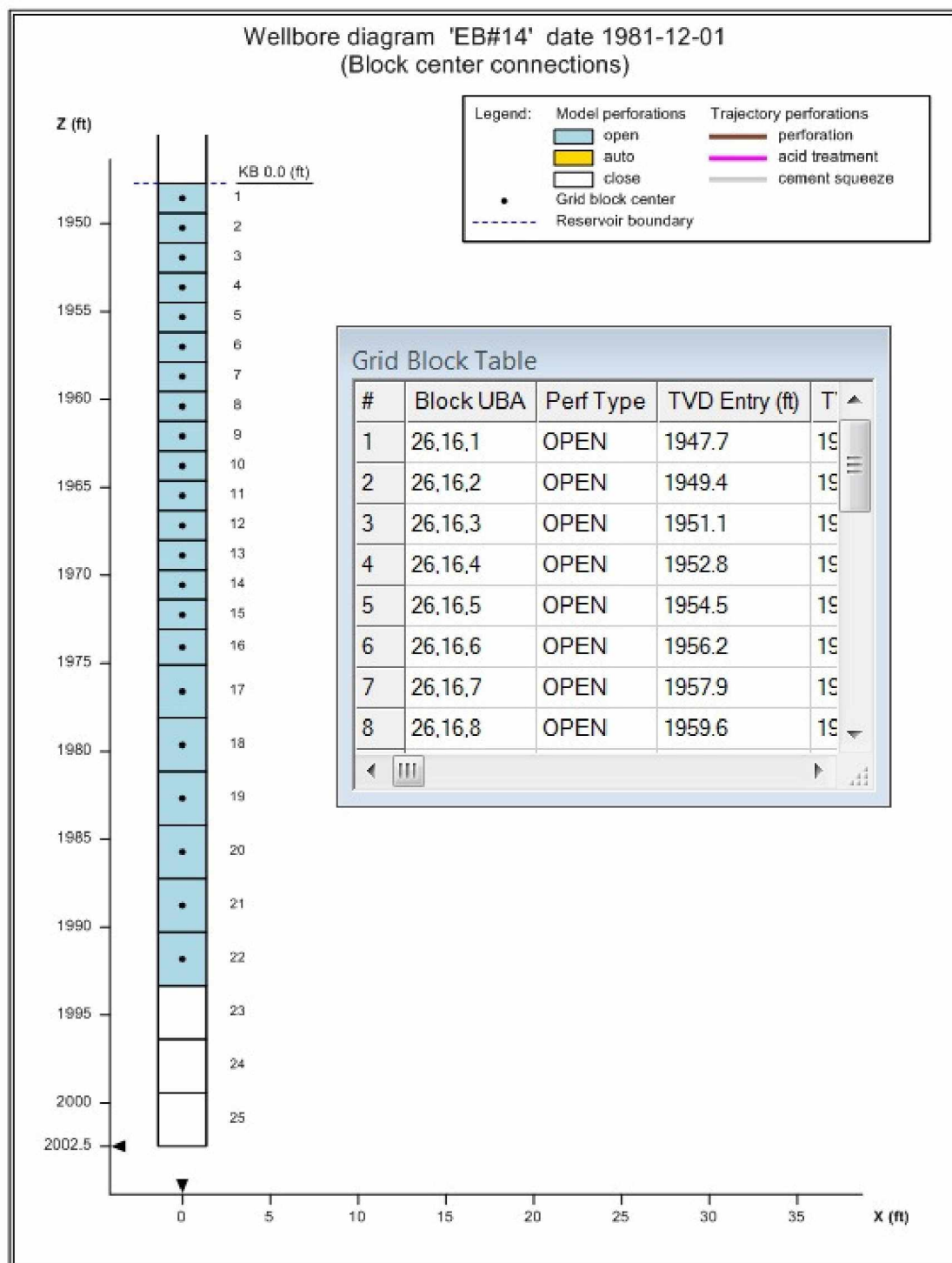


Figure B.2: Wellbore Diagram of EB #14

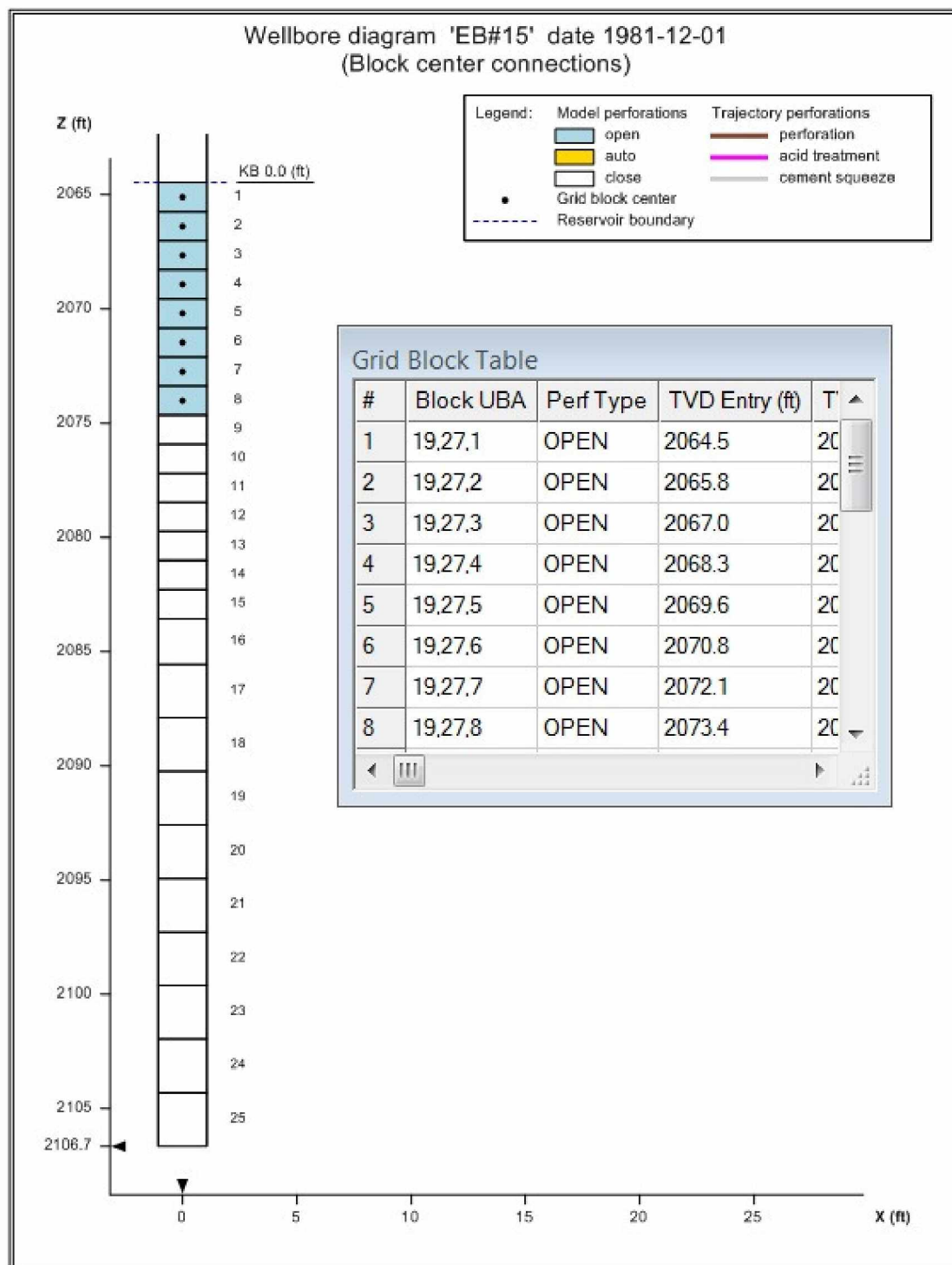


Figure B.3: Wellbore Diagram of EB #15

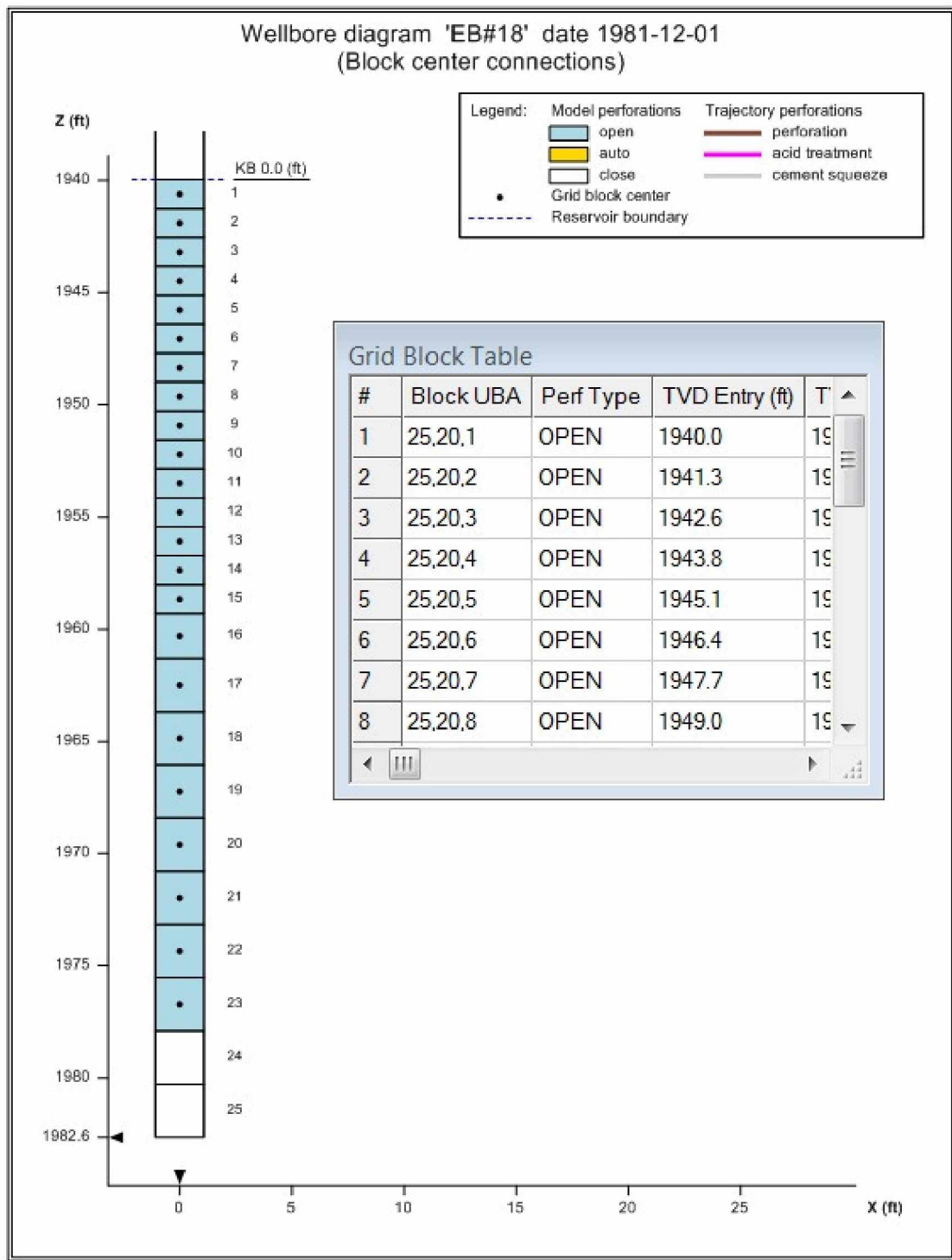


Figure B.4: Wellbore Diagram of EB #18

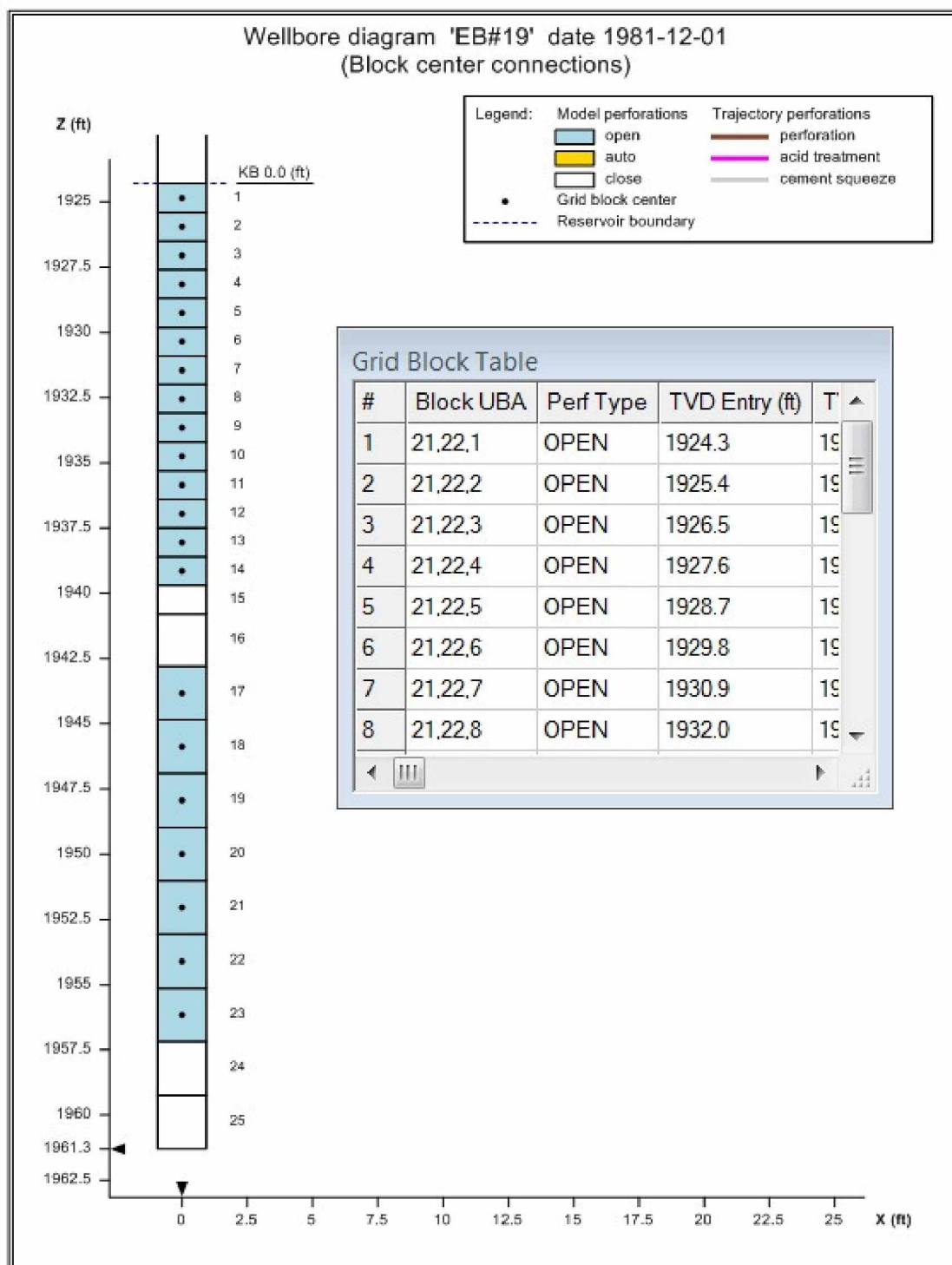


Figure B.5: Wellbore Diagram of EB #19



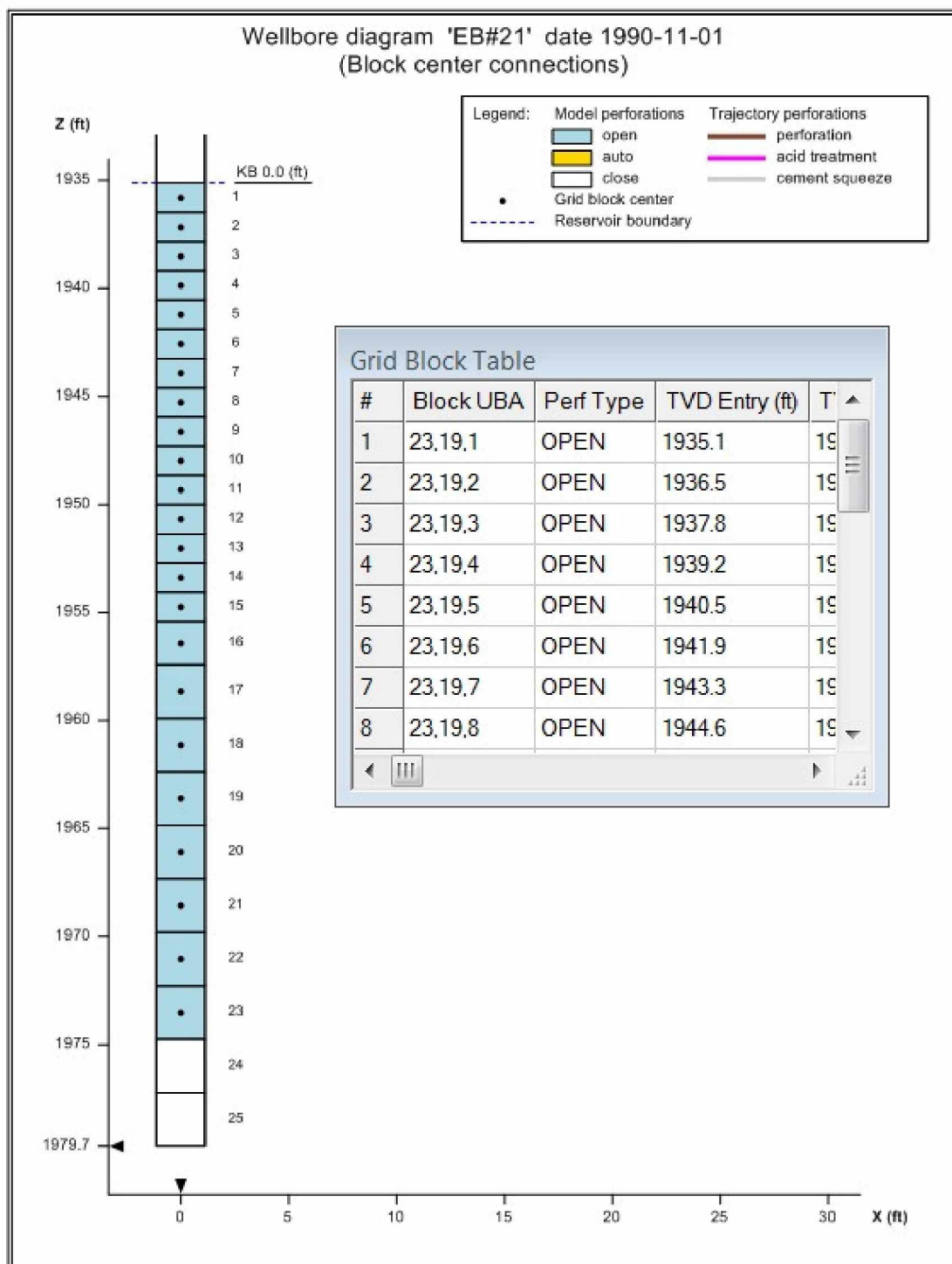


Figure B.6: Wellbore Diagram of EB #21

### APPENDIX C. Wellbore Diagrams of the Existing WAL Wells

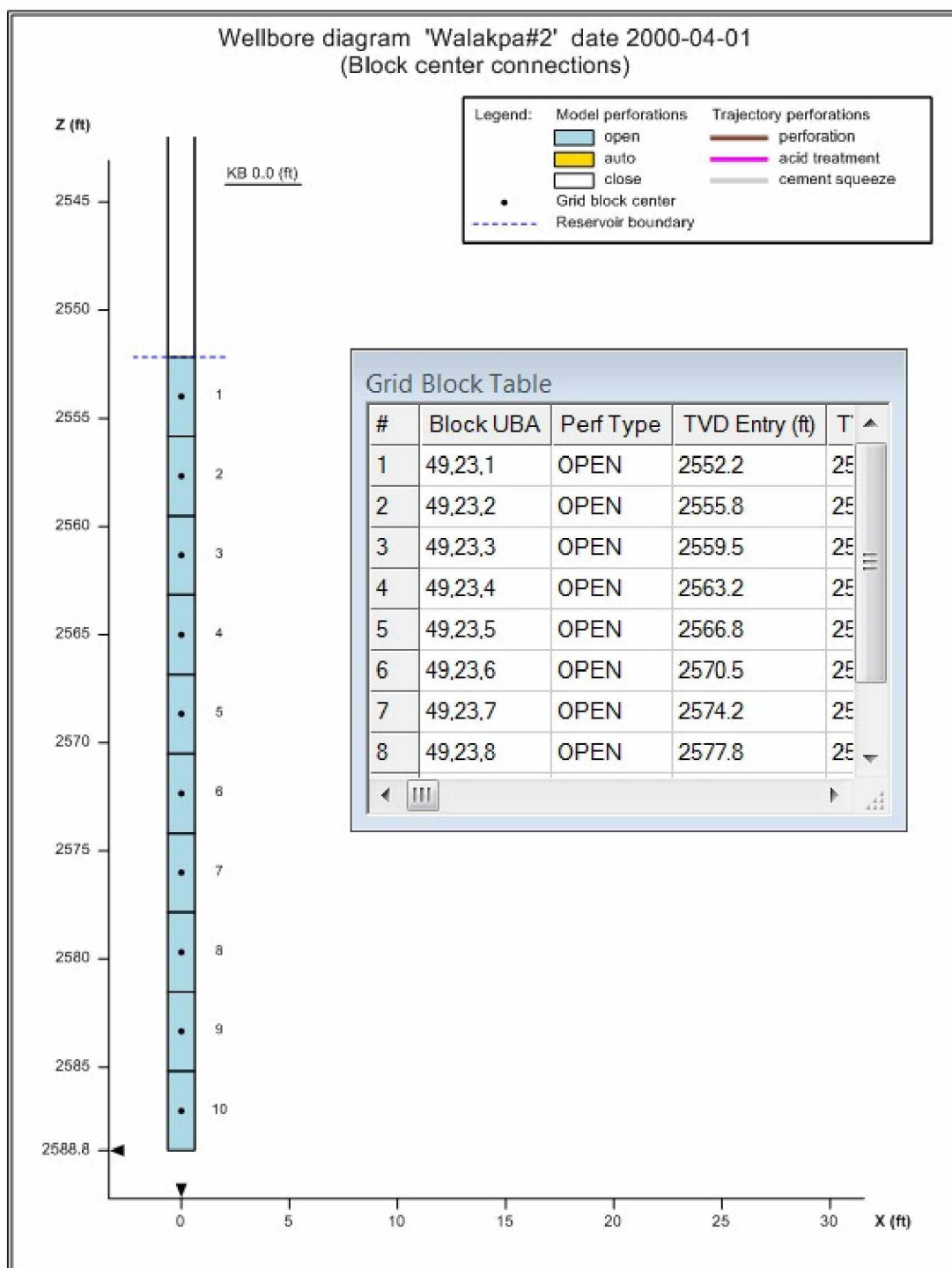


Figure C.1: Wellbore Diagram of WAL #2

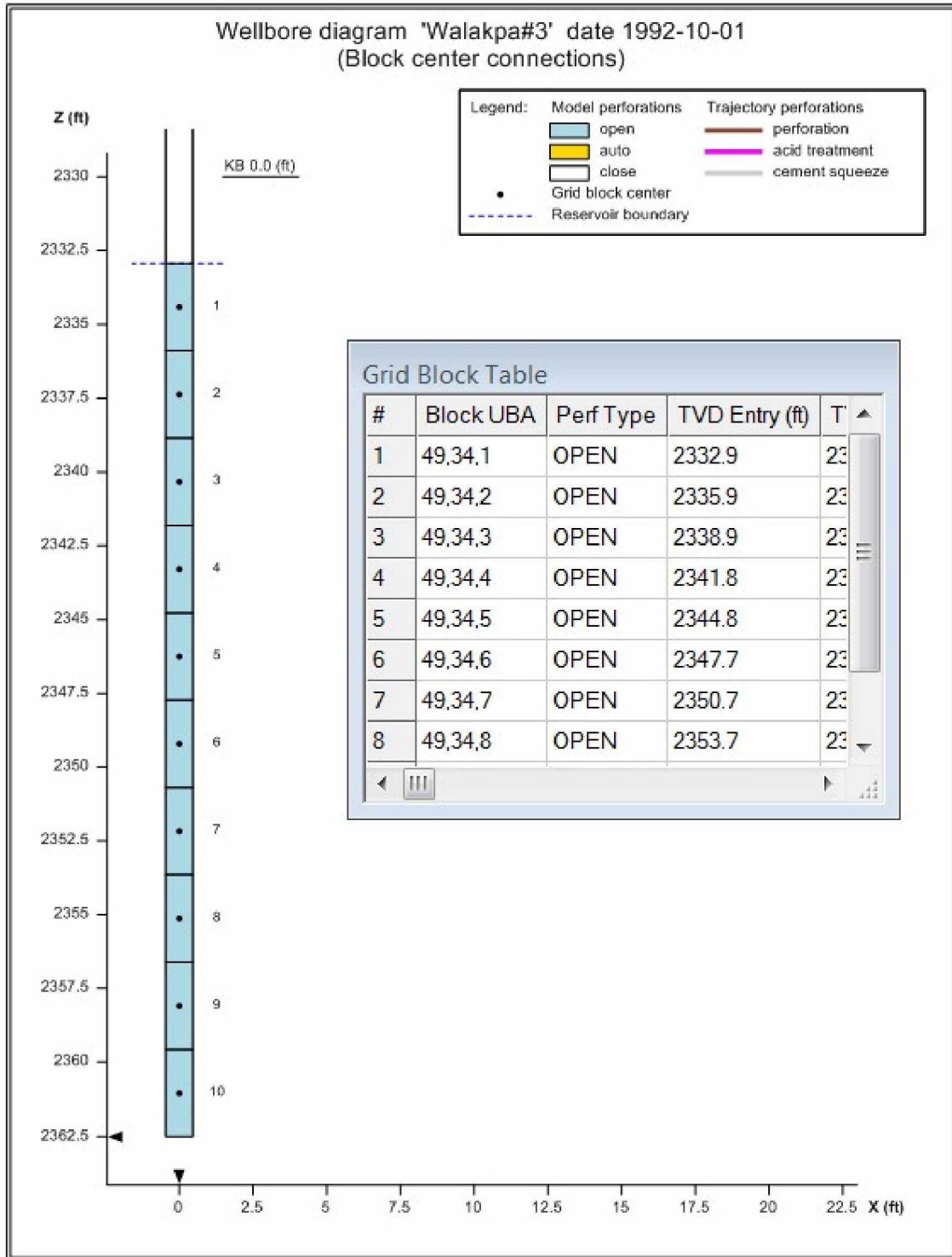


Figure C.2: Wellbore Diagram of WAL #3

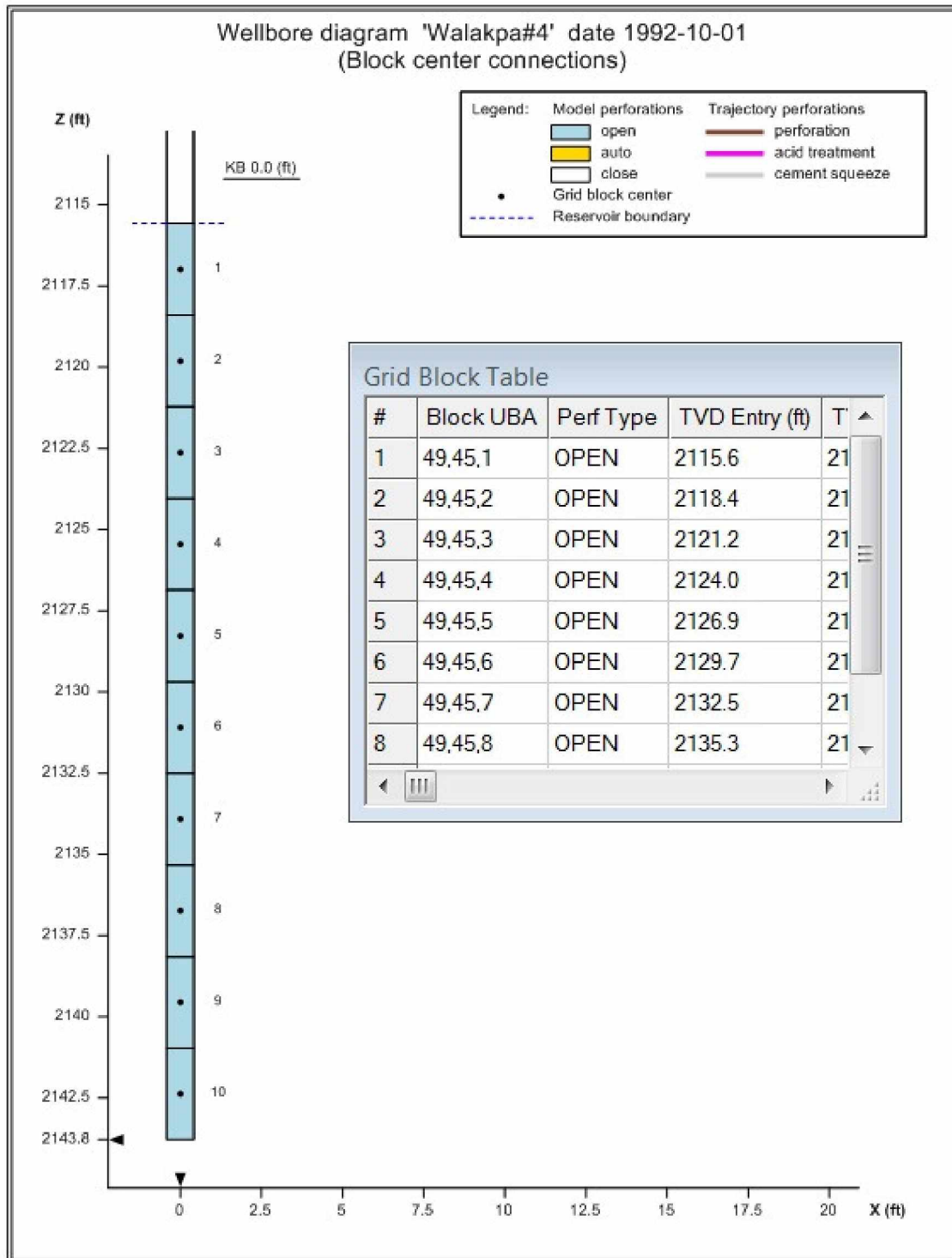


Figure C.3: Wellbore Diagram of WAL #4

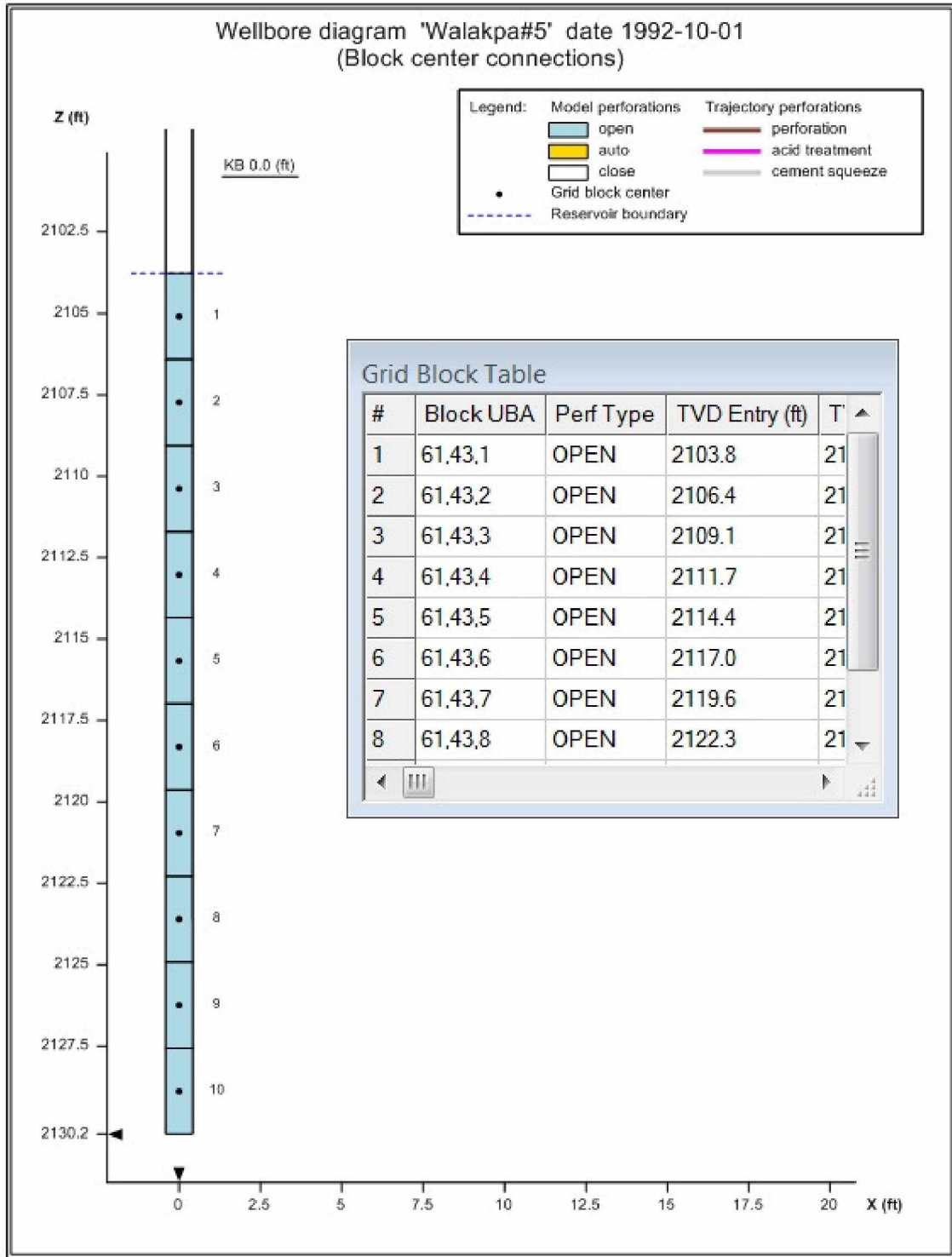


Figure C.4: Wellbore Diagram of WAL #5

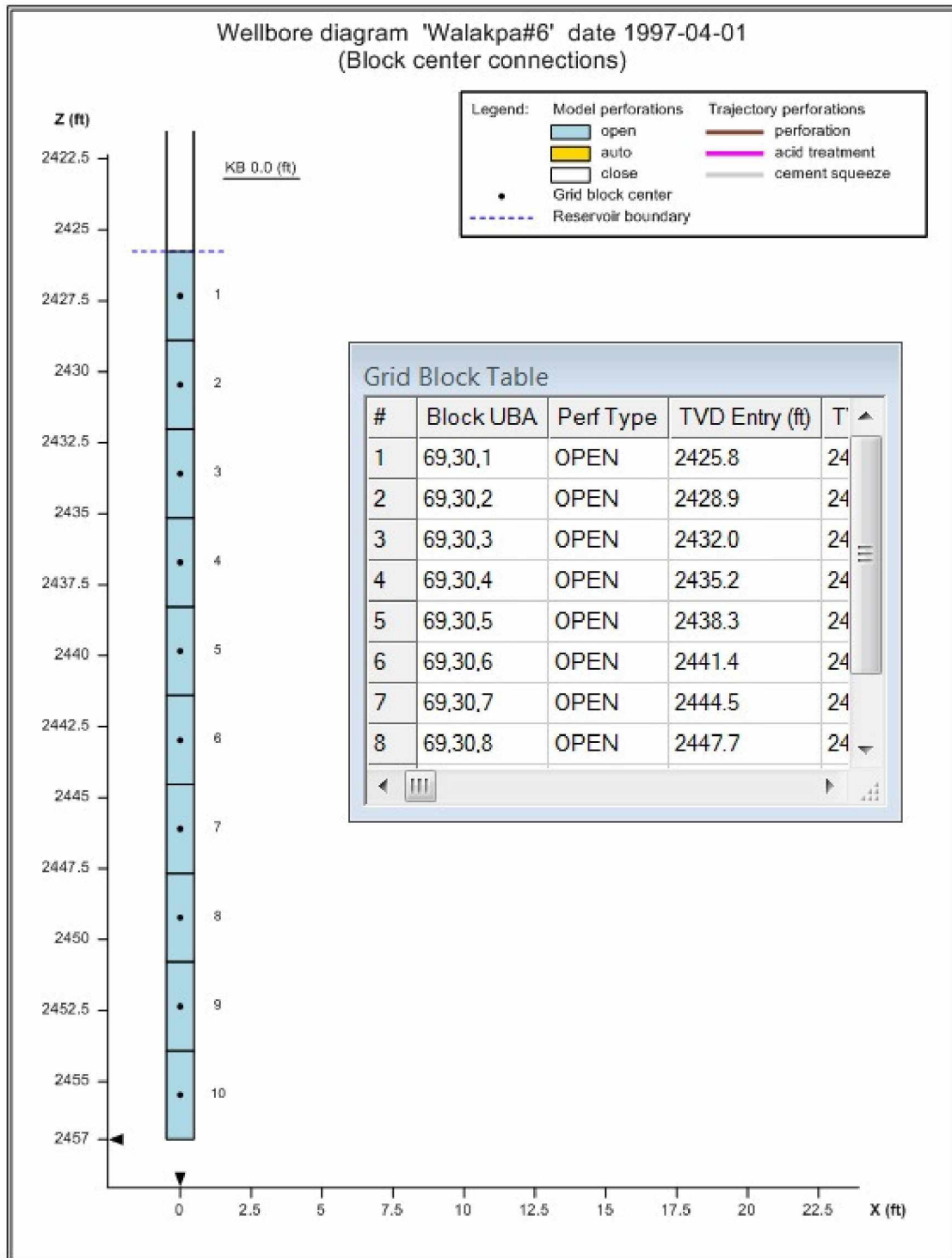


Figure C.5: Wellbore Diagram of WAL #6

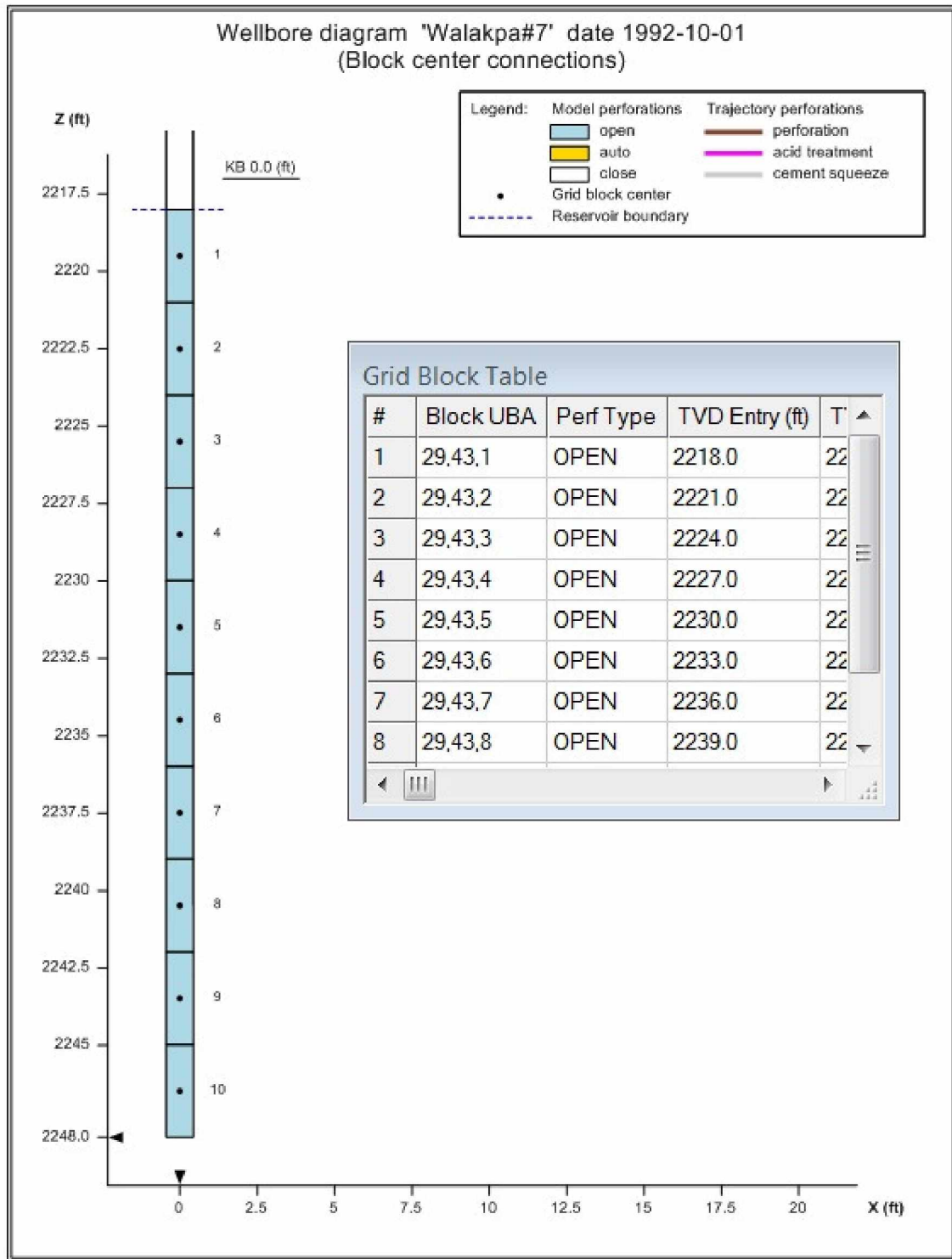


Figure C.6: Wellbore Diagram of WAL #7

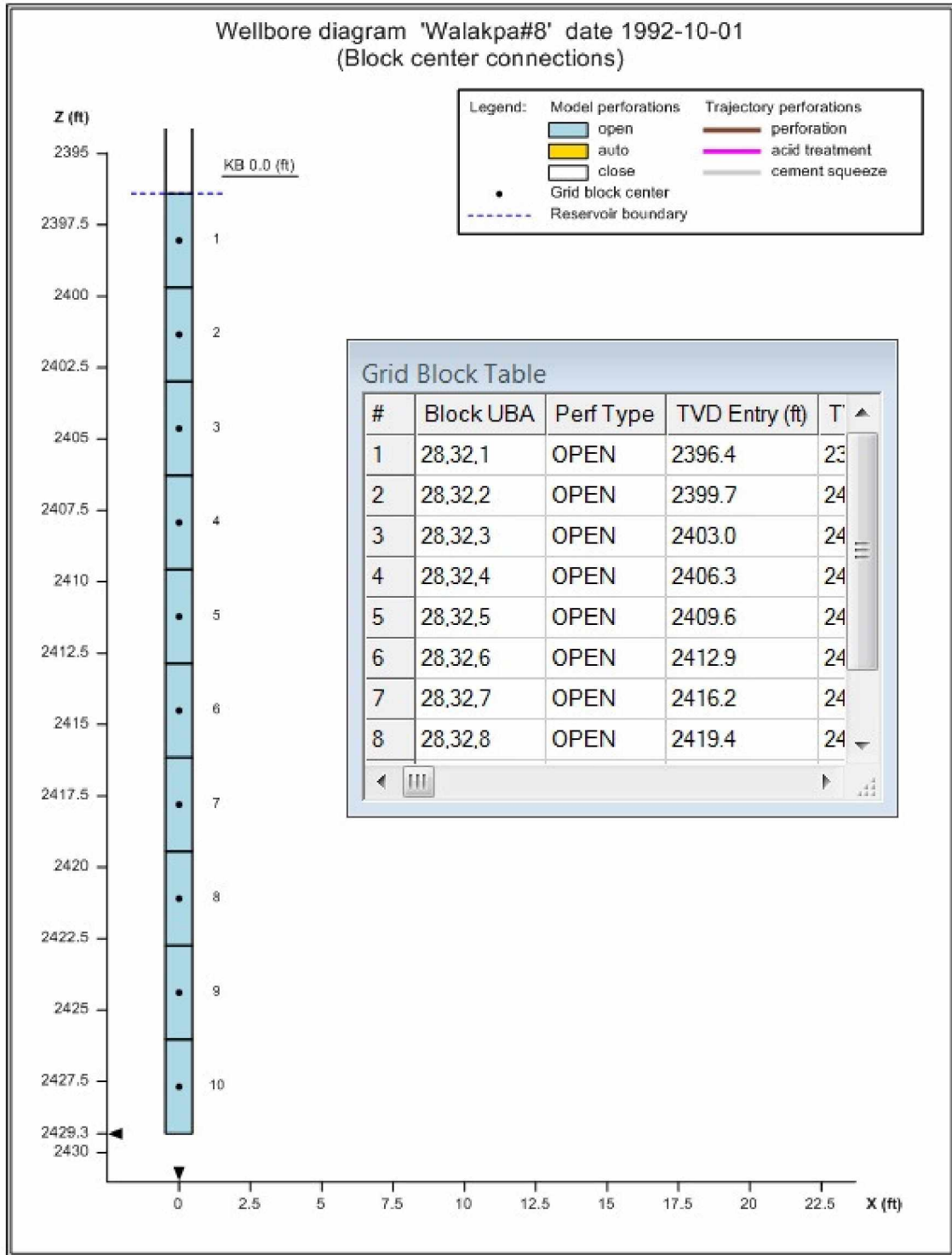


Figure C.7: Wellbore Diagram of WAL #8



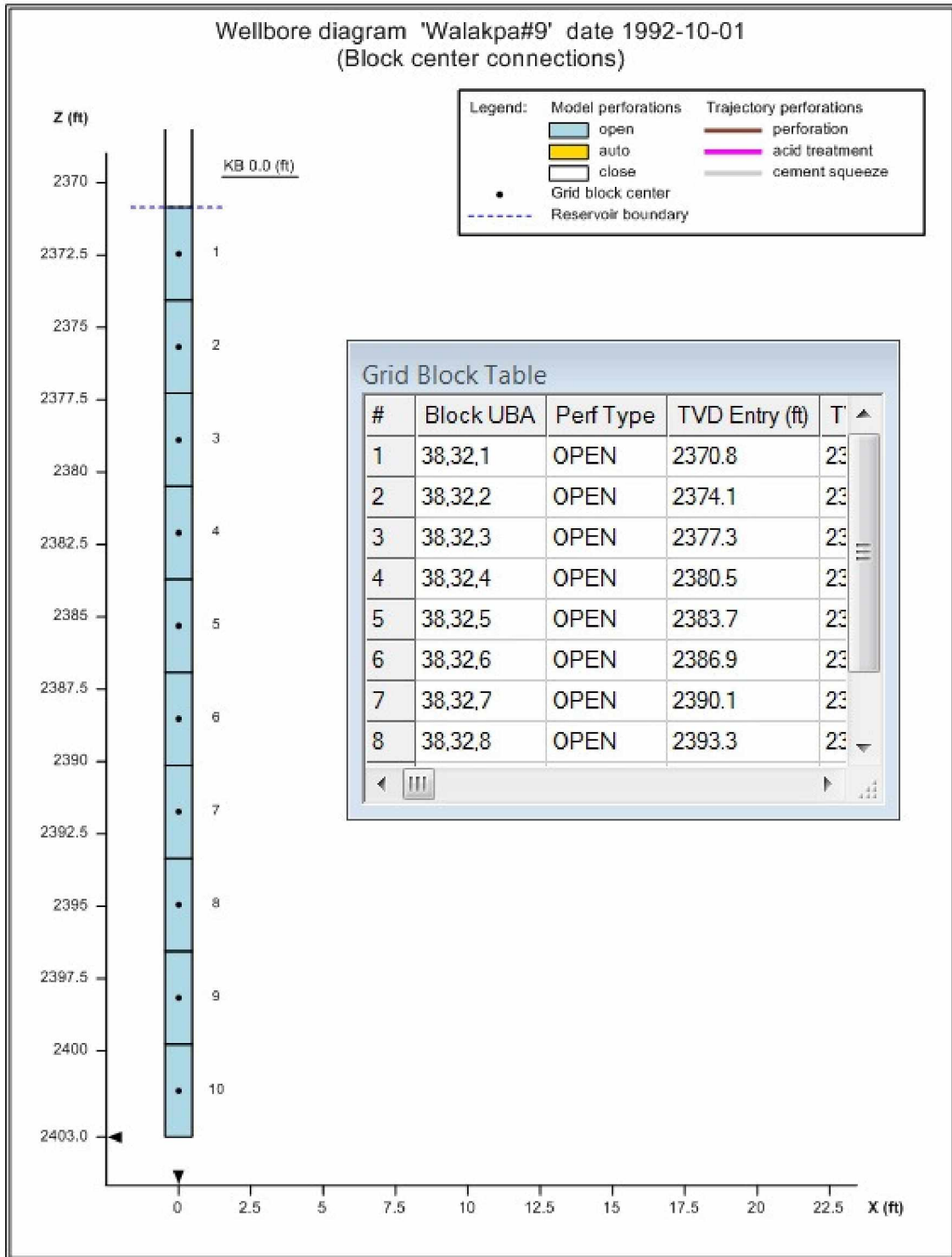


Figure C.8: Wellbore Diagram of WAL #9

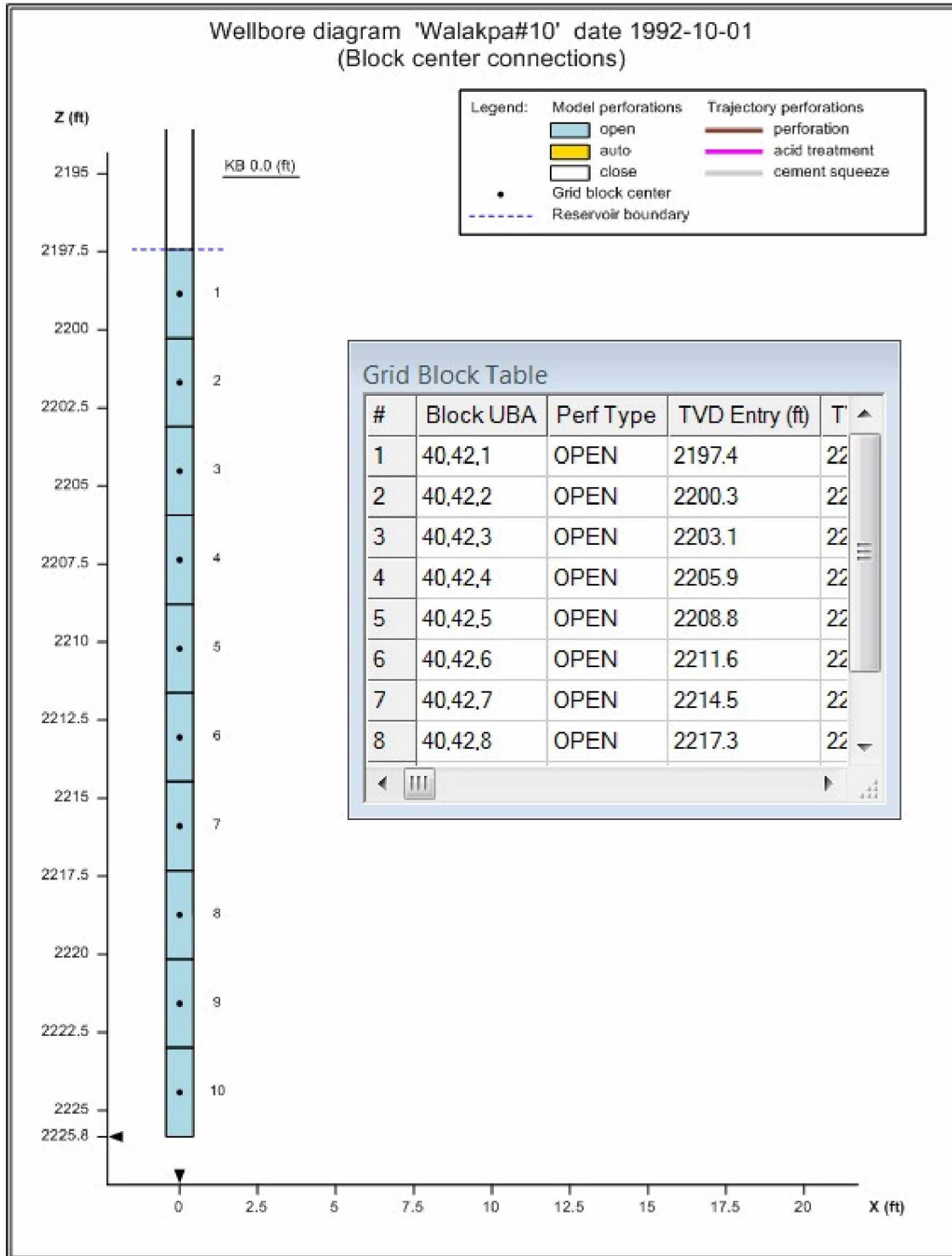


Figure C.9: Wellbore Diagram of WAL #10

### APPENDIX D. Wellbore Diagrams of Planned WAL Wells

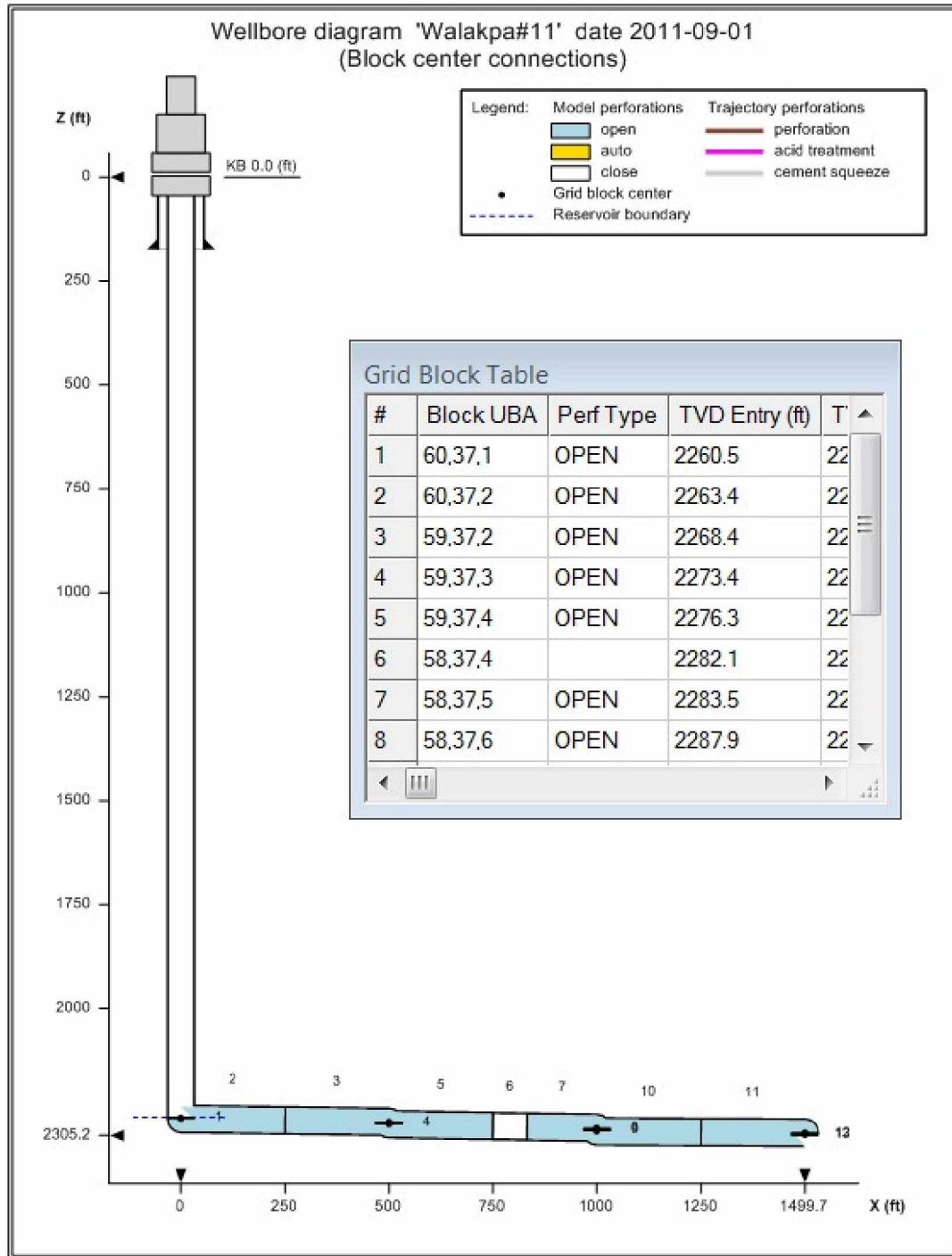


Figure D.1: Wellbore Diagram of WAL #11

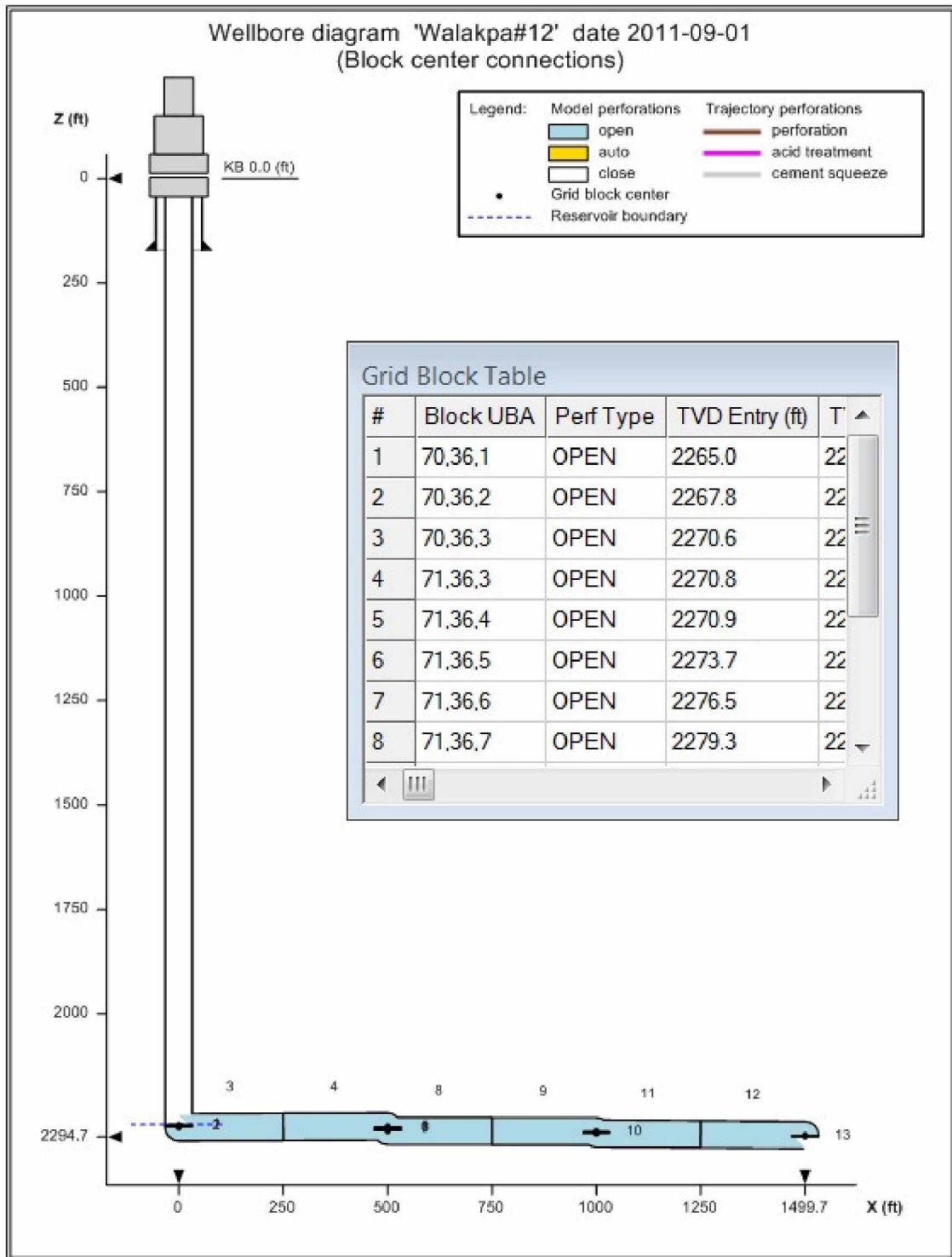


Figure D.2: Wellbore Diagram of WAL #12

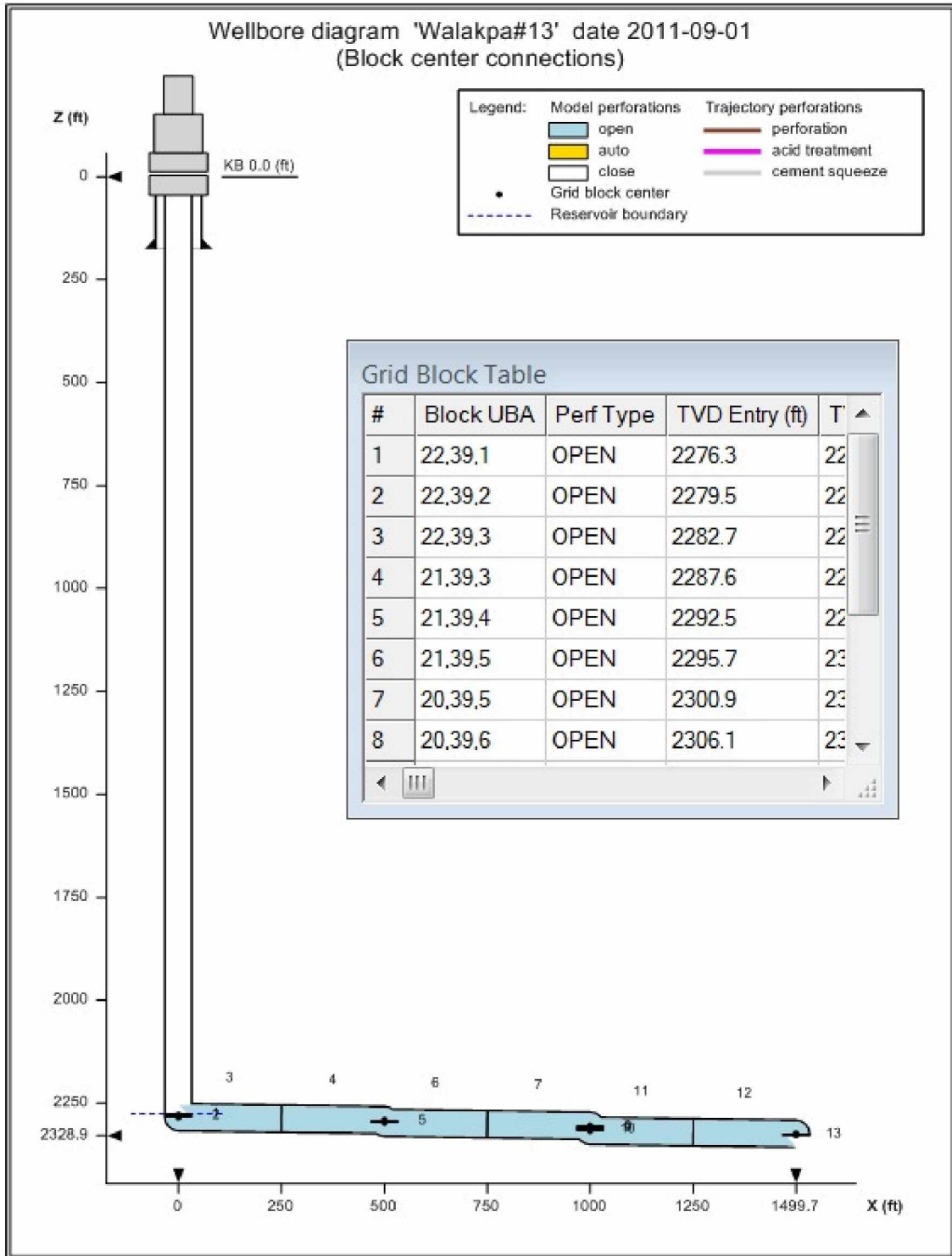


Figure D.3: Wellbore Diagram of WAL #13

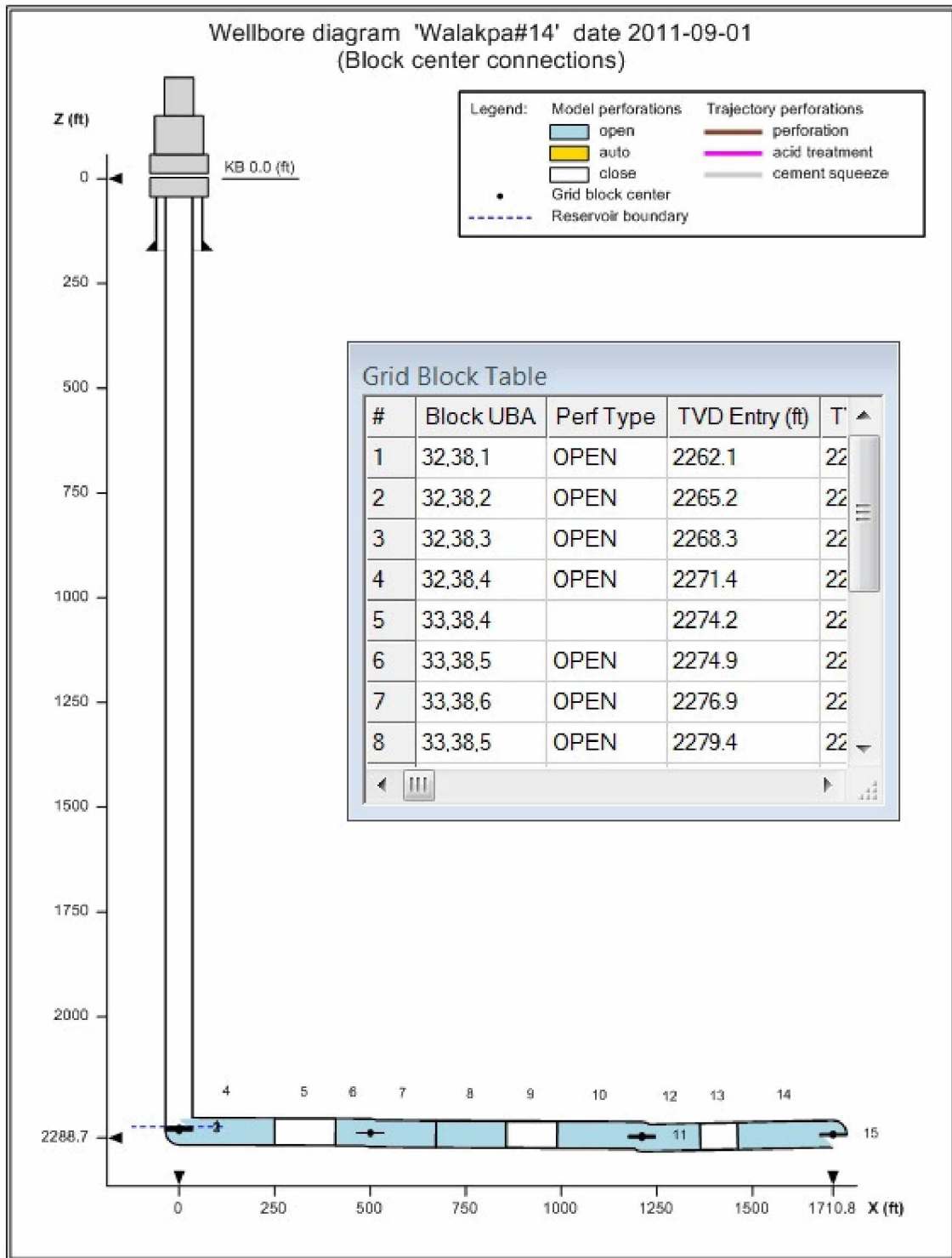


Figure D.4: Wellbore Diagram of WAL #14